الجمهورية الجزائرية الديمقراطية الشعبية
République Algérienne Démocratique et Populaire
وزارة التعليم العالي والبحث العلمي
Ministère de l'Enseignement Supérieur et de la Recherche Scientifique
جامعة فرحات عباس - سطيف 1
Université Ferhat Abbas - Sétif 1

THÈSE

Présentée à l'Institut d'Optique et Mécanique de Précision pour l'obtention du

Diplôme de

DOCTORAT 3ème Cycle LMD

Domaine : Sciences et Technologies
Filière : Optique et Mécanique de Précision
Spécialité : Optique et Photonique Appliquée

Par

MEBARKIA Ishak

THÈME

Etude des propriétés physiques de différents matériaux: $ABrF_4$ (A=Na, K, et Rb) composés ternaires

Soutenue le : 03/12/2022

Devant le jury composé de :

Président	BOUAFIA Mohamed	Prof.	Univ. Ferhat Abbas - Sétif 1
Rapporteur	MANALLAH Aïssa	Prof.	Univ. Ferhat Abbas - Sétif 1
Co-rapporteur	BEENKEN J. D. Wichard	PD Dr.	Univ. Technique – Ilmenau
Examinateur	BELLOUI Bouzid	Prof.	Univ. Ferhat Abbas - Sétif 1
Examinateur	HANINI Faouzi	MCA	Univ. Larbi Tébessi - Tébessa

الجمهورية الجزائرية الديمقراطية الشعبية
People's Democratic Republic of Algeria
وزارة التعليم العالي والبحث العلمي
Ministry of Higher Education and Scientific Research
جامعة فرحات عباس - سطيف 1
Ferhat Abbas University - Setif 1

THESIS

Submitted to the Institute of Optics and Precision Mechanics in Partial Fulfillment of the Requirements for the Award of the Degree of

3rd Cycle LMD DOCTORATE

Domain: Science and Technology
Faculty: Optics and Precision Mechanics
Specialty: Optics and Applied Photonics

By

MEBARKIA Ishak

SUBJECT

The study of the physical properties of different materials: $ABrF_4$ (A=Na, K, and Rb) ternary compounds

Discussed publicly at: 03/12/2022

Members of the assessment committee:

Chairman	BOUAFIA Mohamed	Prof.	Ferhat Abbas University-Setif 1
Supervisor	MANALLAH Aïssa	Prof.	Ferhat Abbas University-Setif 1
Co-supervisor	BEENKEN J. D. Wichard	PD Dr.	Technical University – Ilmenau
Examiner	BELLOUI Bouzid	Prof.	Ferhat Abbas University-Setif 1
Examiner	HANINI Faouzi	MCA	Larbi Tebessi University Tebessa

Acknowledgements

*First of all, praise is to almighty God "**Allah**", who gave me faith, courage, and patience to do this work. Then I ask Allah to make easy my progress in seeking science and to have the knowledge to help people and benefit humanity.*

*I would like to express my gratitude to **Prof. Aïssa Manallah** for his permission to be my academic supervisor, his guidance, and his valuable suggestions which were very useful to me during my four years Ph.D. program*

*I am thankful to the German Academic Exchange Service **DAAD** for the internship at the Technical University of Ilmenau in the framework of the **ILSE** project. I would also like to acknowledge the **DAAD-Project ILSE** leaders, **Prof. Mohamed Bouafia** and **Prof. Dr. Stefan Krischok**.*

*I am very appreciative to **PD Dr. Wichard Beenken** for his help, patience, and being my co-supervisor. Wichard gave me very in-time valuable instructions and put me in contact with experts in the field at TU Ilmenau, like **Prof. Dr. Erich Runge** who gave me precious advice regarding many theoretical issues in his classes.*

*Furthermore, I would like to thank the members of the assessment committee, **Prof. Bouzid Belloui** and **Dr. Faouzi Hanini** who honored me by accepting to judge and enrich this work.*

Last but not least, I would like to thank my dear parents, my family and all my friends for their support and encouragement.

Ishak Mebarkia

Dedication

I dedicate this modest work

To my dear parents

To my family

To my friends

To all those who love science

Table of contents

List of Abbreviations

BCT_2	Body Centered Tetragonal lattice Type 2
BFGS	Broyden–Fletcher–Goldfarb–Shanno
BZ	Brillouin zone
B88	Becke 1988
CASTEP	CAmbridge Serial Total Energy Package
CB	Conduction Band
CBM	Conduction Band minimum
CST	Constant
DBS	Direct Band gap Semiconductor
DFT	Density Functional Theory
EOS	Equation Of States
GGA	Generalized Gradient Approximation
HP	Hartree Product
IBS	Indirect Band gap Semiconductor
LDA	Local Density Approximation
OTFG	On-The-Fly pseudopotential Generation
PBE	Perdew-Burke-Ernzerhof
PBE-sol	Perdew-Burke-Ernzerhof for solids
PDOS	Partial Density Of States
PP-PW	Pseudopotential Plane Wave
PW91	Perdew-Wang 1991
TDOS	Total Density Of States
USPP	Ultra-Soft Pseudopotential
UV	Ultraviolet
VB	Valence Band
VBM	Valence Band Maximum
WC	Wu-Cohen
2D	Two-Dimensional
3D	Three-Dimensional

List of Figures

List of Tables

General Introduction

General Introduction

For several years great effort has been devoted to discovering new efficient optical materials that are required for Ultraviolet (UV) region applications in the fields of medical treatment, optical communications, semiconductor processing, electrical and electronics industries; etc. The alkali metal complex fluorides single crystals, that have a large UV optical absorption range, wide-band gaps, and lower refractive indices compared to those of oxides, are promising UV optical materials to fulfill this objective [1,2].

One of the motivating categories belonging to the alkali metal complex fluorides family is known as the alkali metal tetrafluoridobromate crystals, which are favorable for optoelectronic technologies such as UV optical components, optical amplifiers, and diode-pumped lasers, etc. [3,4]. Among these materials, there are $NaBrF_4$, $KBrF_4$, and $RbBrF_4$ ternary compounds, which are belonging to the same crystalline structure and sharing one of the alkali elements such that Sodium "Na", Potassium "K", and Rubidium "Rb" as a cation with an anion formed by Bromine bonded with four Fluorine "BrF_4" [5-8].

The objective of this research work is to predict the structural, mechanical, electronic, and optical properties of ternary compounds $ABrF_4$ with (A = Na, K, and Rb) using the ab-initio (first-principles) method of the Density Functional Theory. To the knowledge of the authors, no theoretical nor experimental study of the mechanical, electronic, and optical properties has been carried out on the herein studied compounds. The results presented in this work may be useful in evaluating potential technological applications of $NaBrF_4$, $KBrF_4$, and $RbBrF_4$ materials.

To cognize the different physical properties (structural, elastic, electronic ...) of materials as complex systems formed by interacting electrons and nuclei, it is necessary to study the physical environment in which the electrons move, and this is done through calculation methods. The resolution methods can be subdivided into three groups: I. Empirical methods, which use experimental data to find the parameter values. II. Semi-empirical methods, which require atomic parameters and experimental results to predict other properties that are not yet determined. III. Ab-initio (first-principle) methods, which only use the atomic constants as an input parameter for solving the Schrödinger equation.

The first principle is associated with the fundamental principles of quantum mechanics. These methods replace very expensive and even sometimes unrealizable experiments in the laboratory, they are a tool of choice for the prediction of the physical properties of new materials. The ab initio method that we used in this thesis is the pseudopotential plane wave (PP-PW) method within the framework of the density functional theory (DFT), implemented in the Cambridge serial total energy package (CASTEP) code. The exchange-correlation functional is treated in the generalized gradient approximation proposed by Perdew, Burke, and Ernzerhof for solids (GGA PBE-sol). The work of this thesis is divided into three chapters and organized as follows:

Firstly, a brief introduction on the materials to be studied, followed by a first chapter where we will present the foundations of the density functional theory (DFT) by means of which this work is carried out. This method is used to solve the electronic problem resulting from the introduction of the Born-Oppenheimer approximation in the Schrödinger multi-electron equation, and the approximations used to deal with the exchange-correlation energy part.

The second chapter is based on the description of the two approaches employed to solve the mono-electron Kohn-Sham equations, the plane wave approach for the expansion of the mono-electron Kohn-Sham orbitals, and the pseudo-potential approach for dealing with the Coulomb electrons-nuclei interaction (external potential). This chapter ends with a brief description of the calculation code used in this work to simulate the physical properties of the considered systems.

The last chapter is devoted to presenting and discussing the results obtained concerning the structural, mechanical, electronic, and optical properties of $NaBrF_4$, $KBrF_4$, and $RbBrF_4$ compounds.

Finally, the thesis is crowned by a conclusion containing the main consequences of this work.

References

[1] S. Stepleton, Synthesis of Complex Fluorides for Optical Applications, All Diss. (2009). https://tigerprints.clemson.edu/all_dissertations/418.

[2] A.J. Stevenson, H. Serier-Brault, P. Gredin, M. Mortier, Fluoride materials for optical applications: Single crystals, ceramics, glasses, and glass–ceramics, J. Fluor. Chem. 132 (2011) 1165–1173. https://doi.org/10.1016/J.JFLUCHEM.2011.07.017.

[3] O. Materials, Bulk Crystal Growth of Electronic , Optical & Wiley Series in Materials for Electronic and Optoelectronic, 2005. https://books.google.dz/books

[4] R. Burkhalter, I. Dohnke, J. Hulliger, Growing of bulk crystals and structuring waveguides of fluoride materials for laser applications, 2001. https://doi.org/10.1016/S0960-8974(01)00002-X.

[5] S.I. Ivlev, R. V. Ostvald, F. Kraus, A new look at NaBrF4: the most BrF3-rich tetrafluoridobromate(III) by mass, Monatshefte Fur Chemie. 147 (2016) 1661–1668. https://doi.org/10.1007/s00706-016-1799-2.

[6] S.I. Ivlev, F. Kraus, Redetermination of the crystal structure of K[BrF 4] from single-crystal X-ray diffraction data , IUCrData. 3 (2018). https://doi.org/10.1107/s2414314618006466.

[7] A. V. Malin, S.I. Ivlev, R. V. Ostvald, F. Kraus, Rubidium tetrafluoridobromate(III): redetermination of the crystal structure from single-crystal X-ray diffraction data, IUCrData. 4 (2019). https://doi.org/10.1107/s2414314619015955.

[8] A. V. Malin, S.I. Ivlev, R. V. Ostvald, F. Kraus, Redetermination of the crystal structure of caesium tetrafluoridobromate (III) from single-crystal X-ray diffraction data, IUCrData. 5 (2020) 3–8. https://doi.org/10.1107/s2414314620001145.

Chapter I

The Density Functional Theory

Chapter I: The Density Functional Theory

I.1 Introduction

Condensed matter physics is the branch of physics concerned with understanding and exploiting systems composed of interacting electrons and nuclei. The study of the different physical properties of a group of particles is carried out with the help of quantum mechanics by solving the time-independent Schrödinger equation.

There are analytical and exact numerical solutions to Schrodinger's equation for simple systems with a small number of atoms and molecules. However, the calculation of the ground state of a system with many particles forming a crystal is impossible to solve directly, since each particle interacts with all the other ones due to the strong correlation between the electrons, thus the Schrödinger equation becomes mathematically unsolvable. In most cases, the use of a certain number of approximations and assumptions turns out to be absolutely essential. for this reason, many approaches aiming at obtaining useful information on all these systems are in continuous development.

In this chapter, we focus on the Density Functional Theory, which has been acquired today its letters of nobility thanks to its success and effectiveness in computing the electronic structure of matter. Therefore, this theory takes a primordial place in computational physics and is described in an ab-initio or first-principle way[1].

I.2 Schrödinger equation for crystal

Any crystalline solid can be considered as a single system composed of electrons as light particles and nuclei as heavy particles. The ground state of the system can be described by solving the time-independent Schrödinger equation established by the Austrian-Irish physicist Erwin Schrödinger in 1925 with the following form [1]:

$$\widehat{\boldsymbol{H}}\,\boldsymbol{\Psi}(\boldsymbol{r_i}, \boldsymbol{R_\alpha}) = \boldsymbol{E}\,\boldsymbol{\Psi}(\boldsymbol{r_i}, \boldsymbol{R_\alpha}) \qquad \textbf{(I.1)}$$

Where $\boldsymbol{E}$ is the total energy of the crystal, $\boldsymbol{\Psi}$ is the many-body wave function which is in terms

[1] ab initio (or "from first principles") relies on basic and established laws of physics without additional assumptions.

of the spatial coordinates of electrons $\boldsymbol{r_i}$ $(\boldsymbol{i = 1 \ldots N_e})$ and of nuclei $\boldsymbol{R_\alpha}$ $(\boldsymbol{\alpha = 1 \ldots N_\alpha})$ where $\boldsymbol{N_e}$ and $\boldsymbol{N_\alpha}$ are respectively the number of electrons and ions in the system. Lastly, $\widehat{\boldsymbol{H}}$ represents the Hamiltonian operator which given by:

$$\widehat{\boldsymbol{H}} = \widehat{\boldsymbol{T}}_{\boldsymbol{e}} + \widehat{\boldsymbol{T}}_{\boldsymbol{Z}} + \widehat{\boldsymbol{U}}_{\boldsymbol{e}} + \widehat{\boldsymbol{U}}_{\boldsymbol{Z}} + \widehat{\boldsymbol{U}}_{\boldsymbol{eZ}} \qquad \textbf{(I.2)}$$

Where:

- $\widehat{\boldsymbol{T}}_{\boldsymbol{e}} = -\frac{\hbar^2}{2\boldsymbol{m_e}} \sum_{\boldsymbol{i=1}}^{\boldsymbol{N_e}} \boldsymbol{\nabla}_{\boldsymbol{r_i}}^{\boldsymbol{2}}$: is the electronic kinetic energy.
- $\widehat{\boldsymbol{T}}_{\boldsymbol{Z}} = -\frac{\hbar^2}{2\boldsymbol{M_\alpha}} \sum_{\boldsymbol{i=1}}^{\boldsymbol{N_\alpha}} \boldsymbol{\nabla}_{\boldsymbol{R_\alpha}}^{\boldsymbol{2}}$: is the nuclei kinetic energy.
- $\widehat{\boldsymbol{U}}_{\boldsymbol{e}} = \frac{\boldsymbol{1}}{\boldsymbol{8\pi\varepsilon_0}} \sum_{\boldsymbol{i=1}}^{\boldsymbol{N_e}} \sum_{\boldsymbol{j\neq i}}^{\boldsymbol{N_e}} \frac{\boldsymbol{e^2}}{|\boldsymbol{r_i - r_j}|}$: is the potential of the repulsive interaction (electron-electron).
- $\widehat{\boldsymbol{U}}_{\boldsymbol{Z}} = \frac{\boldsymbol{1}}{\boldsymbol{8\pi\varepsilon_0}} \sum_{\boldsymbol{\alpha=1}}^{\boldsymbol{N_\alpha}} \sum_{\boldsymbol{\beta\neq\alpha}}^{\boldsymbol{N_\alpha}} \frac{\boldsymbol{Z_\alpha Z_\beta e^2}}{|\boldsymbol{R_\alpha - R_\beta}|}$: is the potential of the repulsive interaction (nucleus-nucleus).
- $\widehat{\boldsymbol{U}}_{\boldsymbol{eZ}} = -\frac{\boldsymbol{1}}{\boldsymbol{4\pi\varepsilon_0}} \sum_{\boldsymbol{i=1}}^{\boldsymbol{N_e}} \sum_{\boldsymbol{\alpha=1}}^{\boldsymbol{N_\alpha}} \frac{\boldsymbol{Z_\alpha e^2}}{|\boldsymbol{r_i - R_\alpha}|}$: is the potential of the attractive interaction (electron-nucleus).

The Hamiltonian operator can therefore be written as:

$$\widehat{\boldsymbol{H}} = -\frac{\hbar^2}{2\boldsymbol{m_e}} \sum_{\boldsymbol{i=1}}^{\boldsymbol{N_e}} \boldsymbol{\nabla}_{\boldsymbol{r_i}}^{\boldsymbol{2}} - \frac{\hbar^2}{2\boldsymbol{M_\alpha}} \sum_{\boldsymbol{i=1}}^{\boldsymbol{N_\alpha}} \boldsymbol{\nabla}_{\boldsymbol{R_\alpha}}^{\boldsymbol{2}} + \frac{\boldsymbol{1}}{\boldsymbol{8\pi\varepsilon_0}} \sum_{\boldsymbol{i=1}}^{\boldsymbol{N_e}} \sum_{\boldsymbol{j\neq i}}^{\boldsymbol{N_e}} \frac{\boldsymbol{e^2}}{|\boldsymbol{r_i - r_j}|} + \frac{\boldsymbol{1}}{\boldsymbol{8\pi\varepsilon_0}} \sum_{\boldsymbol{\alpha=1}}^{\boldsymbol{N_\alpha}} \sum_{\boldsymbol{\beta\neq\alpha}}^{\boldsymbol{N_\alpha}} \frac{\boldsymbol{Z_\alpha Z_\beta e^2}}{|\boldsymbol{R_\alpha - R_\beta}|} - \frac{\boldsymbol{1}}{\boldsymbol{4\pi\varepsilon_0}} \sum_{\boldsymbol{i=1}}^{\boldsymbol{N_e}} \sum_{\boldsymbol{\alpha=1}}^{\boldsymbol{N_\alpha}} \frac{\boldsymbol{Z_\alpha e^2}}{|\boldsymbol{r_i - R_\alpha}|} \qquad \textbf{(I.3)}$$

Where:

$\boldsymbol{\nabla^2}$: is the Laplacian operator.

$\hbar$: is the reduced Planck constant.

$\boldsymbol{m_e}$: is the mass of the electron.

$\boldsymbol{e}$: is the electron charge.

$|\boldsymbol{r_i - r_j}|$: is the distance between the electrons $\boldsymbol{i}$ and $\boldsymbol{j}$.

$\boldsymbol{M_\alpha}$: is the mass of the nucleus.

$\boldsymbol{Z_\alpha}$, $\boldsymbol{Z_\beta}$: are the atomic numbers of the nuclei $\boldsymbol{\alpha}$ and $\boldsymbol{\beta}$, respectively.

$|\boldsymbol{R_\alpha - R_\beta}|$: is the distance between the nuclei $\boldsymbol{\alpha}$ and $\boldsymbol{\beta}$.

The Schrödinger equation **(I.1)** gives the eigenvalues of the energy and their corresponding eigenstates, which is contains $3(\boldsymbol{Z+1})\boldsymbol{N_\alpha}$ variables. For a crystalline solid the number of atoms $\boldsymbol{N_\alpha}$ is about 10^{22} atoms/cm^3, then it is impossible to obtain a solution because it is an N-body problem that is only solved by a certain number of approximations.

I.3 The different approximations

I.3.1 The Born–Oppenheimer approximation

In 1927, the German physicist Max Born and the American physicist Julius Robert Oppenheimer proposed the Born-Oppenheimer approximation [2] also called the adiabatic approximation to simplify the resolution of Schrödinger equation.

This approximation is based on the fact that the mass of the nuclei is much higher than that of the electrons, then the atomic nuclei are hypothesized immobile, hence their kinetic energies are null and the interaction potentials between them are constant. Given that $\widehat{\boldsymbol{T}}_{\boldsymbol{Z}} = \boldsymbol{0}$ and $\widehat{\boldsymbol{U}}_{\boldsymbol{Z}} = \boldsymbol{CST}$ we can define a wave function $\boldsymbol{\Psi_e}$ as a wave function of the electrons, and a new Hamiltonian of the electrons, which is given by:

$$\widehat{\boldsymbol{H}}_{\boldsymbol{e}} = \widehat{\boldsymbol{T}}_{\boldsymbol{e}} + \widehat{\boldsymbol{U}}_{\boldsymbol{e}} + \widehat{\boldsymbol{U}}_{\boldsymbol{eZ}} = -\frac{\hbar^2}{2m_e}\sum_{i=1}^{N_e}\nabla_{r_i}^2 + \frac{1}{8\pi\varepsilon_0}\sum_{i=1}^{N_e}\sum_{j\neq i}^{N_e}\frac{e^2}{|r_i - r_j|} - \frac{1}{4\pi\varepsilon_0}\sum_{i=1}^{N_e}\sum_{\alpha=1}^{N_\alpha}\frac{Z_\alpha e^2}{|r_i - R_\alpha^0|} \quad \textbf{(I.4)}$$

The multi-electronic Schrödinger equation can then be written as follows:

$$\widehat{\boldsymbol{H}}_{\boldsymbol{e}}\boldsymbol{\Psi_e}(\boldsymbol{r_i}, \boldsymbol{R_\alpha^0}) = \boldsymbol{E_e}\boldsymbol{\Psi_e}(\boldsymbol{r_i}, \boldsymbol{R_\alpha^0}) \quad \textbf{(I.5)}$$

In this equation, the R_α^0 does not appear as a variable but rather appears as a parameter, and E_e represents the energy of electrons moving in the field created by fixed ions.

It is right that this approximation reduced the problem to the behavior of electrons and minimized the number of variables, but it is not sufficient to solve the Schrödinger equation due to the interaction of a high number of electrons between themselves "$\widehat{U}_e$". This is why the Born–Oppenheimer approximation is very often required other complementary approximations.

I.3.2 The self-consistent field approximation

I.3.2.1 The Hartree approximation

In 1928, the English physicist Douglas Rayner Hartree proposed the first approach, known as Hartree approximation [3] to solve the problem of many electrons. This approximation considers the electrons are independent, where each of them moves alone in the mean-field created by nuclei and other electrons, hence the problem of N-electron in interaction is simplified to a single-electron problem.

The behavior of each electron is described by a single Hamiltonian $\boldsymbol{h}$, and the total Hamiltonian of electrons $\widehat{\boldsymbol{H}}_{\boldsymbol{e}}$ can be written as a sum of N-single Hamiltonians, as follows taking into consideration the Hartree atomic units[2]:

$$\widehat{\boldsymbol{H}}_{\boldsymbol{e}} = \sum_{\boldsymbol{i}=\boldsymbol{1}}^{\boldsymbol{N_e}} \boldsymbol{h_i} \qquad \textbf{(I.6)}$$

$$\boldsymbol{h_i} = -\frac{\boldsymbol{1}}{\boldsymbol{2}} \boldsymbol{\nabla}_{\boldsymbol{r_i}}^{\boldsymbol{2}} + \boldsymbol{\mu_i}(\boldsymbol{r_i}) + \boldsymbol{u_i}(\boldsymbol{r_i}) \qquad \textbf{(I.7)}$$

Where:

- $\boldsymbol{\mu_i}(\boldsymbol{r_i}) = \frac{\boldsymbol{1}}{\boldsymbol{2}} \sum_{\boldsymbol{j}\neq\boldsymbol{i}}^{\boldsymbol{N_e}} \frac{\boldsymbol{1}}{|\boldsymbol{r_i}-\boldsymbol{r_j}|}$: is the Hartree potential, also called the self-consistent potential which represents the Coulomb repulsion exerted on electron $\boldsymbol{i}$ by all the other electrons $\boldsymbol{j} \neq \boldsymbol{i}$.
- $\boldsymbol{u_i}(\boldsymbol{r_i}) = -\sum_{\boldsymbol{\alpha}=\boldsymbol{1}}^{\boldsymbol{N_\alpha}} \frac{\boldsymbol{Z_\alpha}}{|\boldsymbol{r_i}-\boldsymbol{R_\alpha^0}|}$: is the potential energy which represents the Coulomb attraction of the electron $\boldsymbol{i}$ with all nuclei of the crystal.

The total energy of electrons $\boldsymbol{E_e}$ is the sum of the energies of the separated electrons $\boldsymbol{\varepsilon}$:

$$\boldsymbol{E_e} = \sum_{\boldsymbol{i}=\boldsymbol{1}}^{\boldsymbol{N_e}} \boldsymbol{\varepsilon_i} \qquad \textbf{(I.8)}$$

The mono-electronic Schrödinger equation can then be written as follows:

$$\left[-\frac{\boldsymbol{1}}{\boldsymbol{2}} \boldsymbol{\nabla}_{\boldsymbol{r_i}}^{\boldsymbol{2}} + \boldsymbol{V_{eff}}(\boldsymbol{r_i})\right] \boldsymbol{\psi_i}(\boldsymbol{r_i}) = \boldsymbol{\varepsilon_i}\, \boldsymbol{\psi_i}(\boldsymbol{r_i}) \qquad \textbf{(I.9)}$$

[2] The Hartree atomic units are a system of units widely used to simplify formal or numerical calculations in quantum physics, especially in atomic physics. They consist in setting $\hbar = \boldsymbol{m_e} = \frac{\boldsymbol{e^2}}{\boldsymbol{4\pi\varepsilon_0}} = \boldsymbol{1}$.

Where $\boldsymbol{V_{eff}(r_i)}$ is the effective potential given by:

$$\boldsymbol{V_{eff}(r_i) = \mu_i(r_i) + u_i(r_i)} \quad \textbf{(I.10)}$$

Solving the mono-electronic Schrödinger equation **(I.9)** for each electron gives the wave function of the respective electron $\boldsymbol{\psi}$, and the total wave function of electrons $\boldsymbol{\Psi_e}$ is written as:

$$\boldsymbol{\Psi_e^{HP}(r_1, r_2, r_3 \dots r_{N_e}) = \prod_{i=1}^{N_e} \psi_i(r_i)} \quad \textbf{(I.11)}$$

This function is a product of single-electron spin-orbitals. It is called the Hartree Product (HP).

This approach simplified the solution of the Schrödinger equation but is non-compatible with Pauli exclusion principle [4] owing to the Hartree product is not satisfactory for fermions such as electrons, because the total wave function $\boldsymbol{\Psi_e^{HP}}$ is not anti-symmetrical with respect to the exchange of any two electrons.

I.3.2.2 The Hartree-Fock approximation

In 1930, the Russian physicist Vladimir Aleksandrovich Fock and the American physicist John Clarke Slater solved the problem of the lack of anti-symmetry in the Hartree approximation [5,6].

To be the total wave function anti-symmetric, the exchange of two electrons must mathematically lead to the appearance of a negative sign as in the following equality:

$$\boldsymbol{\Psi_e(\dots r_i \dots r_j \dots) = -\Psi_e(\dots r_j \dots r_i \dots)} \quad \textbf{(I.12)}$$

In the framework of this approximation the total wave function is written as a Slater determinant of single-electron orbitals and confirms the Pauli exclusion principle, as follows:

$$\boldsymbol{\Psi_e^{HF}(r_1, r_2, r_3 \dots r_{N_e}) = \frac{1}{\sqrt{N_e!}} \begin{bmatrix} \psi_1(r_1) & \cdots & \psi_1(r_{N_e}) \\ \vdots & \ddots & \vdots \\ \psi_{N_e}(r_1) & \cdots & \psi_{N_e}(r_{N_e}) \end{bmatrix}} \quad \textbf{(I.13)}$$

Where $\boldsymbol{\frac{1}{\sqrt{N_e!}}}$ is the normalization factor of the Hartree-Fock total wave function $\boldsymbol{\Psi_e^{HF}}$.

The calculation by the Hartree-Fock method leads to good results, especially in molecular physics, but it does not take into account the effects of electronic correlations, where it assumes that an electron is immersed in an average field created by the other electrons. Thus, it becomes very heavy and gives an overestimation of the energy if the distance between nuclei increases as in the case of a large system.

I.4 Foundations of Density Functional Theory

The fundamental concept of the density functional theory is to express the energy of an electronic system in terms of the electron density $\boldsymbol{\rho(r)}$ that minimizes the energy of the system. It is in fact an old idea dating from 1927 when established by the British physicist Llewellyn Hilleth Thomas [7] and the Italian physicist Enrico Fermi [8] expressing all total energy contributions (kinetic as well as electrostatic) in terms of electron density.

The Thomas-Fermi model consists of subdividing the inhomogeneous system into the behavior of a local homogeneous gas of constant density. Then this model is a local approximation of the density, which did not take into account the exchange and correlation effects of electrons. For this reason, an exchange-energy functional was added by the British physicist Paul Adrien Maurice Dirac in 1930 [9] and an expression for the correlation-energy obtained by the Hungarian physicist Eugene Paul Wigner in 1934 [10].

The application of the electron density as a fundamental variable to describe the properties of the system has existed since the first approaches to the electronic structure of matter, but it has only been proved by the demonstration of other fundamental theorems and equations, which presented the best procedure for the realization of the density functional theory.

I.4.1 The theorems of Hohenberg and Kohn

In 1964, the French-American physicist Pierre Hohenberg and the Austrian-American physicist Walter Kohn demonstrated two fundamental theorems relative to any system of electrons in an external field such as that induced by nuclei [11].

a) The first theorem:

The ground state total energy is uniquely determined by the electron density $\boldsymbol{\rho(r)}$ for a given external potential $\boldsymbol{V_{ext}(r)}$. This theorem signifies that to determine the wave functions, it is sufficient to know the electron density, then the total energy $\boldsymbol{E}$ is represented as a functional of the electron density $\boldsymbol{\rho(r)}$.

From Schrödinger's equation we have:

$$\boldsymbol{E = \langle \Psi | \hat{H} | \Psi \rangle = \langle \Psi | \hat{T}_e + \hat{U}_e + \hat{V}_{ext} | \Psi \rangle = \langle \Psi | \hat{T}_e + \hat{U}_e | \Psi \rangle + \langle \Psi | \hat{V}_{ext} | \Psi \rangle = \langle \Psi | \hat{T}_e + \hat{U}_e | \Psi \rangle + \int V_{ext}(r)\, \rho(r) d^3 r} \quad \textbf{(I.14)}$$

Where $\boldsymbol{T_e}$ and $\boldsymbol{U_e}$ are the kinetic energy and the inter-electron interaction potential respectively that do not depend on the external potential $\boldsymbol{V_{ext}(r)}$.

The total energy can be expressed as functional according to the first theorem of Hohenberg-Kohn as follows:

$$\boldsymbol{E^{HK}[\rho(r)] = F^{HK}[\rho(r)] + V_{ext}[\rho(r)]} \quad \textbf{(I.15)}$$

$\boldsymbol{F^{HK}[\rho(r)]}$ is a universal functional of Hohenberg-Kohn, which is universal for any many-electron system. This functional contains the kinetic and Coulomb contributions to the energy which is given by:

$$\boldsymbol{F^{HK}[\rho(r)] = \langle \Psi | \hat{T}_e + \hat{U}_e | \Psi \rangle = T_e[\rho(r)] + U_e[\rho(r)]} \quad \textbf{(I.16)}$$

$\boldsymbol{V_{ext}[\rho(r)]}$ is a non-universal functional, which is depends on the studied system and given by:

$$\boldsymbol{V_{ext}[\rho(r)] = \int V_{ext}(r)\, \rho(r) d^3 r} \quad \textbf{(I.17)}$$

b) ***The second theorem:***

The minimum value of the total energy functional $\boldsymbol{E[\rho(r)]}$ is the exact ground state energy of the system $\boldsymbol{E_0}$ and the electron density $\boldsymbol{\rho(r)}$ that minimizes this functional is the exact ground state electron density $\boldsymbol{\rho_0}$. This theorem based on the variational principle, which means that the ground state electron density $\boldsymbol{\rho_0}$ is the one that minimizes the total energy, and this minimum total energy is the ground state total energy $\boldsymbol{E_0}$, as follows:

$$\boldsymbol{E_0 = E[\rho_0(r)] \leq E[\rho(r)]} \quad \textbf{(I.18)}$$

Furthermore, all other ground state properties are also a functional of the ground state electron density $\boldsymbol{\rho_0}$ and all properties of the system can be determined by this ground state electron density.

I.4.2 The equations of Kohn and Sham

In 1965, Walter Kohn and the American physicist Lu Jeu Sham added equations which made the density functional theory a practical tool for obtaining the ground state energy of an electronic system [12].

The ansatz[2] of Kohn and Sham is based on replacing the system of interacting electrons with a simple fictitious system of non-interacting electrons immersed in an effective potential, chosen such that the electron density is identical to that of the real system. For this reason, the self-consistent mono-electronic Schrödinger equation defined in equation **(I.9)** is modified to write as follows:

$$\left[-\frac{1}{2}\nabla_{r_i}^2 + V_{eff}^{KS}(r)\right]\psi_i(r) = \varepsilon_i\,\psi_i(r) \qquad \textbf{(I.19)}$$

Where $V_{eff}^{KS}(r)$ is the Kohn-Sham effective potential, which is given by:

$$V_{eff}^{KS}(r) = V_H(r) + V_{ext}(r) + V_{XC}(r) \qquad \textbf{(I.20)}$$

Where:

- $V_H(r)$ is the classical Hartree potential (The self-consistent potential), which can be expressed as a function of the electron density as follows:

$$V_H(r) = \int \frac{\rho(r')}{|r-r'|} d^3r' \qquad \textbf{(I.21)}$$

- $V_{ext}(r)$ is the external potential created by the nuclei.

- $V_{XC}(r)$ is the exchange-correlation potential defined as a functional derivative of the exchange-correlation energy E_{XC} with respect to the electron density $\rho(r)$:

$$V_{XC}(r) = \frac{\delta E_{XC}[\rho(r)]}{\delta\rho(r)} \qquad \textbf{(I.22)}$$

[2]The ansatz is an assumption about the form of an unknown function that is made in order to facilitate the solution of an equation or other problem.

The electron density for $\boldsymbol{N_e}$ electron system is expressed as follows:

$$\boldsymbol{\rho(r) = \sum_{i=1}^{N_e} |\psi_i(r)|^2} \quad \textbf{(I.23)}$$

Where $\boldsymbol{\psi_i(r)}$ are the Kohn-Sham orbitals which describing by the following expression:

$$\boldsymbol{\psi_i(r) = \sum_j C_{ij} \phi_j(r)} \quad \textbf{(I.24)}$$

Where $\boldsymbol{C_{ij}}$ are the expansion coefficients expressing $\boldsymbol{\psi_i(r)}$ in a given basis set $\boldsymbol{\phi_j(r)}$

Resolving the Schrödinger equation in the approach of the Kohn-Sham is done by solving the equation **(I.19)** via ab-initio methods which principally consist to determine the expansion coefficients $\boldsymbol{C_{ij}}$ for occupied orbitals that minimize the total energy. This is done according to the basis set, in which the Hamiltonian $\boldsymbol{H}$ and the overlap matrixes $\boldsymbol{S}$ are calculated, then finding the exact expansion coefficients $\boldsymbol{C_i}$ from the following secular equation [13]:

$$\boldsymbol{(H - \phi \varepsilon_i S) C_i = 0} \quad \textbf{(I.25)}$$

The self-consistent algorithm (i.e., iterative algorithm) used to solve the Kohn-Sham equations is illustrated by an organization chart in the Figure I.1, which is based on an initial guess of the electron density, calculates the Kohn-Sham effective potential, and solves the Kohn-Sham equations, then evaluates the electron density and compare it to the initial guessed density. this algorithm iterates until the desired convergence is reached where the total energy is minimized.

The theorems of Hohenberg and Kohn as well as the development leading to the Kohn-Sham mono-particle equations are perfectly rigorous and are obtained from exact and well-defined parameters except for the exchange-correlation energy functional $\boldsymbol{E_{XC}[\rho(r)]}$ that appears in the Kohn-Sham effective potential equation makes any exact solution impossible since its analytic form is unknown, for this reason, several approximations have been proposed.

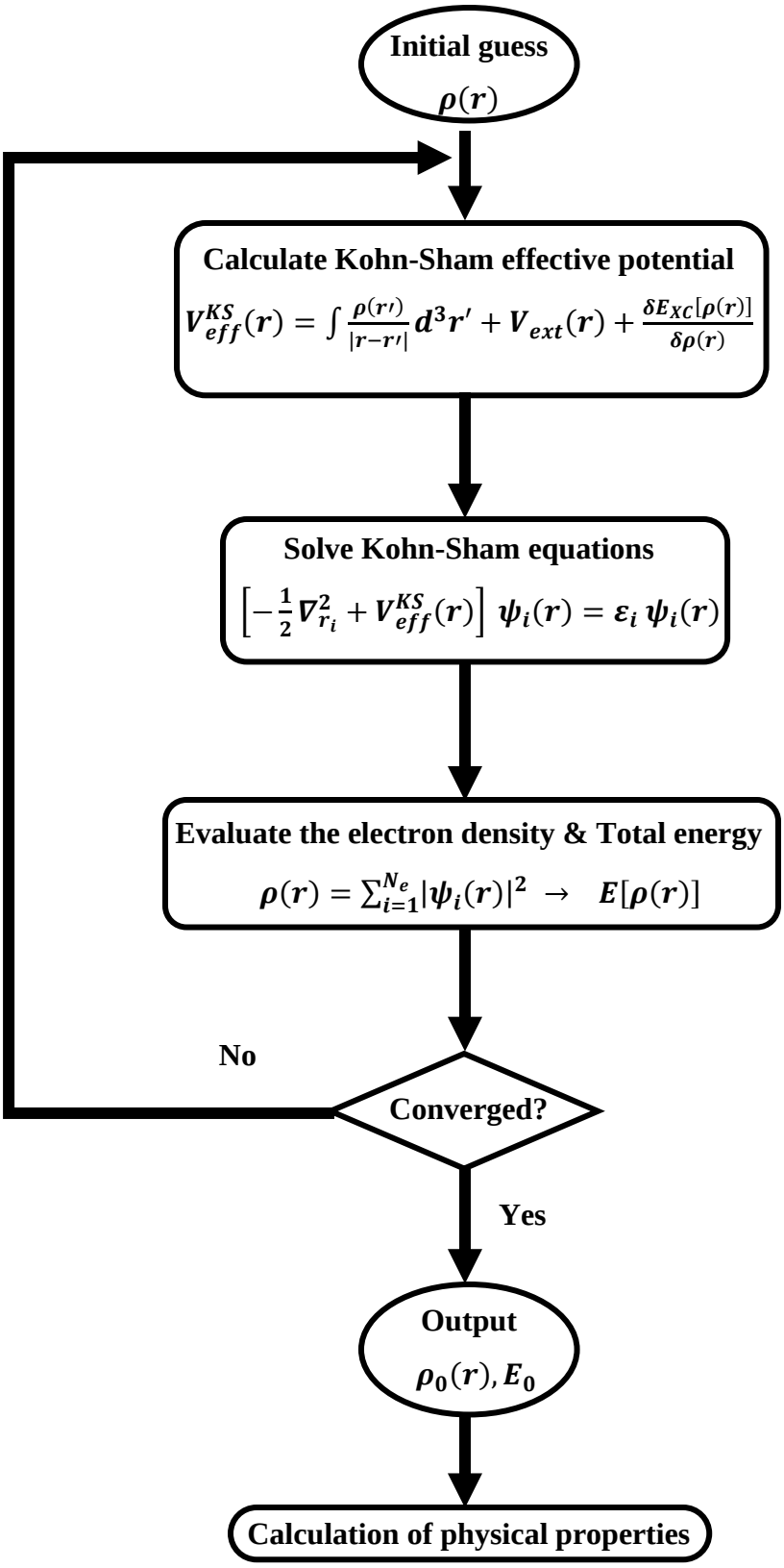

Figure I.1 The organization chart of Kohn-Sham equations resolution within the self-consistent algorithm based on an initial guess and convergence criteria.

I.4.3 The exchange-correlation energy approximations

Several approximations were proposed and tested on different types of systems to determine the exchange-correlation energy expression. In solid-state physics, the most common approximations are the local density approximation (LDA), and the generalized gradient approximation (GGA).

I.4.3.1 The local density approximation

The local density approximation (LDA) is the oldest and simplest approximation proposed by Kohn and Sham in 1965 [12]. In this approach, the electron density assumed varies sufficiently slowly in the system to be similar to that of a homogeneous electron gas, which implies that the effects of exchange and correlation have a local character. In this case, the exchange-correlation energy can be written in this form:

$$\boldsymbol{E_{XC}^{LDA}[\rho(r)] = \int \varepsilon_{XC}^{LDA}[\rho(r)]\,\rho(r)d^3r} \qquad \textbf{(I.26)}$$

Where $\boldsymbol{\varepsilon_{XC}^{LDA}[\rho(r)]}$ is the exchange-correlation energy per particle of an electron gas of uniform density $\boldsymbol{\rho(r)}$, which has been parameterized for different values of the electron density, by U. Von Barth and L. Hedin (1972) [14], O. Gunnarsson and B. I. Lundqvist (1976) [15], S. H. Vosko, L. Wilk, and M. Nusair (1980) [16], and J. P. Perdew and Alex Zunger (1980) [17].

The LDA is an honest approximation for systems with slowly varying electron density, but this condition is rarely fulfilled for real electronic systems, for this reason, many developments have been made to improve the results obtained.

I.4.3.2 The generalized gradient approximation

In 1986, the American physicist John P. Perdew proposed the generalized gradient approximation (GGA) [18] which is a semi-local approximation where it considers the exchange correlation energy no longer as a function only of the electron density, but more generally as a function $\boldsymbol{f_{XC}}$ of the electron density $\boldsymbol{\rho(r)}$ and its local variation $\boldsymbol{\vec{\nabla}\,\rho(r)}$

$$\boldsymbol{E_{XC}^{GGA}[\rho(r)] = \int f_{XC}\{\rho(r), \vec{\nabla}\,\rho(r)\}\,d^3r} \qquad \textbf{(I.27)}$$

There are many forms of f_{XC} function, the most frequently used are "B88" introduced by Axel D. Becke in 1988 [19], "PW91" announced by John P. Perdew and Yue Wang in 1991 [20], "PBE" proposed by John P. Perdew, Kieron Burke, and Matthias Ernzerhof in 1996 [21], "PBE-sol" developed especially for solids in 2008 [22], and "WC" suggested also for solids by Zhigang Wu and R. E. Cohen in 2006 [23].

References

[1] E. Schrödinger, An Undulatory Theory of the Mechanics of Atoms and Molecules, Phys. Rev. 28 (1926) 1049. https://doi.org/10.1103/PhysRev.28.1049.

[2] M. Born, R. Oppenheimer, Zur Quantentheorie der Molekeln, Ann. Phys. 389 (1927) 457–484. https://doi.org/10.1002/andp.19273892002.

[3] D.R. Hartree, The Wave Mechanics of an Atom with a Non-Coulomb Central Field Part I Theory and Methods, Math. Proc. Cambridge Philos. Soc. 24 (1928) 89–110. https://doi.org/10.1017/S0305004100011919.

[4] W. PAULI, On the Connexion between the Completion of Electron Groups in an Atom with the Complex Structure of Spectra, Old Quantum Theory. (1967) 184–203. https://doi.org/10.1016/b978-0-08-012102-4.50019-x.

[5] V. Fock, Näherungsmethode zur Lösung des quantenmechanischen Mehrkörperproblems, Zeitschrift Für Phys. 1930 611. 61 (1930) 126–148. https://doi.org/10.1007/BF01340294.

[6] J.C. Slater, Cohesion in Monovalent Metals, Phys. Rev. 35 (1930) 509. https://doi.org/10.1103/PhysRev.35.509.

[7] L.H. Thomas, The calculation of atomic fields, Math. Proc. Cambridge Philos. Soc. 23 (1927) 542–548. https://doi.org/10.1017/S0305004100011683.

[8] E. Fermi, Eine statistische Methode zur Bestimmung einiger Eigenschaften des Atoms und ihre Anwendung auf die Theorie des periodischen Systems der Elemente, Zeitschrift Für Phys. 48 (1928) 73–79. https://doi.org/10.1007/BF01351576.

[9] P.A.M. Dirac, Note on Exchange Phenomena in the Thomas Atom, Math. Proc. Cambridge Philos. Soc. 26 (1930) 376–385. https://doi.org/10.1017/S0305004100016108.

[10] E. Wigner, On the interaction of electrons in metals, Phys. Rev. 46 (1934) 1002–1011. https://doi.org/10.1103/PhysRev.46.1002.

[11] P. Hohenberg, W. Kohn, Inhomogeneous electron gas, Phys. Rev. 136 (1964) B864. https://doi.org/10.1103/PHYSREV.136.B864/FIGURE/1/THUMB.

[12] W. Kohn, L.J. Sham, Self-consistent equations including exchange and correlation effects, Phys. Rev. 140 (1965) A1133. https://doi.org/10.1103/PHYSREV.140.A1133/FIGURE/1/THUMB.

[13] G. Kresse, J. Furthmüller, Efficient iterative schemes for *ab initio* total-energy calculations using a plane-wave basis set, Phys. Rev. B. 54 (1996) 11169. https://doi.org/10.1103/PhysRevB.54.11169.

[14] U. Von Barth, L. Hedin, A local exchange-correlation potential for the spin polarized case. I, J. Phys. C Solid State Phys. 5 (1972) 1629–1642. https://doi.org/10.1088/0022-3719/5/13/012.

[15] O. Gunnarsson, B.I. Lundqvist, Exchange and correlation in atoms, molecules, and solids by the spin-density-functional formalism, Phys. Rev. B. 13 (1976) 4274. https://doi.org/10.1103/PhysRevB.13.4274.

[16] S.H. Vosko, L. Wilk, M. Nusair, Accurate spin-dependent electron liquid correlation energies for local spin density calculations: a critical analysis, Can. J. Phys. 58 (1980) 1200–1211. https://doi.org/10.1139/p80-159.

[17] J.P. Perdew, A. Zunger, Self-interaction correction to density-functional approximations for many-electron systems, Phys. Rev. B. 23 (1981) 5048–5079. https://doi.org/10.1103/PhysRevB.23.5048.

[18] J.P. Perdew, Density-functional approximation for the correlation energy of the inhomogeneous electron gas, Phys. Rev. B. 33 (1986) 8822. https://doi.org/10.1103/PhysRevB.33.8822.

[19] A.D. Becke, Density-functional exchange-energy approximation with correct asymptotic behavior, Phys. Rev. A. 38 (1988) 3098. https://doi.org/10.1103/PhysRevA.38.3098.

[20] J.P. Perdew, Y. Wang, Accurate and simple analytic representation of the electron-gas correlation energy, Phys. Rev. B. 45 (1992) 13244. https://doi.org/10.1103/PhysRevB.45.13244.

[21] J.P. Perdew, K. Burke, M. Ernzerhof, Generalized gradient approximation made simple, Phys. Rev. Lett. 77 (1996) 3865–3868. https://doi.org/10.1103/PhysRevLett.77.3865.

[22] J.P. Perdew, A. Ruzsinszky, G.I. Csonka, O.A. Vydrov, G.E. Scuseria, L.A. Constantin, X. Zhou, K. Burke, Restoring the density-gradient expansion for exchange in solids and surfaces, Phys. Rev. Lett. 100 (2008) 1–4. https://doi.org/10.1103/PhysRevLett.100.136406.

[23] Z. Wu, R.E. Cohen, More accurate generalized gradient approximation for solids, Phys. Rev. B - Condens. Matter Mater. Phys. 73 (2006). https://doi.org/10.1103/PhysRevB.73.235116.

Chapter II

Plane Waves and Pseudopotential Method

Chapter II: Plane Waves and Pseudopotential Method

II.1 Introduction

The first chapter shows the transition from a multi-body problem (The multi-electronic Schrödinger equation) to a one-body problem (The Kohn-Sham mono-particle equations) using the density functional theory.

In order to simplify the resolution of the Kohn-Sham equations, it is necessary to make other technical approximations, it is essentially the choice of implementations that describe the basic nature (potential and orbitals).

In this chapter, we are only interested in the description of two approximations available in our computational code (CASTEP), which allowed us to calculate the physical properties of herein studied crystals. A plane waves basis to describe the wave functions (i.e., the orbitals), and a pseudo-approach characterizing the potential. These approximations are usually coupled together in a single approach known as the plane wave Pseudopotential method (PP-PW).

II.2 Plane waves

II.2.1 The theorem of Bloch

In 1928, the Swiss-American physicist Felix Bloch proposed wave functions describing the quantum states of electrons subjected to a periodic potential such that in the crystalline solid [1]. These wave functions often called Bloch waves $\boldsymbol{\psi}_{\boldsymbol{n},\vec{\boldsymbol{k}}}(\vec{\boldsymbol{r}})$ which are the solutions of the time independent Schrödinger equation, where written as a product of a plane wave $\boldsymbol{e}^{\boldsymbol{i}\,\vec{\boldsymbol{k}}\,\vec{\boldsymbol{r}}}$ by a function $\boldsymbol{f}_{\boldsymbol{n},\vec{\boldsymbol{k}}}(\vec{\boldsymbol{r}})$ having the periodicity of the crystal lattice:

$$\boldsymbol{\psi}_{\boldsymbol{n},\vec{\boldsymbol{k}}}(\vec{\boldsymbol{r}}) = \boldsymbol{f}_{\boldsymbol{n},\vec{\boldsymbol{k}}}(\vec{\boldsymbol{r}})\boldsymbol{e}^{\boldsymbol{i}\,\vec{\boldsymbol{k}}\,\vec{\boldsymbol{r}}} \qquad \textbf{(II.1)}$$

Where $\vec{\boldsymbol{k}}$ is a wave vector of reciprocal space confined in the first Brillouin zone[1], the subscript $\boldsymbol{n}$ is the band index having discrete values, which is present because there are different wave functions with the same wave vector $\vec{\boldsymbol{k}}$, and $\boldsymbol{f}_{\boldsymbol{n},\vec{\boldsymbol{k}}}(\vec{\boldsymbol{r}})$ is a function of period $\boldsymbol{R}$ i.e:

---

1 Brillouin zone is a symmetric primitive cell in wave vector space, which has all the symmetries of the point group of the reciprocal lattice.

$$f_{n,\vec{k}}(\vec{r}) = f_{n,\vec{k}}(\vec{r} + \vec{R}) \quad \textbf{(II.2)}$$

The vector $\vec{R}$ is the translation vector of the direct lattice (Bravais lattice). The periodic function $f_{n,\vec{k}}(\vec{r})$ can be decomposed by Fourier transform on a plane wave basis of reciprocal lattice wave vectors $\vec{K}$:

$$f_n(\vec{r}) = \sum_{\vec{K}} C_{n,\vec{K}} e^{i\,\vec{K}\,\vec{r}} \quad \textbf{(II.3)}$$

Thus, the wave functions can be written as a sum of plane waves:

$$\psi_{n,\vec{k}}(\vec{r}) = \sum_{\vec{K}} C_{n,(\vec{K}+\vec{k})} e^{i\,(\vec{K}+\vec{k})\,\vec{r}} \quad \textbf{(II.4)}$$

From this equation, the only unknowns remaining to be determined are the Fourier coefficients $C_{n,(\vec{K}+\vec{k})}$. Furthermore, the indices $\vec{k}$ and $\vec{K}$ (The plane wave vector and the reciprocal lattice vector, respectively) have an infinity number in the Brillouin zone, which makes the problem of an infinity number of plane waves that reproduce the ground-state of a system.

The large number problem of $\vec{k}$ is fixed by the operation of sampling the Brillouin zone, and the infinity number problem of $\vec{K}$ is solved by verifying the condition of the cut-off energy.

II.2.2 Sampling the Brillouin Zone

Among the steps followed to solve the Kohn-Sham equations, evaluate the electron density, and achieve the convergence is the diagonalization of the Hamiltonian in order to determine the eigenstates (wave functions), but the number of this latter is infinitely large, due to the large number of the plane wave vector $\vec{k}$ in the Brillouin zone. To overcome this problem, it is possible to perform the calculation by sampling the Brillouin zone into specific sets of k points.

In order to reach a limit number of points k, the crystalline solid must be reduced to a supercell, and transformed it into the reciprocal lattice containing the first Brillouin zone characterized by the plane wave vector $\vec{k}$. By symmetry operation, the first Brillouin zone will be reduced to an irreducible Brillouin zone. Finally, this irreducible Brillouin zone will be sampled at a number of points k.

Therefore, *k*-points sampling consists of dividing the irreducible Brillouin zone into small volumes to perform the integration numerically. Different methods have been proposed to carry out the integration in the Brillouin zone such as the methods of: Joannopoulos-Cohen introduced by John D. Joannopoulos and Marvin L. Cohen in 1972 [2], Chadi-Kohn developed by D. J. Chadi and Marvin L. Cohen in 1973 [3], Monkhorst-Pack announced by Hendrik J. Monkhorst and James D. Pack in 1976 [4], and Evarestov-Smirnov proposed by R. A. Evarestov and V. P. Smirnov in 1983 [5].

For our calculations, we used the Monkhorst-Pack method, which is the most popular sampling approach. This method consists in establishing a sampling in the three directions $(\vec{k_1} \wedge \vec{k_2}).\vec{k_3}$ from the space of the Brillouin zone. The increase in the number of *k*-points makes the calculation more precise, but very long and it requires more powerful and efficient computer equipment.

II.2.3 The cut-off Energy

The plane wave basis is purely mathematical, usually used in ab initio calculations. To solve the infinity number problem of $\vec{K}$ in the Brillouin zone, we only take into account the vectors which verify the following condition:

$$\frac{\hbar^2}{2m_e}\left|\vec{K} + \vec{k}\right|^2 \leq E_{cut} \qquad \textbf{(II.5)}$$

E_{cut} is the cut-off energy which represents the maximum energy of plane waves, which limits the infinity number of plane waves to a plane wave basis set having low kinetic energy, since they are more important than those with great kinetic energy.

The limitation of the plane wave basis leads to errors in the calculation of the total energy. The order of magnitude of this error can be reduced by increasing the value of the cut-off energy. In principle, the value of cut-off energy should be increased until the total energy converged, which means that the choice of E_{cut} determines the degree of accuracy of the calculation.

II.3 The pseudopotential approximation

In 1934, the German physicist Hans Gustav Adolf Hellmann introduced the pseudopotential, which he called "Zusatzpotential" i.e., additional potential [6]. Almost at the same time, the Italian physicist Enrico Fermi suggested the use of the pseudopotential approximation [7]. Since that time, many works established to develop the pseudopotential approximation to be a powerful approximation used in the ab-initio calculations today to simplify the description of complex systems.

The basic idea of the pseudopotential approximation consists in considering the electrons of strongly bonded cores as fixed charges, and one treats only the valence electrons since only the valence states take part in the atomic bonds and consequently in the majority of physical properties. Therefore, in the pseudopotential method the real Coulombic potential (The effective potential in Kohn-Sham equations $\boldsymbol{V_{eff}^{KS}(r) \sim Z/r}$) is replaced by a pseudopotential interacting only with the valence electrons $\boldsymbol{V^{ps}(r)}$, and the real wave functions of the valence electrons $\boldsymbol{\psi_i^v(r)}$ of energies $\boldsymbol{\varepsilon_i^v}$ are replaced by pseudo-wave functions $\boldsymbol{\psi_i^{ps}(r)}$. Finally, the Kohn-Sham equations can be written as the following form:

$$\left[-\frac{1}{2}\nabla_{r_i}^2 + V^{ps}(r)\right]\psi_i^{ps}(r) = \varepsilon_i^v\,\psi_i^{ps}(r) \qquad \textbf{(II.6)}$$

Practically, the pseudopotentials are constructed in such a way that beyond a certain cut-off radius $\boldsymbol{r_{cut}}$ defines a sphere inside which are located the core electrons. Therefore, the pseudopotential $\boldsymbol{V^{ps}(r)}$ and the pseudo-wave functions $\boldsymbol{\psi_i^{ps}(r)}$ must be identical to the real Coulombic potential $\boldsymbol{Z/r}$ and the real wave functions of the valence electrons $\boldsymbol{\psi_i^v(r)}$ outside the sphere of radius $\boldsymbol{r_{cut}}$, as showing in Figure II.1.

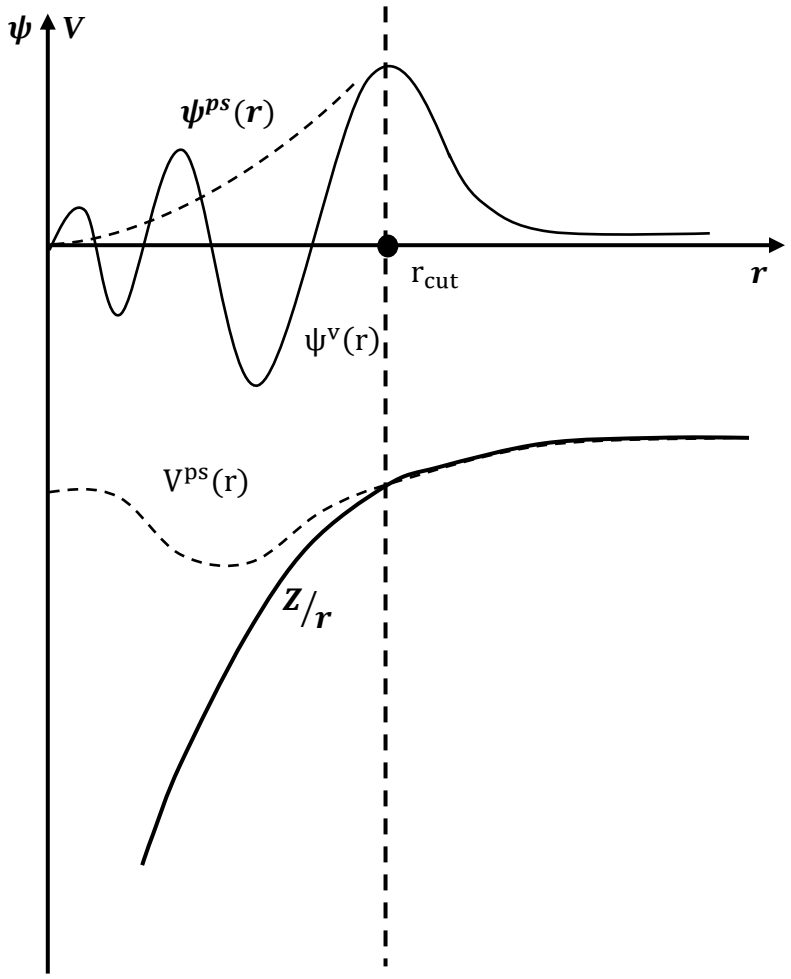

Figure II.1 The illustration of real Coulombic potential (solid lines) and pseudopotential (dashed lines), their corresponding wave functions, and the radius r_{cut} at which real and pseudo values are matched.

The pseudopotential approximation is of great interest in the theoretical calculation of the electronic structure of matter due to its simplification for solving the Kohn-Sham equations. the most popular used pseudopotentials in the ab-initio calculation are the Norm-conserving and the ultra-soft pseudopotentials.

II.3.1 The norm-conserving pseudopotentials

The approach of Norm-conserving pseudopotentials was introduced by D. R. Hamann, M. Schlüter, and C. Chiang in 1979 [8], which consists to make the electron density determined by the norm of real wave functions of valence electrons (i.e., $|\boldsymbol{\psi}_i^v(\boldsymbol{r})|^2$) and the electron density determined by the pseudo-wave functions $\boldsymbol{\psi}_i^{ps}(\boldsymbol{r})$ identical. This idea leads to define a set of criteria necessary for the construction of this type of pseudopotential, such are:

- The Eigenvalues of the energy corresponding to real wave functions must be identical to those corresponding to the pseudo-wave functions.

$$\boldsymbol{\varepsilon_i = \varepsilon_i^{ps}} \qquad \textbf{(II.7)}$$

- The real wave functions of the valence electrons must be identical to the pseudo-wave functions beyond a chosen cut-off radius (i.e., outside the core region).

$$\boldsymbol{\psi_i^v(r \geq r_{cut}) = \psi_i^{ps}(r \geq r_{cut})} \qquad \textbf{II.8)}$$

- Inside the core region, the real wave functions differ from the pseudo-wave functions, but they have the same norm, i.e., along $\boldsymbol{r_{cut}}$, the real valence electron density and the pseudo-electron density must be identical for each valence orbital, this is the conservation property of the norm.

$$\boldsymbol{\int_0^{r_c} |\psi_i^v(r)|^2 dr = \int_0^{r_c} \left|\psi_i^{ps}(r)\right|^2 dr} \qquad \textbf{(II.9)}$$

- Beyond the cut-off radius, the pseudopotential varies continuously, i.e., the logarithmic derivatives of the real wave functions and the pseudo-wave functions must be identical, as well as their derivatives with respect to energy.

This pseudopotential makes the calculations more precise due to its transferability, but it requires a large number of plane waves to describe the wave functions correctly, therefore a large cut-off energy and computation time.

II.3.2 The Ultra-Soft pseudopotentials

In 1990, the American physicist David Vanderbilt introduced another approximation of pseudopotential that reduces the number of plane waves, therefore reducing the cut-off energy [9]. In this approach, the norm-conservation property is ignored. On the other hand, the pseudo-wave functions are arbitrarily smoothed as much as possible in the core region, hence it is called ultra-soft pseudopotential.

To achieve this approximation, a larger cut-off radius $\boldsymbol{r}_{cut}$ than that of norm-conserving pseudopotentials is used. For this reason, a small number of plane waves is needed, which reduces the computation time and makes their convergence fast.

II.4 The used calculation code

Our calculations in this thesis were performed using the numerical modeling code CASTEP (*Cambridge Serial Total Energy Package*), which is part of a set of numerical simulation software named Materials Studio. The CASTEP program created by the condensed matter group of Cambridge university in 1989, and developed to be a first principles quantum mechanical code using to calculate the electronic structure [10,11].

CASTEP employs the Density Functional Theory (DFT) within the plane wave Pseudopotential method (PW-PP) to simulate many physical properties of large range materials including crystals, surfaces, molecules, and liquids.

The self-consistent method used in our calculation by CASTEP to solve the Kohn-Sham equations is the Broyden–Fletcher–Goldfarb–Shanno algorithm (BFGS) [12], and the pseudopotential approximation choice is the Ultra-Soft Pseudo-Potential Generated on the Fly (OTFG-USPP), which minimizes the error with respect to fully converged all-electron DFT calculations [13].

References

[1] F. Bloch, Über die Quantenmechanik der Elektronen in Kristallgittern, Zeitschrift Für Phys. 52 (1929) 555–600. https://doi.org/10.1007/BF01339455.

[2] J.D. Joannopoulos, M.L. Cohen, Electronic charge densities for ZnS in the wurtzite and zincblende structures, J. Phys. C Solid State Phys. 6 (1973) 1572. https://doi.org/10.1088/0022-3719/6/9/015.

[3] D.J. Chadi, M.L. Cohen, Special points in the brillouin zone, Phys. Rev. B. 8 (1973) 5747–5753. https://doi.org/10.1103/PhysRevB.8.5747.

[4] Hendrik J Monkhorst, J.D. Pack, Special points for Brillouin-zone integration Monkhorst and Pack, Phys. Rev. B. 13 (1976) 5188–5192. http://prb.aps.org/pdf/PRB/v13/i12/p5188_1.

[5] R.A. Evarestov, V.P. Smirnov, Special points of the brillouin zone and their use in the solid state theory, Phys. Status Solidi. 119 (1983) 9–40. https://doi.org/10.1002/pssb.2221190102.

[6] H. Hellmann, A new approximation method in the problem of many electrons, J. Chem. Phys. 3 (1935) 61. https://doi.org/10.1063/1.1749559.

[7] E. Fermi, Sopra lo Spostamento per Pressione delle Righe Elevate delle Serie Spettrali, Nuovo Cim. 11 (1934) 157–166. https://doi.org/10.1007/BF02959829.

[8] D.R. Hamann, M. Schlüter, C. Chiang, Norm-Conserving Pseudopotentials, Phys. Rev. Lett. 43 (1979) 1494–1497. https://doi.org/10.1103/PhysRevLett.43.1494.

[9] D. Vanderbilt, Soft self-consistent pseudopotentials in a generalized eigenvalue formalism, Phys. Rev. B. 41 (1990) 7892. https://doi.org/10.1103/PhysRevB.41.7892.

[10] M.C. Payne, M.P. Teter, D.C. Allan, T.A. Arias, J.D. Joannopoulos, Iterative minimization techniques for *ab initio* total-energy calculations: molecular dynamics and conjugate gradients, Rev. Mod. Phys. 64 (1992) 1045. https://doi.org/10.1103/RevModPhys.64.1045.

[11] S.J. Clark, M.D. Segall, C.J. Pickard, P.J. Hasnip, M.I.J. Probert, K. Refson, M.C. Payne, First principles methods using CASTEP, Zeitschrift Fur Krist. 220 (2005) 567–570. https://doi.org/10.1524/zkri.220.5.567.65075.

[12] J.D. Head, M.C. Zerner, A Broyden-Fletcher-Goldfarb-Shanno optimization procedure for molecular geometries, Chem. Phys. Lett. 122 (1985) 264–270. https://doi.org/10.1016/0009-2614(85)80574-1.

[13] K. Lejaeghere, V. Van Speybroeck, G. Van Oost, S. Cottenier, Error estimates for solid-state density-functional theory predictions: An overview by means of the ground-state elemental crystals, Crit. Rev. Solid State Mater. Sci. 39 (2014) 1–24. https://doi.org/10.1080/10408436.2013.772503.

Chapter III

Study of the physical properties of $ABrF_4$ (A= Na, K, and Rb)

Chapter III: Study of the physical properties of $ABrF_4$ (A= Na, K, and Rb)

III.1 Introduction

The alkali metal tetrafluoridobromates are a motivating category belonging to the alkali metal complex fluorides family, which are inherently centrosymmetric and favorable for optoelectronic technologies, viz., for manufacturing ultra-violet optical components to generate long-wavelength radiation, optical amplifiers, and diode-pumped lasers, etc. [1,2].

The ternary compound of alkali metal tetrafluoridobromate with the general formula $ABrF_4$ consists of sharing one of the alkali elements (A= Na, K, Rb, and Cs) as a cation with BrF_4 anion. Since the 1950s, several attempts have been carried out to determine the crystal structure of $ABrF_4$ (A=Na, K, Rb, and Cs) ternary compounds. During the past century, all syntheses on these crystals executed using powder X-ray diffraction data and powder neutron diffraction data [3–7], have been agreeing that $NaBrF_4$, $KBrF_4$, $RbBrF_4$, and $CsBrF_4$ crystallize in tetragonal space group type I4/mcm (No. 140). While the fractional coordinates of the atoms, the anisotropic displacement parameters, and the standard uncertainties are still vague.

In the recent few years, various experimental methods supported by theoretical calculations have been performed to investigate the synthesis and characterization with higher precision. Ivlev et al. (2016) [8] done the first refinement of the crystal structure of $NaBrF_4$ using single-crystal X-ray diffraction data and indicate that Na, Br, and F atoms are located in the Wyckoff sites 4a (0 , 0 , 1/4), 4d (1/2 , 0 , 0) and 16l (0.33524 , 0.16476 , 0.13080), respectively. They reinforced also this study using of powder X-ray diffraction data, Raman and Infrared spectroscopy, and theoretical studies using first-principles calculations based on the density functional theory (DFT) within the generalized gradient approximation (GGA) and local density approximation (LDA). Subsequently, Ivlev and Kraus (2018) [9] redetermined the crystal structure of $KBrF_4$ from single-crystal X-ray diffraction data, where suggest that K, Br, and F atoms occupy the Wyckoff sites 4a (1/2, 1/2, 1/4), 4d (1/2,0,1/2) and 16l (0.65508, 0.15508, 0.37889), respectively. The same principle was carried out on the $RbBrF_4$ compound in two successive publications, where Ivlev et al. (2015) [10] revisited this compound by powder X-ray diffraction data, also using of Infrared and Raman spectroscopy, as well as theoretical calculations based on hybrid density functional method. Whereas Malin et al. (2019) [11],

performed the first determination of the crystal structure of $RbBrF_4$ based on single-crystal X-ray diffraction data, which the authors confirmed that the Wyckoff positions regarding Rb, Br, and F atoms, respectively are 4a (1/2, 1/2, 3/4), 4d (1/2, 0,1/2) and 16l (0.6501, 0.1501, 0.61660).

Recently, research has demonstrated that $CsBrF_4$ crystallizes in orthorhombic structure space group type Immm (No. 71), rather than the tetragonal structure, where Ivlev et al. (2013) [12] executed the synthesis of $CsBrF_4$ crystal using powder X-ray diffraction data process, whereas Malin et al. (2020) [13] has been done the redetermination of this crystal structure using single-crystal X-ray diffraction data to improve the results of the fractional coordinates of the atoms and the anisotropic displacement parameters with high precision.

Due to the high content of bromine trifluoride BrF_3 in these crystals and their chemical characteristics, which makes them useful fluorinating oxidizers in different fields of chemical technologies [14–19]. It is significant to emphasize that until now, neither the experimental studies nor the theoretical calculations were published regarding the fundamental physical properties of these compounds, such as mechanical, electronic, and optical properties, which motivates us to investigate these properties and remove the theoretical lacking of the alkali metal tetrafluoridobromates that crystallize in tetragonal structure (i.e., $NaBrF_4$, $KBrF_4$, and $RbBrF_4$).

III.2 Calculation methods

All first-principle calculations were performed within the framework of the density functional theory (DFT) using the Cambridge Serial Total Energy Package (CASTEP) code based on the plane-wave pseudo-potential (PP-PW) method [20]. The electronic exchange potential was described using the generalized gradient approximation (GGA) with the Perdew-Burke-Ernzerhof (PBE-sol) exchange-correlation function developed especially for solids [21]. The pseudo-atomic calculations were performed as the valence electron structures $5s^1$ for Rb, $4s^1$ for K, $3s^1$ for Na, $4s^2\ 4p^5$ for Br and $2s^2\ 2p^5$ for F.

The plane-wave basis set cut-off energy was 60 Ry and the Brillouin zone (BZ) sampling with 4×4×2 mesh of Monkhorst-Pack special *k*-points [22], which corresponds to three irreducible points in the first BZ. The self-consistent convergence of the total energy change 2×10^{-5} eV/atom, the maximum force is 0.05 eV/Å, the maximum stress within 0.1 GPa, and the maximum atom displacement within 0.002 Å.

III.3 Results and discussion

III.3.1 Structural properties

$NaBrF_4$, $KBrF_4$, and $RbBrF_4$ compounds crystallize at ambient conditions in the tetragonal structure with the space group I4/mcm (No. 140), where the conventional cell contains four formula units (Z=4) in which F, Br, and the alkali atoms are predicted experimentally to positioned at the Wyckoff sites given in Table III.1.

Table III.1 The experimental values of the atom positions in Wyckoff sites of $ABrF_4$ (A = Na, K and Rb) ternary compounds.

	$NaBrF_4$	**$KBrF_4$**	**$RbBrF_4$**
Alkali atom	**4a (0, 0, 1/4)[a,b]**	**4c (0, 0, 0)[c]**	**4c (0, 0, 0)[g]**
		4a (0, 0, 1/4)[d,e]	**4a (0, 0, 1/4)[h]**
		4a (1/2, 1/2, 1/4)[f]	**4a (1/2, 1/2, 3/4)[i]**
Br	**4d (1/2, 0, 0) [a,b]**	**4b (0, 1/2, 1/4)[c]**	**4d (0, 1/2, 0)[g,h]**
		4d (0, 1/2, 0)[d,e]	**4d (1/2, 0, 1/2)[i]**
		4d (1/2, 0, 1/2)[f]	
F	**16l (0.6633, -0.1633, 0.1299)[a]**	**16l (0.161, 0.661, 0.147)[c]**	**16l (0.1490, -0.3510, 0.1162)[g]**
	16l (0.33524, 0.16476, 0.13080)[b]	**16l (0.152, 0.652, 0.880)[d]**	**16l (0.151, -0.349, 0.1193)[h]**
		16l (0.152, 0.652, 0.121)[e]	**16l (0.6501, 0.1501, 0.61660)[i]**
		16l (0.65508, 0.15508, 0.37889)[f]	

Note: The experimental values mean by:

- Powder X-ray diffraction data: [a]Ref.8, [c]Ref.3, [d]Ref.4, [g]Ref.7, [h]Ref.10.
- Powder neutron diffraction data: [e]Ref.5.
- Single crystal X-ray diffraction data: [b]Ref.8, [f]Ref.9, [i]Ref.11.

To determine the equilibrium structural parameters including the lattice parameters (***a*** and ***c***), the internal coordinates of Fluorine atom (x_F, y_F, and z_F), and the inter-atomic distances, we have used the latest experimental parameters obtained by single-crystal X-ray diffraction data to build the initial crystal structure, then both ***c/a*** ratio and the internal coordinates x_F, y_F and z_F are relaxed for each volume. The conventional cell of $NaBrF_4$ is illustrated in Figure III.1. as a prototype for the herein studied compounds, where the $[BrF_4]^-$ anion shows the square-planar structure and the coordination of the cation element by F atoms is a square anti-prismatic polyhedron. Table III.2. mentions the calculated results for the ground states parameters such as the lattice constants ***a*** and ***c*** (in angström), the tetragonal ratio ***c/a***, the internal coordinates x_F, y_F, and z_F, the bond lengths that connect the Fluorine atom to other elements "***Br–F*** and ***A–F*** (in angström)", the values of minimum and maximum angle ***F-Br-F*** (in degree), the Bulk modulus B_0 (in GPa) and the Bulk modulus pressure derivative B_0' for the studied ternary compounds using GGA PBE-sol approximation along with the experimental data, as well as the other theoretical calculations for comparison.

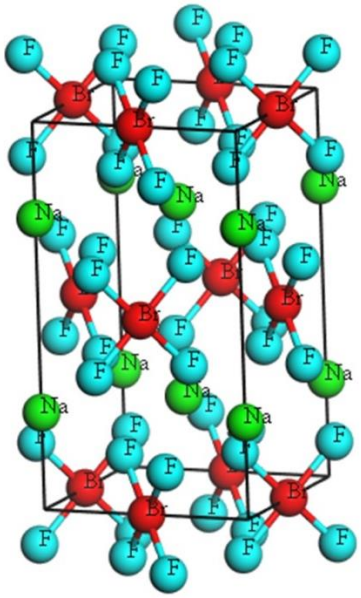

Figure III.1 The conventional cell of $NaBrF_4$ ternary compound.

Table III.2 The ground states structural parameters of $ABrF_4$ (A = Na, K and Rb).

Compounds	Parameters	Present work	Other calculations	Experimental works
$NaBrF_4$	*A*	5.7814	5.546[d], 5.788[e]	5.762[a], 5.7848[b], 5.7239[c]
	C	10.4294	10.09[d], 10.44[e]	10.327[a], 10.400[b], 10.331[c]
	c/a	1.8039	1.8193[d], 1.8037[e]	1.7922[a], 1.7978[b], 1.8048[c]
	x_F	0.33452	/	0.6633[b], 0.33524[c]
	y_F	0.16548	/	–0.1633[b], 0.16476[c]
	z_F	0.13140	/	0.1299[b], 0.13080[c]
	Br–F	1.926	1.909[d], 1.933[e]	1.90[b], 1.899[c]
	Na–F	2.4871	2.362[d], 2.487[e]	2.499[b], 2.4674[c]
	F–Br–F#1	89.265	88.6[d], 89.2[e]	89.4[b], 89.25[c]
	F–Br–F#2	90.735	91.4[d], 90.8[e]	90.6[b], 90.75[c]
	B_0	28.09621	/	/
	B'_0	6.89523	/	/
$KBrF_4$	*A*	6.1769	/	6.192[a], 6.162[f], 6.174[g], 6.17[h], 6.0999[i]
	C	11.1626	/	11.108[a],11.081[f], 11.103[g], 11.1[h], 11.0509[i]
	c/a	1.8071	/	1.7939[a],1.7982[f], 1.7983[g], 1.7990[h], 1.8116[i]
	x_F	0.65585	/	0.161[f], 0.152[g], 0.152[h], 0.65508[i]
	y_F	0.15585	/	0.661[f], 0.652[g], 0.652[h], 0.15508[i]
	z_F	0.37835	/	0.147[f], 0.880[g], 0.121[h], 0.37889[i]
	Br–F	1.9229	/	1.81[f], 1.88[g], 1.89[h], 1.8924[i]
	K–F	2.7384	/	2.84[f], 2.75[g], 2.77[h], 2.7112[i]
	F–Br–F#1	90.15	/	89.1[h], 89.98[i]
	F–Br–F#2	89.85	/	90.9[h], 90.02[i]
	B_0	20.42155	/	/
	B'_0	6.42551	/	/
$RbBrF_4$	*A*	6.3895	6.20[m], 6.94[n]	6.401[a], 6.351[j], 6.37181[k], 6.2991[l]
	C	11.5819	11.74[m], 8.93[n]	11.1538[a], 11.489[j], 11.4934[k], 11.4659[l]
	c/a	1.8126	1.8935[m], 1.2867[n]	1.7425[a], 1.8090[j], 1.8037[k], 1.8202[l]
	x_F	0.6508	0.154[m], 0.1458[n]	0.1490[j], 0.151[k], 0.6501[l]
	y_F	0.1508	-0.346[m], -0.3542[n]	-0.3510[j], -0.349[k], 0.1501[l]
	z_F	0.6171	0.1145[m], 0.1411[n]	0.1162[j], 0.1193[k], 0.61660[l]
	Br–F	1.9225	1.91[m], 1.91[n]	1.8903[j], 1.932[k], 1.8905[l]
	Rb–F	2.8769	2.84[m], 2.94[n]	2.7653[j], 2.851[k], 2.8447[l]
	F–Br–F#1	90.28	89.7[m], 82.7[n]	89.861[j], 90.4[k], 90.01[l]
	F–Br–F#2	89.72	90.3[m], 97.3[n]	90.139[j], 89.6[k], 89.99[l]
	B_0	18.27326	/	/
	B'_0	6.75771	/	/

Note: [a]Ref.6, [b, c, d, e]Ref.8, [f]Ref.3, [g]Ref.4, [h]Ref.5, [i]Ref.9, [j]Ref.7, [k, m, n]Ref.10, [l]Ref.11

The calculated cell volumes $\boldsymbol{V}$ at fixed applied hydrostatic pressures in a [-2,2] GPa range with a step of 1 GPa and the associated total energies $\boldsymbol{E}$ were fitted to the following Birch-Murnaghan isothermal equation of states (EOS) [23], to obtain the bulk modulus $\boldsymbol{B_0}$ and its pressure derivative $\boldsymbol{B_0'}$, as shown in Figure III.2.

$$\boldsymbol{E(V) = E_0 + \frac{9V_0B_0}{16}\left\{\left[\left(\frac{V_0}{V}\right)^{\frac{2}{3}} - 1\right]^3 B_0' + \left[\left(\frac{V_0}{V}\right)^{\frac{2}{3}} - 1\right]^2 \left[6 - 4\left(\frac{V_0}{V}\right)^{\frac{2}{3}}\right]\right\}} \qquad \textbf{(III.1)}$$

Where $\boldsymbol{E_0}$ and $\boldsymbol{V_0}$ are the energy and volume at zero pressure, respectively. We can notice that there is an excellent agreement between our calculated results of the optimized structural parameters and the earlier experimental ones for all studied compounds, whereas the results obtained in this study are in good agreement with the available theoretical values except for the $NaBrF_4$ compound, which the authors took their experimental values obtained from single-crystal X-ray diffraction data, then optimized the structures by LDA and GGA PBE-sol approximations, contrary to $RbBrF_4$ when the theoretical calculations based on the experimental values obtained by powder X-ray diffraction data and treated by PBE0 hybrid density functional method. We note also the nonexistence of theoretical investigation for the $KBrF_4$ compound.

For $NaBrF_4$, $KBrF_4$ and $RbBrF_4$ compounds, the calculated lattice constants $\boldsymbol{a}$ and $\boldsymbol{c}$ as well as $\boldsymbol{c/a}$ ratio deviate from the measured ones by only (1.0046%, 0.9525%, 0.0499%), (1.2623%, 1.0108%, 0.2484%) and (1.4351%, 1.0117%, 0.4175%), respectively. These insignificant deviations confirm the validity of our performed calculations. Moreover, the lattice constants $\boldsymbol{a}$ and $\boldsymbol{c}$ and the bond lengths that connect the Fluorine atom F to the Alkali elements A increase when the A atom is replaced in the sequence Na→K→Rb in the $ABrF_4$ series. This trend can be justified by the increase of the atomic radii in the same sequence, when ($\boldsymbol{r^{Na}}$ = 1.90) < ($\boldsymbol{r^{K}}$ = 2.43) < ($\boldsymbol{r^{Rb}}$ = 2.65).

The ***F–Br–F#*** angles are defined as differing only slightly from 90° and their sum equal 180°, where our calculations have achieved with good coincidence to the experimental and theoretical studies. Furthermore, the bulk modulus calculated in this sub-section will be used later to confirm the reliability of our calculations by comparing it with the corresponding one in the next sub-section.

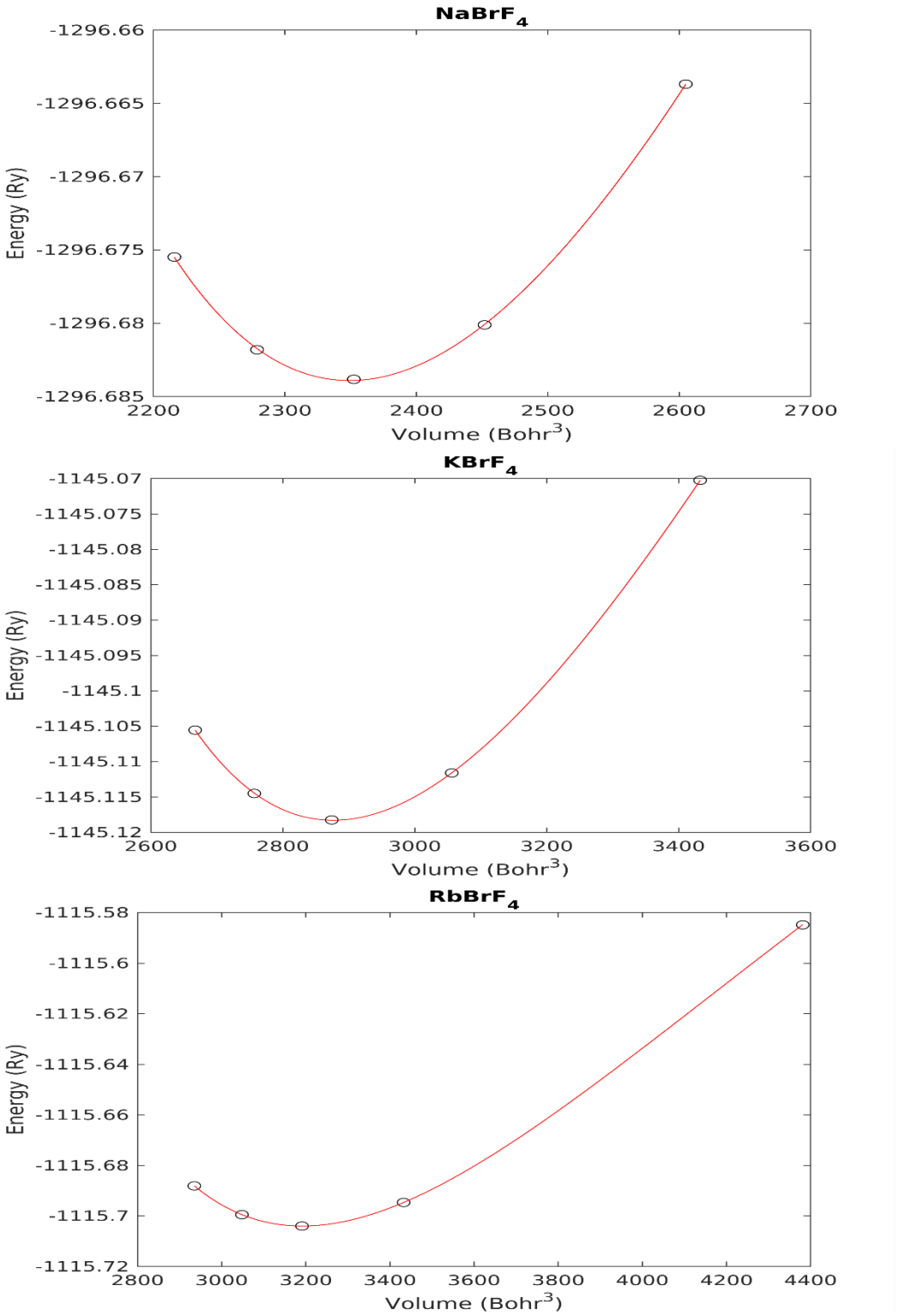

Figure III.2 The total energy versus cell volume data for $ABrF_4$ (A = Na, K, and Rb) compounds. The black circles are the calculated results and the red lines represent the $\boldsymbol{E(V)}$ Birch–Murnaghan EOS fits.

III.3.2 Mechanical properties

The examination of the elastic constants and the polycrystalline moduli of crystals have proved their eligibility to realize many mechanical properties such as stability, strength, stiffness, hardness, and brittleness or ductility behavior of materials and some other physical properties, such as inter-atomic potentials, phonon spectra and equation of state [24]. Usually, the elastic constants of polycrystalline materials depend on the elastic constants of the component single crystals, and to calculate the elastic constants of polycrystals, numerical simulations of the aggregate mass have been used, or have used some well-known approximations such as those of Voigt, Reuss and Hill [25].

Since the herein studied compounds crystallize within a tetragonal structure at ambient conditions, six elastic stiffness constants are considered ($\boldsymbol{C_{11}}$, $\boldsymbol{C_{12}}$, $\boldsymbol{C_{13}}$, $\boldsymbol{C_{33}}$, $\boldsymbol{C_{44}}$, and $\boldsymbol{C_{66}}$). The calculated elastic stiffness and compliance constants ($\boldsymbol{C_{ij}}$ and $\boldsymbol{S_{ij}}$) for $ABrF_4$ (A=Na, K and Rb) ternary compounds, are listed in Table III.3. These values can be considered as a reference for future research works because we note the absence of any previous data on the elastic constants in the literature for these studied materials.

According to the following four necessary and sufficient conditions for elastic stability in the tetragonal structures [26]: $\boldsymbol{C_{11} > |C_{12}|}$; $\boldsymbol{(C_{11} + C_{12})C_{33} > 2(C_{13})^2}$; $\boldsymbol{C_{44} > 0}$; $\boldsymbol{C_{66} > 0}$, the elastic Stiffness constants $\boldsymbol{C_{ij}}$ of the herein studied compounds as shown in Table III.3 confirm the previous mechanical stability conditions showing that $NaBrF_4$, $KBrF_4$, and $RbBrF_4$ compounds are mechanically stable. Moreover, this study has shown that all studied compounds have $\boldsymbol{C_{33} > C_{11}}$ where $\boldsymbol{(C_{33}/C_{11}) > 1}$ as indicate in Table III.3, which specifies that the bonding strength along **[001]** direction is stronger than the bonding strength along **[100]** and **[010]** directions. While $\boldsymbol{C_{66} > C_{44}}$ or $\boldsymbol{(C_{66}/C_{44}) > 1}$, which indicates that along **[100]** direction, the shear deformation in the plan **(001)** is more difficult than the corresponding one in the plan **(010)**.

Table III.3 The calculated values of the elastic stiffness constants C_{ij} (in GPa), the ratios C_{33}/C_{11} and C_{66}/C_{44}, the Cauchy pressures $[C_{12} - C_{66}]$ and $[C_{13} - C_{44}]$, and the elastic compliance constants S_{ij} (in 1/GPa) for $ABrF_4$ (A=Na, K and Rb) ternary compounds.

Compounds	$NaBrF_4$	$KBrF_4$	$RbBrF_4$
C_{11}	37.95067	25.94675	21.71127
C_{12}	26.55510	15.94402	12.68495
C_{13}	18.15587	13.96060	15.50370
C_{33}	57.82495	34.06575	33.23418
C_{44}	17.60895	10.26875	9.15633
C_{66}	22.36172	13.00377	9.80792
C_{33}/C_{11}	1.52	1.31	1.53
C_{66}/C_{44}	1.27	1.27	1.07
$C_{12} - C_{66}$	4.19	2.94	2.88
$C_{13} - C_{44}$	0.55	3.69	6.35
S_{11}	0.0532921	0.0664076	0.0804797
S_{12}	-0.0344613	-0.0335651	-0.0303074
S_{13}	-0.0059125	-0.0134593	-0.0234053
S_{33}	0.0210064	0.0403866	0.0519266
S_{44}	0.0567893	0.0973828	0.1092140
S_{66}	0.0447193	0.0769008	0.1019585

The polycrystalline moduli in our study have been calculated by using the Voigt [27] and Reuss [28] approximations. The bulk modulus $\boldsymbol{B}$ and shear modulus $\boldsymbol{G}$ can be evaluated by the obtained elastic Stiffness constants $\boldsymbol{C_{ij}}$ as follows [29]:

$$\boldsymbol{B_V = \frac{2(C_{11}+C_{12})+C_{33}+4C_{13}}{9}} \quad \textbf{(III.2)}$$

$$\boldsymbol{B_R = \frac{(C_{11}+C_{12})C_{33}-2C_{13}^2}{C_{11}+C_{12}+2C_{33}-4C_{13}}} \quad \textbf{(III.3)}$$

$$\boldsymbol{G_V = \frac{2C_{11}-C_{12}-2C_{13}+C_{33}+6C_{44}+3C_{66}}{15}} \quad \textbf{(III.4)}$$

$$\boldsymbol{G_R = \frac{15}{\frac{18B_V}{(C_{11}+C_{12})C_{33}-2C_{13}^2}+\frac{6}{(C_{11}-C_{12})}+\frac{6}{C_{44}}+\frac{3}{C_{66}}}} \quad \textbf{(III.5)}$$

In the above equations, the subscripts ($\boldsymbol{V}$ and $\boldsymbol{R}$) of bulk modulus and shear modulus indicate the Voigt approximation and Reuss approximation, respectively. According to the Hill approximation [30], the polycrystalline moduli (Bulk modulus $\boldsymbol{B}$, shear modulus $\boldsymbol{G}$, Young's modulus $\boldsymbol{E}$, Poisson's ratio $\boldsymbol{\nu}$, and Lamé's coefficients $\boldsymbol{\mu}$ and $\boldsymbol{\lambda}$) can be estimated by the following equations:

$$\boldsymbol{B = \frac{B_V+B_R}{2}} \quad \textbf{(III. 6)}$$

$$\boldsymbol{G = \frac{G_V+G_R}{2}} \quad \textbf{(III.7)}$$

$$\boldsymbol{E = \frac{9BG}{3B+G}} \quad \textbf{(III.8)}$$

$$\boldsymbol{\nu = \frac{3B-2G}{6B+2G}} \quad \textbf{(III.9)}$$

$$\boldsymbol{\mu = \frac{E}{2(1+\nu)}} \quad \textbf{(III.10)}$$

$$\boldsymbol{\lambda = \frac{\nu E}{(1+\nu)(1-2\nu)}} \quad \textbf{(III.11)}$$

The results of the mechanical properties of our studied compounds are listed in Table III.4. We can note the excellent agreement between the values of the bulk modulus $\boldsymbol{B}$ calculated from the elastic Stiffness constants $\boldsymbol{C_{ij}}$ as shown in Table III.4, and the corresponding ones $\boldsymbol{B_0}$ fitted to the Birch–Murnaghan EOS in the previous sub-section for all studied compounds. This consequence is good proof of the reliability of our calculation. On the other hand, the Bulk modulus value decreases when the alkali atom A is replaced in the following sequence Na→K→Rb in the $ABrF_4$ compounds, suggesting the increase in volume $\boldsymbol{V}$ of the considering compounds, which is in agreement with the Cohen's approximation $\boldsymbol{B \sim V^{-1}}$ [31].

Table III.4 The calculated values of Bulk modulus $\boldsymbol{B}$ (in GPa), shear modulus $\boldsymbol{G}$ (in GPa), Young modulus $\boldsymbol{E}$ (in GPa), Poisson ratio $\boldsymbol{\nu}$, Lamé's coefficients $\boldsymbol{\mu}$ and $\boldsymbol{\lambda}$, Pugh's ratio $\boldsymbol{B/G}$ and Vickers hardness $\boldsymbol{H_V}$ for $ABrF_4$ (A=Na, K and Rb) ternary compounds.

Compounds	**$NaBrF_4$**	**$KBrF_4$**	**$RbBrF_4$**
$\boldsymbol{B_V}$	**28.82888**	**19.29885**	**18.22682**
$\boldsymbol{B_R}$	**28.55676**	**19.14445**	**17.05031**
$\boldsymbol{G_V}$	**16.23989**	**9.51452**	**7.82174**
$\boldsymbol{G_R}$	**12.81612**	**8.57269**	**7.07155**
$\boldsymbol{B}$	**28.69282**	**19.22165**	**17.63857**
$\boldsymbol{G}$	**14.52800**	**9.04361**	**7.44664**
$\boldsymbol{E}$	**37.29029**	**23.45273**	**19.58395**
$\boldsymbol{\nu}$	**0.28339**	**0.29665**	**0.31495**
$\boldsymbol{\mu}$	**14.52804**	**9.04358**	**7.44665**
$\boldsymbol{\lambda}$	**19.00749**	**13.19258**	**12.67414**
$\boldsymbol{B/G}$	**1.9750**	**2.1254**	**2.3687**
$\boldsymbol{H_V}$	**2.1937**	**1.3656**	**1.1244**

The shear modulus $\boldsymbol{G}$ and the young modulus $\boldsymbol{E}$ are usually used to predict the rigidity of solids. Our obtained results indicate that $\boldsymbol{G}$ and $\boldsymbol{E}$ moduli decrease when moving from $NaBrF_4$ to $KBrF_4$ to $RbBrF_4$ which fundamentally originates from decrease $\boldsymbol{C_{44}}$ and indicating the diminution in the stiffness of these compounds in the same direction.

Several methods were developed to predict the mechanical nature of the material and classify it as brittle (fragile) or ductile (malleable). In this study, we have used the three most common methods to prove the reliability of our calculation. Pugh [32] has suggested an empirical relationship linking the bulk modulus $\boldsymbol{B}$ to the shear modulus $\boldsymbol{G}$, when the material is ductile the $\boldsymbol{B/G}$ ratio is greater than **1.75**; otherwise, the material is brittle. As shown in Table III.4, the values of $\boldsymbol{B/G}$ are larger than **1.75** for all herein studied compounds, which indicate their ductile nature. However, Frantsevich [33] proposed a rule regarding the value of Poisson's ratio $\boldsymbol{\nu}$. If $\boldsymbol{\nu > 0.26}$, the compound is classifying as malleable, while if $\boldsymbol{\nu < 0.26}$, the compound is considered fragile. Our calculated values of Poisson's ratio for $NaBrF_4$, $KBrF_4$, and $RbBrF_4$ compounds are larger than **0.26**, signalizing once more the ductile behavior of these compounds, which is good agreement with Pugh evaluation. Moreover, the criteria of the Cauchy [34] pressures $[\boldsymbol{C_{12} - C_{66}}]$ and $[\boldsymbol{C_{13} - C_{44}}]$ indicating the ductile particularity of the material when the two Cauchy pressures have positive values. As shown in Table III.3 the calculated elastic stiffness constants lead to positive values of Cauchy pressures for all studied compounds, which confirm once again that these compounds are mechanically ductile.

One of the usefulness of Poisson's ratio is to inform about the character of the chemical bonding. Regarding the covalent materials, the value of Poisson's ratio is small ($\boldsymbol{\nu \simeq 0.1}$), while for ionic materials it takes higher value ($\boldsymbol{\nu \simeq 0.25}$) [35]. As shown in Table III.4, the values of Poisson's ratio for all studied compounds are Close to **0.25**, suggesting the ionic character is present in their chemical bonding. Furthermore, the ionic crystals can be classified into two groups via the value of Poisson's ratio: central force crystals and non-central force crystals [36]. For central force crystals, the Poisson's ratio takes a value greater than **0.25** and less than **0.5**, whereas for non-central force crystals it equals **0.25** or **0.5** [37]. Since the calculated value of Poisson's ratio for $NaBrF_4$, $KBrF_4$ and $RbBrF_4$ are lying between the range of **0.25** to **0.50**, these compounds present central force.

The hardness of materials is a very important mechanical property in industrial applications, such as used to estimate the corrosion and strength in the machine parts manufacturing industries [38]. Numerous semi-empirical models have been established to calculate the hardness of materials. In this study, we have calculated the Vickers hardness $\boldsymbol{H_V}$ affirmed by Chen, which is linearly correlating with the shear modulus $\boldsymbol{G}$ [39] such as $\boldsymbol{H_V = 0.151\, G}$. The calculated values of Vickers hardness are listed in Table III.4. Which indicates that $NaBrF_4$ is the hardest material between the herein studied compounds.

The micro-cracks existing in the crystals are usually due to elastic anisotropy. Therefore, it is significant to estimate the elastic anisotropy in materials with a view to ameliorate their strength and perfect their structure to some extent [40]. In practical terms, every elastic single crystal is anisotropic [41]. In this case, it is worthy to predict theoretically the elastic anisotropy by using some anisotropy indexes, such as:

- The Universal anisotropy $\boldsymbol{A^U}$ which is valid to all types of elastic single crystals, as introduced and established by Shivakumar's work [41], based on bulk and shear moduli:

$$\boldsymbol{A^U = 5\frac{G_V}{G_R} + \frac{B_V}{B_R} - 6 \geq 0} \qquad \textbf{(III.12)}$$

- The percentage elastic anisotropy for compression $\boldsymbol{A_B}$ and shear $\boldsymbol{A_G}$, as given [40]:

$$\boldsymbol{A_B = \frac{B_V - B_R}{B_V + B_R}} \qquad \textbf{(III.13)}$$

$$\boldsymbol{A_G = \frac{G_V - G_R}{G_V + G_R}} \qquad \textbf{(III.14)}$$

In the relations mentioned above of $\boldsymbol{A^U}$, $\boldsymbol{A_B}$, and $\boldsymbol{A_G}$, the subscripts $\boldsymbol{V}$ and $\boldsymbol{R}$ refer to the Voigt and Reuss estimates, respectively. For an isotropic system, these elastic anisotropy indexes ($\boldsymbol{A^U}$, $\boldsymbol{A_B}$, and $\boldsymbol{A_G}$) take a value of zero, i.e. the magnitude of the deviation of these elastic anisotropy indexes from zero measures the degree of elastic anisotropy possessed by a crystal.

The shear anisotropic factors $\boldsymbol{A_1}$, $\boldsymbol{A_2}$, and $\boldsymbol{A_3}$ are based on the elastic stiffness constants $\boldsymbol{C_{ij}}$, which give an estimation of the degree of anisotropy in bonding between atoms in different crystallographic planes. Regarding the tetragonal structure, only the shear anisotropic factors along the shear planes **(100)** and **(001)** are sufficient and can be written as following [42]:

$$A_1 = A_{(100)} = \frac{4C_{44}}{C_{11}+C_{33}-C_{13}} \quad \textbf{(III.15)}$$

$$A_2 = A_{(001)} = \frac{2C_{66}}{C_{11}-C_{12}} \quad \textbf{(III.16)}$$

In the situation of an isotropic crystal, the shear anisotropic factors A_1 and A_2 must be equal to one, where each value greater or lesser than the unity is a measurement of the level of the mechanical anisotropy in the matter. In this study, these anisotropic indexes have been calculated and listed in Table III.5, which suggests that the elastic properties of the herein studied compounds are anisotropic. Moreover, from these calculated values, $NaBrF_4$ exhibits the highest universal anisotropic A^U than the other studied compounds, and we can notice that the percentage elastic anisotropy for shear modulus A_G is larger than the percentage elastic anisotropy for Bulk modulus A_B for all studied compounds, which indicates that the shear modulus appears more grounded directional reliance than the bulk modulus. On the other hand, the shear anisotropic factor A_2 along the shear plane **(001)** is greater than the shear anisotropic factor A_1 along the shear plane **(100)**, which principally result from the obtained stiffness elastic constants, where $C_{66} > C_{44}$, show the atomic bondings in the crystallographic plane **(001)** is more anisotropic than the corresponding ones lying on the crystallographic plane **(100)**.

Table III.5 Universal anisotropic index A^U, bulk (compression) and shear anisotropic A_B and A_G, shear anisotropic factors A_1 and A_2 for $ABrF_4$ (A=Na, K and Rb) ternary compounds.

Compounds	A^U	A_B	A_G	A_1	A_2
$NaBrF_4$	**1.34526**	**0.00474**	**0.11783**	**1.18451**	**3.92463**
$KBrF_4$	**0.55738**	**0.00402**	**0.05207**	**1.27994**	**2.60004**
$RbBrF_4$	**0.59943**	**0.03335**	**0.05037**	**1.53000**	**2.17318**

A precious design to check the anisotropy of mechanical properties is plotting the polycrystalline moduli in three-dimensional (*3D*) space based on the following mechanical moduli (Bulk modulus B, Young's modulus E, shear modulus G and Poisson's ratio ν) with directional dependence for a tetragonal structure, such as:

$$\boldsymbol{B = \frac{1}{S}} \quad \textbf{(III.17)}$$

$$\boldsymbol{E = \frac{1}{S'}} \quad \textbf{(III.18)}$$

$$\boldsymbol{G = \frac{3}{9S' - S}} \quad \textbf{(III.19)}$$

$$\boldsymbol{\nu = \frac{1}{2}\left(1 - \frac{S}{3S'}\right)} \quad \textbf{(III.20)}$$

Where:

$$\boldsymbol{S = (S_{11} + S_{12} + S_{13})\left(l_1^2 + l_2^2\right) + (2S_{13} + S_{33})l_3^2} \quad \textbf{(III.21)}$$

$$\boldsymbol{S' = S_{11}\left(l_1^4 + l_2^4\right) + (2S_{13} + S_{44})\left(l_1^2 l_3^2 + l_2^2 l_3^2\right) + S_{33} l_3^4 + (2S_{12} + S_{66}) l_1^2 l_2^2} \quad \textbf{(III.22)}$$

In the above relations, $\boldsymbol{S_{ij}}$ is the elastic compliance constants; $\boldsymbol{l_1}$, $\boldsymbol{l_2}$, and $\boldsymbol{l_3}$ refer the directional cosines to the ***x***, ***y***, and ***z*** axes within spherical coordinates, respectively. For the entire isotropy of any polycrystalline modulus previously mentioned, it takes a sphere form in the *3D* space, whereas the curvature from the appearance of the sphere detects the rate of anisotropy. As shown in Figure III.3, for all studied compounds, both young's and shear moduli present a stronger anisotropic degree than that illustrated in bulk modulus and Poisson's ratio. Furthermore, the highest degree of anisotropy for Bulk modulus and the lowest one for shear modulus is showing in the $RbBrF_4$ compound, which affirms the results given in Table III.5. In addition to that, for more distinguished the anisotropy of polycrystalline moduli in their crystallographic planes **(100)**, **(010)** and **(001)**. The projection of the shape of these moduli has been plotted into these planes and showed in Figure III.4. As shown in Figure III.4, the projections on **(010)** and **(100)** planes are identical, which is a consequence of the tetragonal structure of the herein studied compounds. We can confirm for all studied compounds that bulk modulus and Poisson's ratio show weaker anisotropic magnitude compared to that of young's and shear moduli, especially in the plane **(001)** where the bulk modulus appears the shape of the perfect circle. Regarding the shear modulus, it is clear that it showed more anisotropy in the plane **(001)** than in the **(100)** plane, which is reliable to the estimation found in Table III.5, where $\mathbf{A_{(001)} > A_{(100)}}$ for all studied compounds.

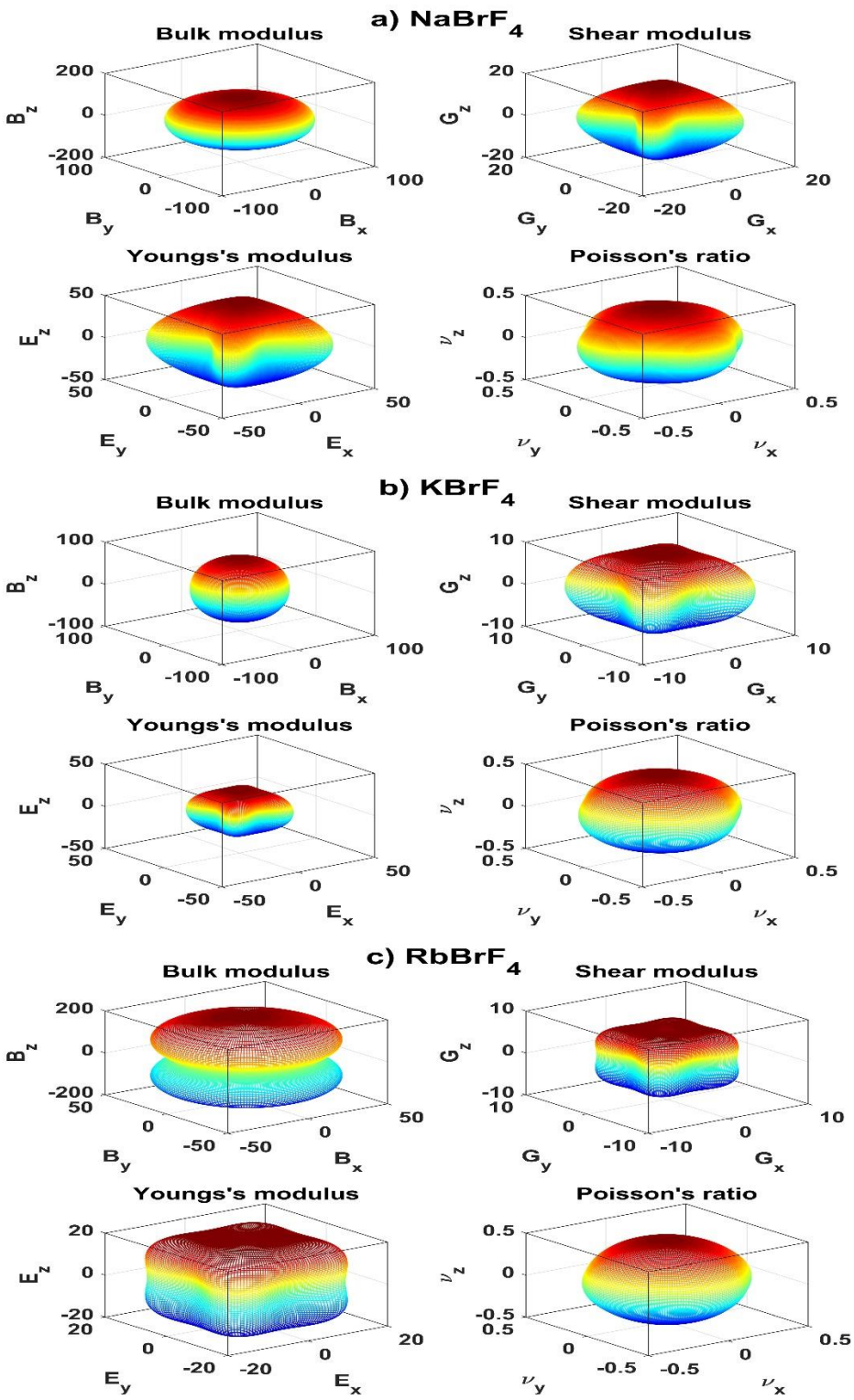

Figure III.3 A *3D* representation of Bulk modulus $\boldsymbol{B}$, shear modulus $\boldsymbol{G}$, Young's modulus $\boldsymbol{E}$ and Poisson's ratio $\boldsymbol{\nu}$ for $ABrF_4$ (A = Na, K and Rb) ternary compounds.

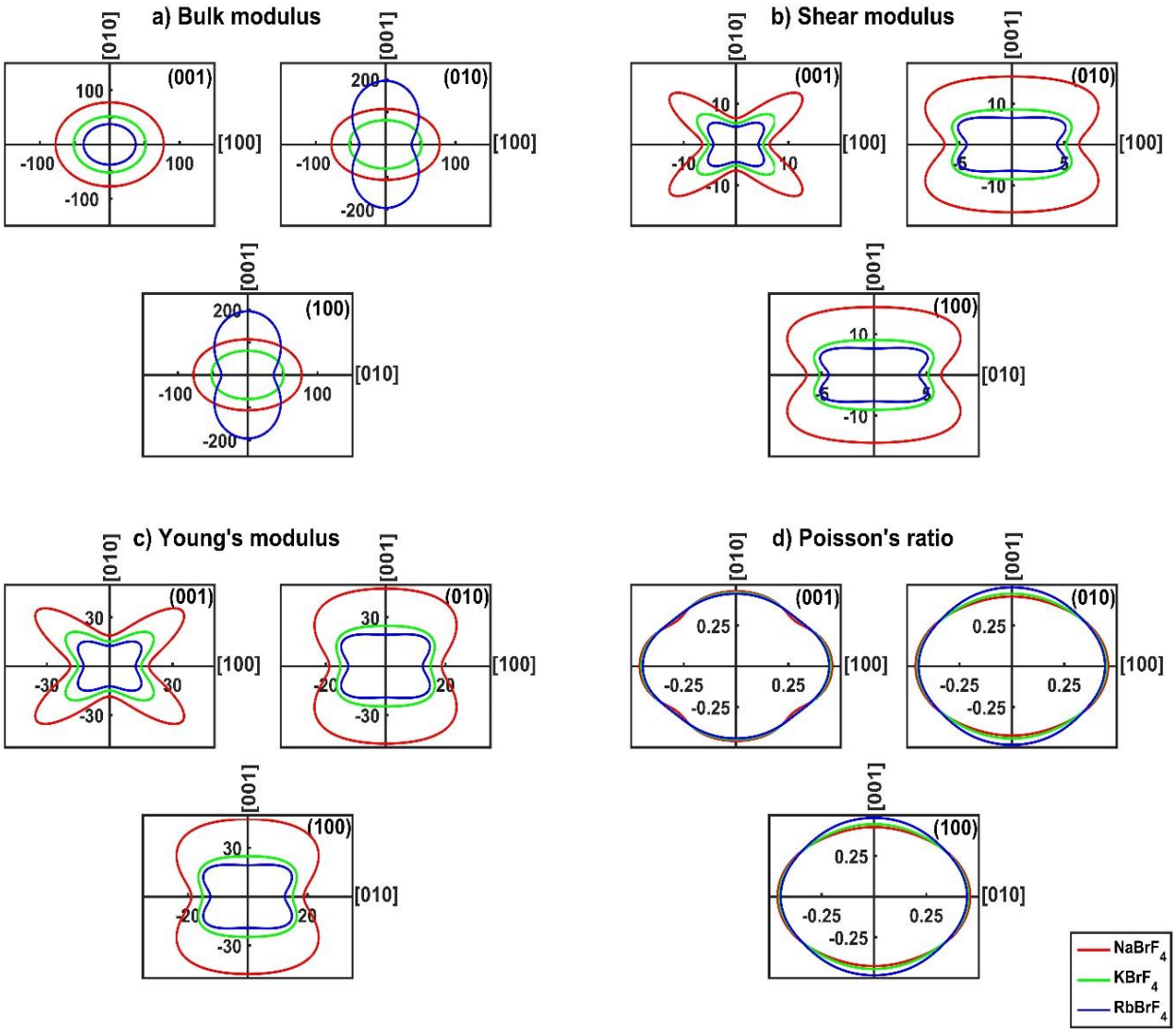

Figure III.4 The planar contours of Bulk modulus ***B***, shear modulus ***G***, Young's modulus ***E*** and Poisson's ratio ***ν*** for $ABrF_4$ (A = Na, K and Rb) ternary compounds are shown for **(001)**, **(010)** and **(100)** crystallographic planes.

The Debye temperature is a significant parameter of solids, Due to its direct correlation to the thermal conductivity, melting temperature, elastic constants, and polycrystalline moduli [43, 44]. Several empirical methods have been developed to calculate Debye temperature $\boldsymbol{\theta_D}$, where, the most common one is proportional to the averaged sound velocity $\boldsymbol{\nu_m}$, by the following equation [44]:

$$\boldsymbol{\theta_D} = \frac{\boldsymbol{h}}{\boldsymbol{k_B}}\left[\frac{3q}{4\pi}\left(\frac{N_A\rho}{M}\right)\right]^{\frac{1}{3}}\boldsymbol{\nu_m} \qquad \textbf{(III.23)}$$

Where $\boldsymbol{h}$ and $\boldsymbol{k_B}$ signify Plank's and Boltzmann's constants, respectively; $\boldsymbol{q}$ is the number of atoms in the unit cell, $\boldsymbol{N_A}$ is Avogadro's number, $\boldsymbol{\rho}$ is the density, $\boldsymbol{M}$ is the molecular weight of the solid, and $\boldsymbol{\nu_m}$ is the average sound velocity which given by:

$$\boldsymbol{\nu_m} = \left[\frac{1}{3}\left(\frac{2}{\nu_t^3} + \frac{1}{\nu_l^3}\right)\right]^{-\frac{1}{3}} \qquad \textbf{(III.24)}$$

Here, $\boldsymbol{\nu_l}$ and $\boldsymbol{\nu_t}$ are respectively the longitudinal and transverse sound velocity calculated from shear modulus $\boldsymbol{G}$, Bulk modulus $\boldsymbol{B}$, and the density $\boldsymbol{\rho}$ under Navier's relations :

$$\boldsymbol{\nu_l} = \left(\frac{B+\frac{4G}{3}}{\rho}\right)^{\frac{1}{2}} \qquad \textbf{(III.25)}$$

$$\boldsymbol{\nu_t} = \left(\frac{G}{\rho}\right)^{\frac{1}{2}} \qquad \textbf{(III.26)}$$

The calculated parameters, such as Debye temperature $\boldsymbol{\theta_D}$, the density $\boldsymbol{\rho}$, as well as the average, longitudinal and transverse sound velocity $\boldsymbol{\nu_m}$, $\boldsymbol{\nu_l}$ and $\boldsymbol{\nu_t}$, respectively are mentioned in Table III.6. Through the results obtained in Table III.6, among the herein studied compounds $NaBrF_4$ exhibits the highest Debye temperature, which implies the largest thermal conductivity and melting temperature, as well as the chemical bonding powerful in the crystal structure and higher hardness, which that in good agreement with our results obtained by calculating the Vickers hardness $\boldsymbol{H_V}$.

Table III.6 The elastic Debye temperature $\boldsymbol{\theta_D}$ (in K), the density $\boldsymbol{\rho}$, the average, longitudinal and transverse sound velocity $\boldsymbol{v_m}$, $\boldsymbol{v_l}$ and $\boldsymbol{v_t}$ (in m/s) for $ABrF_4$ (A=Na, K and Rb) ternary.

Compounds	θ_D	ρ	v_m	v_l	v_t
$NaBrF_4$	**278.13220**	**3.45366**	**2286.15330**	**3730.50832**	**2050.98882**
$KBrF_4$	**218.54463**	**3.05692**	**1920.39024**	**3198.82194**	**1720.00226**
$RbBrF_4$	**181.48469**	**3.42031**	**1651.29016**	**2839.0001**	**1475.52815**

Furthermore, we can be noted that the longitudinal sound velocities of all studied compounds are much faster than transverse sound velocities. In this reason and for deeper study of this phenomenon, the longitudinal and transverse sound velocities ($\boldsymbol{v_l}$ and $\boldsymbol{v_t}$, respectively) in the principal directions are calculated and listed in Table III.7 using Christoffel's equation [45] based on the elastic stiffness constants $\boldsymbol{C_{ij}}$ and the density $\boldsymbol{\rho}$ as follows:

For **[100]**:

$$\begin{cases} [\mathbf{100}]\boldsymbol{v_l} = \sqrt{\dfrac{C_{11}}{\rho}} \\ [\mathbf{001}]\boldsymbol{v_{t1}} = \sqrt{\dfrac{C_{44}}{\rho}} \\ [\mathbf{010}]\boldsymbol{v_{t2}} = \sqrt{\dfrac{C_{66}}{\rho}} \end{cases} \quad \textbf{(III.27)}$$

For **[001]**:

$$\begin{cases} [\mathbf{001}]\boldsymbol{v_l} = \sqrt{\dfrac{C_{33}}{\rho}} \\ [\mathbf{100}]\boldsymbol{v_{t1}} = [\mathbf{010}]\boldsymbol{v_{t2}} = \sqrt{\dfrac{C_{66}}{\rho}} \end{cases} \quad \textbf{(III.28)}$$

For **[110]**:

$$\begin{cases} [\mathbf{110}]\boldsymbol{v_l} = \sqrt{\dfrac{(C_{11}+C_{12}+2C_{66})}{2\rho}} \\ [\mathbf{001}]\boldsymbol{v_{t1}} = \sqrt{\dfrac{C_{44}}{\rho}} \\ [\mathbf{1\bar{1}0}]\boldsymbol{v_{t2}} = \sqrt{\dfrac{(C_{11}-C_{12})}{2\rho}} \end{cases} \quad \textbf{(III.29)}$$

Table III.7 The longitudinal and transverse sound velocities in the principal directions (in km/s) for $ABrF_4$ (A=Na, K and Rb) ternary compounds.

Compounds	**[100]**			**[001]**			**[110]**		
	$[100]\nu_l$	$[001]\nu_{t1}$	$[010]\nu_{t2}$	$[001]\nu_l$	$[100]\nu_{t1}$	$[010]\nu_{t2}$	$[110]\nu_l$	$[100]\nu_{t1}$	$[1\bar{1}0]\nu_{t2}$
$NaBrF_4$	**3.3149**	**2.2580**	**2.5446**	**4.0918**	**2.5446**	**2.5446**	**3.9766**	**2.2580**	**1.2844**
$KBrF_4$	**2.9134**	**1.8328**	**2.0625**	**3.3382**	**2.0625**	**2.0625**	**3.3325**	**1.8328**	**1.2791**
$RbBrF_4$	**2.5195**	**1.6362**	**1.6934**	**3.1172**	**1.6934**	**1.6934**	**2.8099**	**1.6362**	**1.1487**

It is evident that the $NaBrF_4$ compound with large elastic stiffness constants has the fastest sound velocities than the two other compounds. Furthermore, the longitudinal sound velocities of all studied compounds are the fastest along **[001]** principal direction. The anisotropic shown in sound velocities indicates one more elastic anisotropy for these compounds.

Since there are no previous experimental and theoretical data reported in the literature for $NaBrF_4$, $KBrF_4$, and $RbBrF_4$ ternary compounds, we can consider our results as the first prediction of their mechanical properties.

III.3.3 Electronic properties

As $ABrF_4$ (A=Na, K and Rb) compounds crystallize in the tetragonal structure with the space group I4/mcm, the Brillouin zone type is belonging to the Body Centered Tetragonal lattice Type 2 (BCT_2), as shown in Figure III.5 [46].

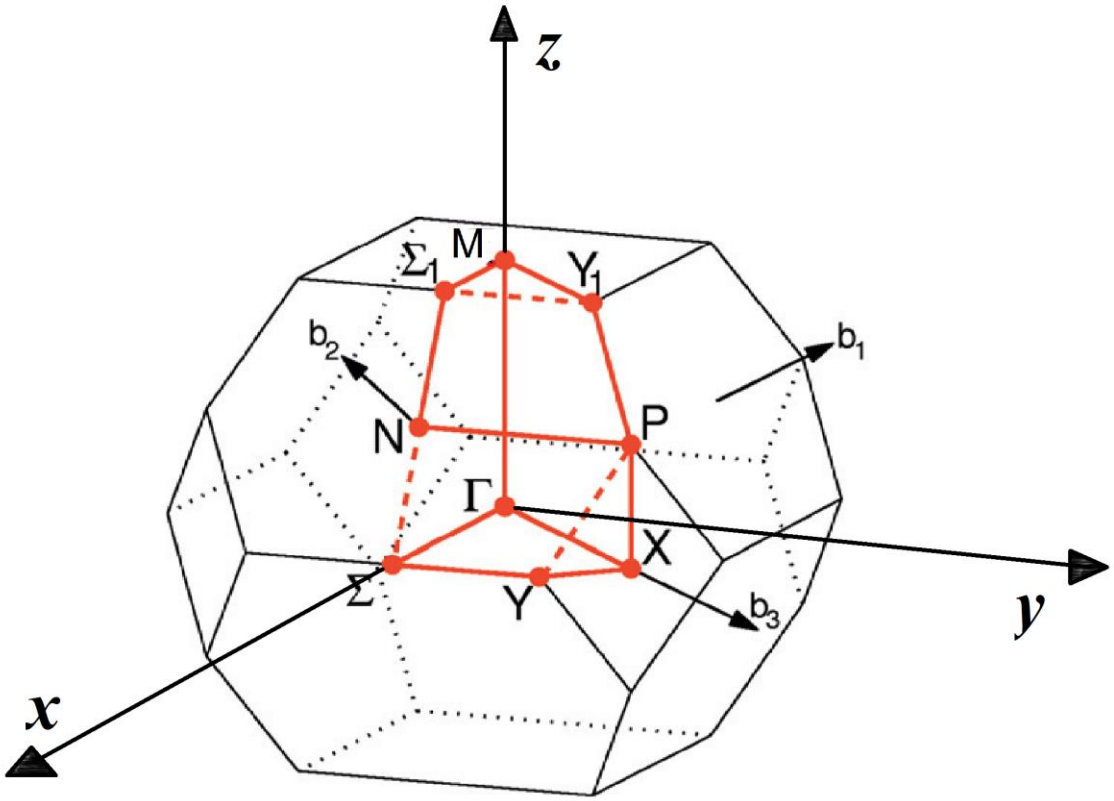

Figure III.5 The Brillouin zone of BCT_2 lattice.

The electronic band structures for our studied compounds are depicted on the left side of Figure III.6 along the Brillouin zone path **Γ-X-P-N-Γ-M**, where **Γ** is the center of the Brillouin zone, **X** is the center of the square face, **P** is the corner point joining three edges, **N** is the center of the face, and **M** is the center of the edge. The horizontal dashed line positioned at 0 eV clarifies the Fermi level ($\mathbf{E_F}$), where the highest energy of the valence band has been selected. The Enlarged view of the band structure around both the maximum of the valence band (VBM) and the minimum of the conduction band (CBM) have been plotted on the right side of Figure III.6.

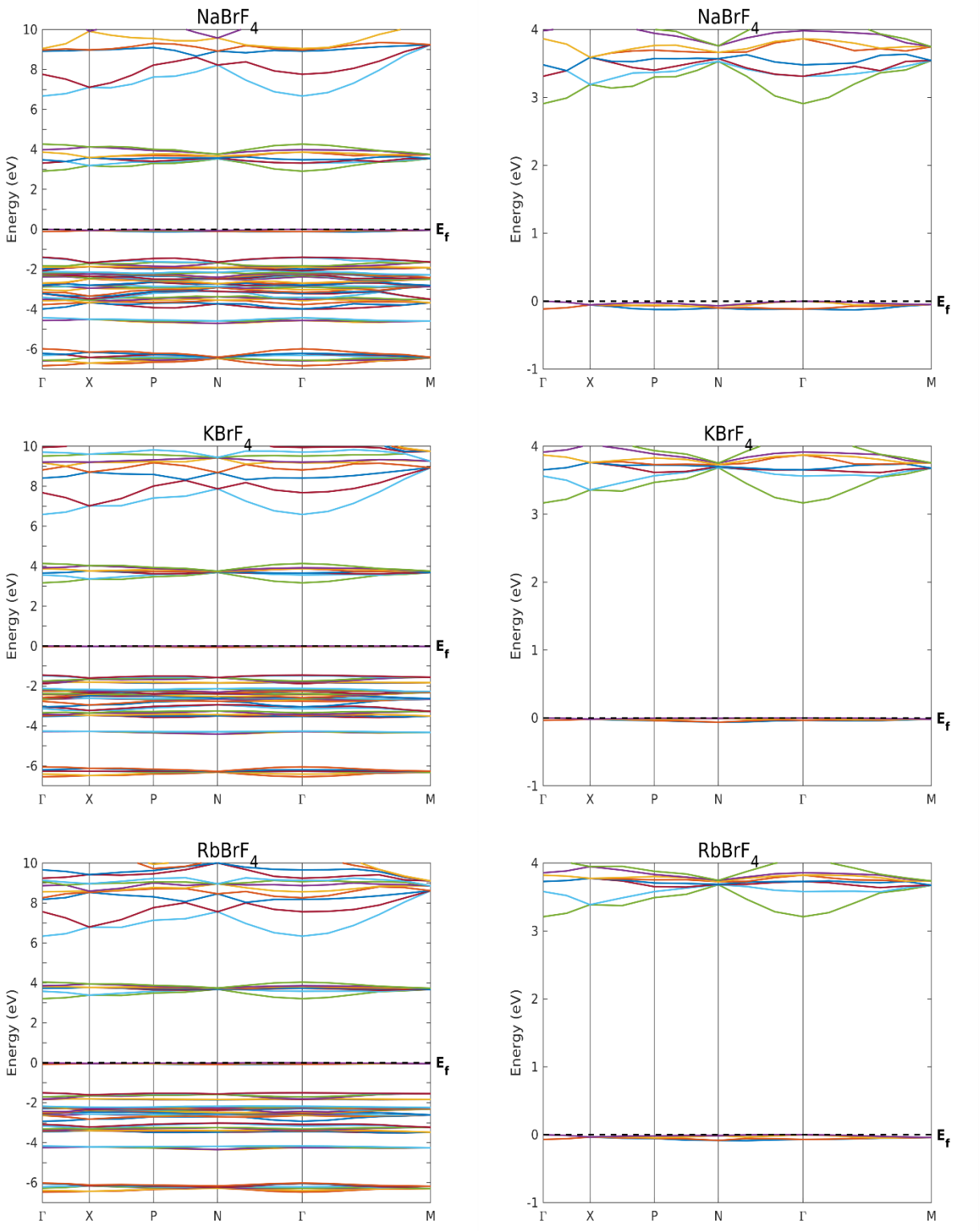

Figure III.6 The band structures (on the left side), and their enlarged view around both VBM and CBM (on the right side) of $ABrF_4$ (A = Na, K and Rb) ternary compounds.

The gap between the conduction and valence bands calculated in this study is 2.909 eV, 3.166 eV and 3.210 eV for $NaBrF_4$, $KBrF_4$ and $RbBrF_4$, respectively, which gives these compounds the property to become wide-band gap semiconductor materials. As shown in Figure III.6, $NaBrF_4$ is a semiconductor compound with a direct band gap, owing to its VBM and its CBM are sited at **Γ** point, where the electron can rise from VB to the CB and change only it's potential (energy), whereas, $KBrF_4$ and $RbBrF_4$ are semiconductors compounds together with an indirect band gap, which their VBM are located near the point **Γ** in the **Γ-N** direction, while their CBM situated at the **Γ** point, where the electron can rise from VB to the CB and change only it's potential (energy) and it's momentum. We can note also that the highest electronegativity value of Na atom (χ^{Na}) makes the band gap of $NaBrF_4$ the smallest among the other compounds, where according to Pauling scale we find: (χ^{Na} = 0.93) > (χ^{K} = χ^{Rb} = 0.82). These results can be considered as a source for future research work since there are no experimental or theoretical band gap values for all studied compounds.

It is clear in Figure III.6, that the topmost part of the valence band (VB) is quasi flat and less dispersive than the lower part of the conduction band (CB), which indicates that the VB holes are heavier than the CB electrons, hence, the VB holes are less mobile than the CB electrons and consequently, the electrons are localized [47]. Furthermore, the contribution of the electrons to the conductivity is predicted to be higher than that of the holes. Thereby, the predominant ionic nature of the chemical bonding is predicted in $ABrF_4$ (A=Na, K and Rb) ternary compounds. We can note also that the VBM appears less dispersive in both $KBrF_4$ and $RbBrF_4$ compounds than that of $NaBrF_4$.

For semiconductors, the effective mass of the charge carriers is an appropriate descriptor of the electronic band structure, which is used to identify the effective density of states and carrier concentrations [48, 49]. The parabolic effective mass approach is one of the best methods applied to calculate the effective mass $\boldsymbol{m}^*$ by parabolic fitting of $\boldsymbol{E}(\boldsymbol{k})$ diagram (the energy $\boldsymbol{E}$ versus the wave vector $\boldsymbol{k}$) around the CBM or the VBM, in agreement with the following relation [50, 51]:

$$\frac{\mathbf{1}}{\boldsymbol{m}^*} = \frac{\mathbf{1}}{\hbar^2}\frac{\boldsymbol{\partial^2 E(k)}}{\boldsymbol{\partial k^2}} \qquad \textbf{(III.30)}$$

The calculated values of the effective mass for electrons $\boldsymbol{m_e^*}$, heavy holes $\boldsymbol{m_{hh}^*}$ and light holes $\boldsymbol{m_{lh}^*}$ are mentioned in Table III.8 for the herein studied compounds. The obtained data show that the value of the effective hole mass is greater than the value of the effective electron mass for all herein studied compounds, which confirm that the VB holes are heavier than the CB electrons, and suggesting that $ABrF_4$ (A = Na, K and Rb) materials are p-type semiconductors. On the other hand, the calculated electron effective mass is smaller in $RbBrF_4$ than that of $NaBrF_4$ and is much smaller than that of $KBrF_4$. Thus, our computations predict higher mobility of electrons in $RbBrF_4$ relative to both $NaBrF_4$ and $KBrF_4$.

Table III.8 The calculated effective masses (in units of the rest free electron mass $\boldsymbol{m_e}$) for $ABrF_4$ (A=Na, K and Rb) ternary compounds. $\boldsymbol{m_e^*}$, $\boldsymbol{m_{hh}^*}$, and $\boldsymbol{m_{lh}^*}$ stand for, respectively, electron, heavy hole, and light hole.

Compounds	$\boldsymbol{m_e^*}$	$\boldsymbol{m_{hh}^*}$	$\boldsymbol{m_{lh}^*}$
$NaBrF_4$	**0,00287**	**0,02654**	**0,01165**
$KBrF_4$	**0,00307**	**0,22927**	**0,01875**
$RbBrF_4$	**0,00272**	**0,06963**	**0,01705**

For understanding the electronic nature better and deeper, the total density of states (TDOS) and partial density of states (PDOS) of all studied compounds are plotted in Figure III.7, where the Fermi level $\mathbf{E_F}$ is considered as the origin of energies.

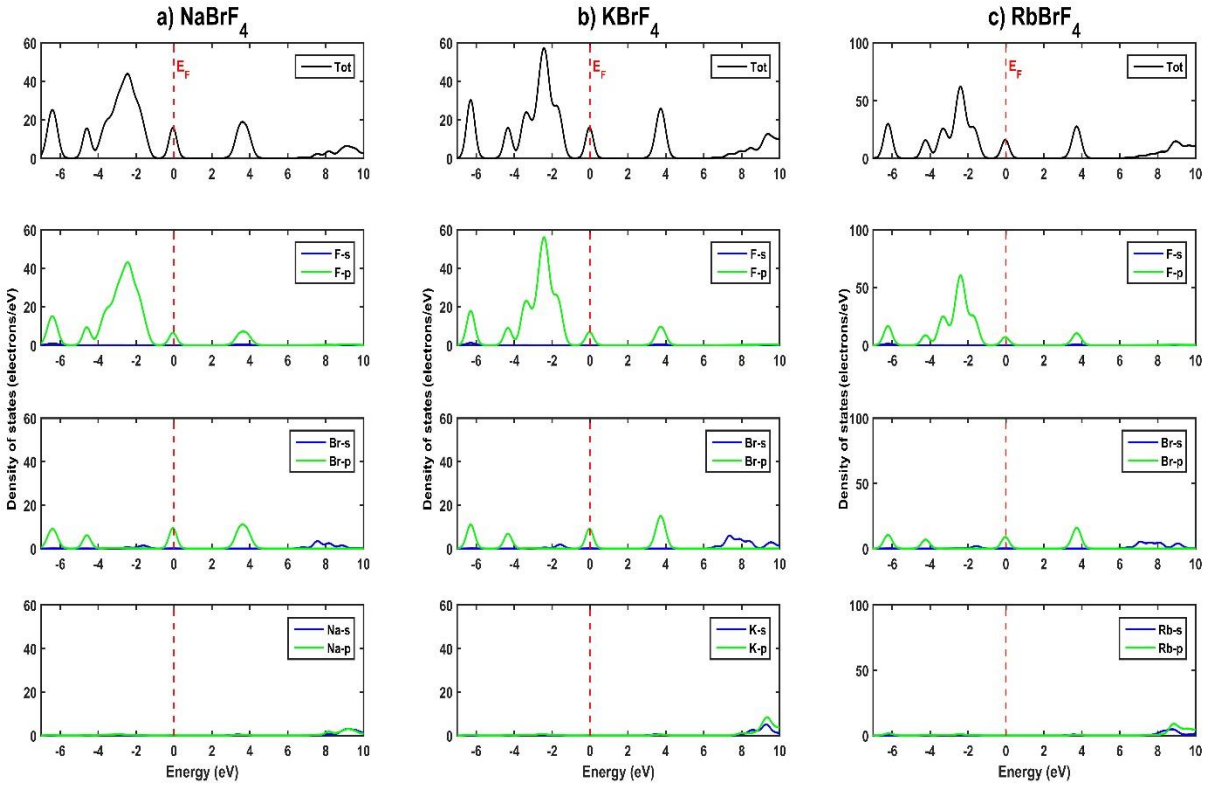

Figure III.7 The calculated total and partial densities of states for $ABrF_4$ (A = Na, K and Rb) ternary compounds.

As shown in Figure III.7, the profile of the density of states of the semiconductors compounds with indirect band gap (IBS) such as $KBrF_4$ and $RbBrF_4$, is almost similar with slight differences can be noted, while the $NaBrF_4$ semiconductor compound with direct band gap (DBS) has a different profile of the density of states. We can note that for all studied compounds, the valence band is dominated by F "p" states with a small contribution of Br "p" states. Whereas, the conduction bands are primarily Br, F, and the alkali element "p" like states with a little participation of Br and the alkali atom "s" states.

Furthermore, to understanding the nature of chemical bonding between the different atoms, the maps of the valance charge densities in the **(010)** plane for $ABrF_4$ (A=Na, K and Rb) ternary compounds are plotted in Figure III.8. It is clear that the ionic character appears in the region between A^+ cations and $(BrF_4)^-$ anions, where demonstrates the reliability of our previously obtained results of Poisson's ratio value and band structure form.

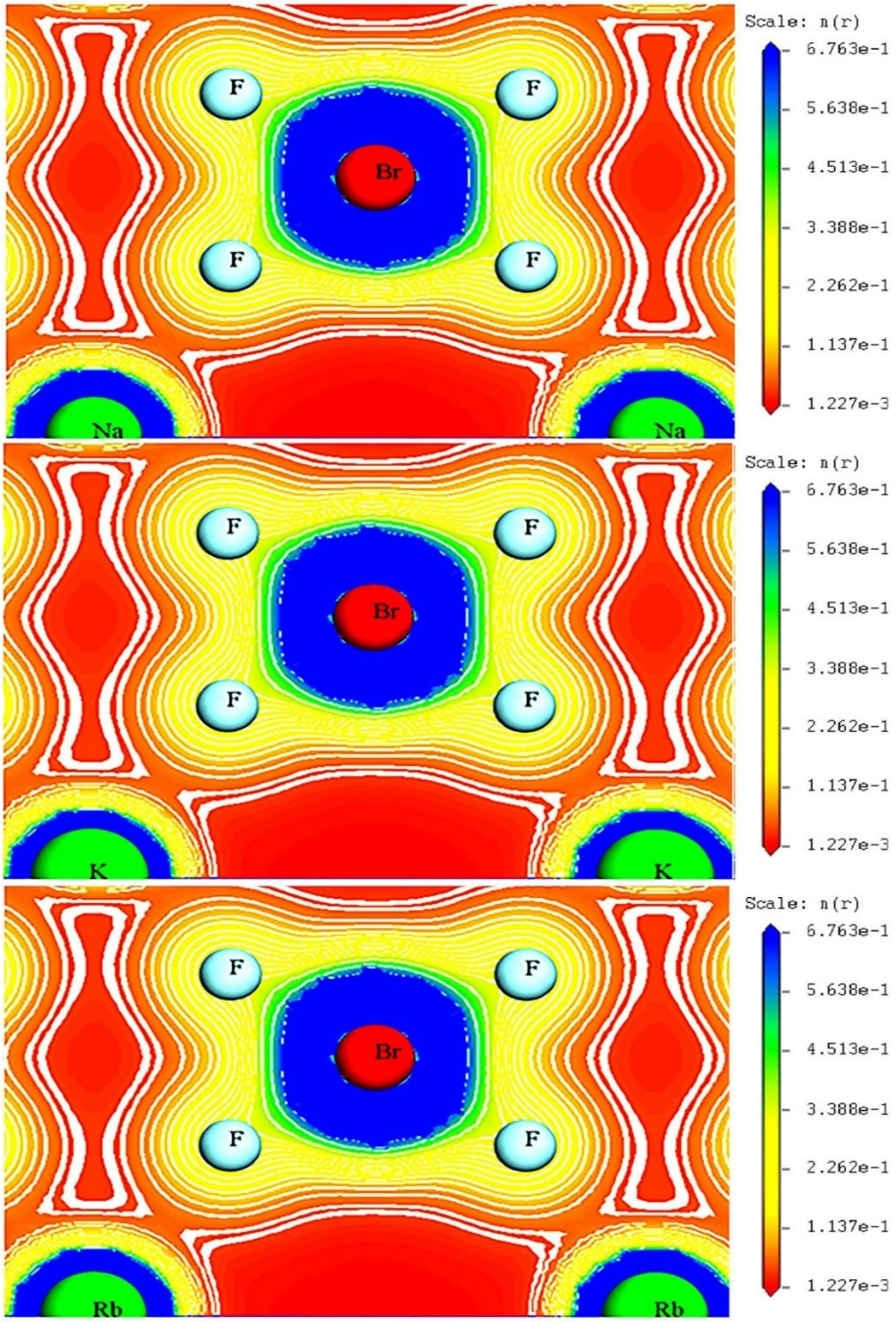

Figure III.8 A *2D* representation of the calculated valence charge densities in the **(010)** crystallographic plane for $ABrF_4$ (A = Na, K and Rb) ternary compounds.

III.3.4 Optical properties

When the materials interact with an external electromagnetic field such as light, the response of the matter generally depends on the frequency of this field. During the light matter interactions, the optical properties of the material appear. The different optical parameters of the material can be calculated from its dielectric permittivity $\boldsymbol{\varepsilon}$, where it is often treated as a complex function of the angular frequency $\boldsymbol{\omega}$ of the applied field:

$$\boldsymbol{\varepsilon(\omega) = \varepsilon_1(\omega) + i\varepsilon_2(\omega)} \quad \textbf{(III.31)}$$

Where $\boldsymbol{\varepsilon_1(\omega)}$ is the real part and $\boldsymbol{\varepsilon_2(\omega)}$ is the imaginary part of the dielectric function. The following equation is used to calculate the imaginary part of the dielectric function [53].

$$\boldsymbol{\varepsilon_2(\omega) = \frac{8}{3\pi\omega^2}\sum_{nn'}\int_{BZ}|P_{nn'}(k)|^2\frac{dS_k}{|\nabla_k\omega_{nn'}(k)|}} \quad \textbf{(III.32)}$$

The photon energy is given by $\boldsymbol{\omega_{nn'}(k)}$, and $\boldsymbol{P_{nn'}(k)}$ is the dipolar matrix element and $\boldsymbol{S_k}$ is a constant energy surface.

The real part of the dielectric function can be estimated from the imaginary part using the normalized Kramers-Kronig relation based on the principal value of the Cauchy integral $\boldsymbol{P}$ as follows [52]:

$$\boldsymbol{\varepsilon_1(\omega) = 1 + \frac{2}{\pi}P\int_0^{+\infty}\frac{\omega'\varepsilon_2(\omega')}{\omega'^2-\omega^2}d\omega'} \quad \textbf{(III.33)}$$

The main optical parameters such as absorption coefficient $\boldsymbol{\alpha(\omega)}$, extinction coefficient $\boldsymbol{k(\omega)}$, refractive index $\boldsymbol{n(\omega)}$, optical reflectivity $\boldsymbol{R(\omega)}$, photoconductivity $\boldsymbol{\sigma(\omega)}$, and energy loss function $\boldsymbol{L(\omega)}$ are given by [53]:

$$\boldsymbol{\alpha(\omega) = \sqrt{2}\omega\left[\sqrt{\varepsilon_1(\omega)^2+\varepsilon_2(\omega)^2}-\varepsilon_1(\omega)\right]^{1/2}} \quad \textbf{(III.34)}$$

$$\boldsymbol{k(\omega) = \alpha(\omega)/2\omega} \quad \textbf{(III.35)}$$

$$\boldsymbol{n(\omega) = \left(1/\sqrt{2}\right)\left[\sqrt{\varepsilon_1(\omega)^2+\varepsilon_2(\omega)^2}+\varepsilon_1(\omega)\right]^{1/2}} \quad \textbf{(III.36)}$$

$$\boldsymbol{R(\omega) = \frac{n(\omega)+ik(\omega)-1}{n(\omega)+ik(\omega)+1}} \quad \textbf{(III.37)}$$

$$\boldsymbol{\sigma(\omega) = \frac{\omega}{4\pi}\varepsilon_2(\omega)} \quad \textbf{(III.38)}$$

$$\boldsymbol{L(\omega) = \frac{\varepsilon_2(\omega)}{\varepsilon_1(\omega)^2+\varepsilon_2(\omega)^2}} \quad \textbf{(III.39)}$$

As $ABrF_4$ (X=Na, K and Rb) ternary compounds are crystallized in tetragonal structure, the dielectric functions include only two components $\boldsymbol{\varepsilon_{xx}}$ and $\boldsymbol{\varepsilon_{zz}}$, where $\boldsymbol{\varepsilon_{xx}}$ concerning the polarization of the applied electric field **E** along the ***x*** and ***y*** directions (i.e., **E** ⊥ ***c***-axis), while $\boldsymbol{\varepsilon_{zz}}$ is related to the polarization of E along ***z*** direction (i.e., **E** ∥ ***c***-axis) [53].

In this study, optical spectra of both perpendicular and parallel to the electric field are plotted versus photon energy in the range of (0-40 eV) for the herein studied compounds. Figure III.9 displays the real and the imaginary parts of the dielectric function for $ABrF_4$ (A=Na, K, Rb), where we can notice that the peaks are move and shifted towards the lowermost energy region by replacing the alkali atoms from Na to K to Rb, which this behavior is shown previously in the calculations of the band structure and the density of states. Furthermore, it is clear that the anisotropy between the components of the dielectric function at the energy region less than 25 eV, makes $\boldsymbol{\varepsilon_{zz}}$ the dominant component for these compounds.

The imaginary part of the dielectric constant $\boldsymbol{\varepsilon_2}$ (called also the absorptive part) has a significant peak located at the lower energy region with a small shift between the two components $\boldsymbol{\varepsilon_2^{xx}}$ and $\boldsymbol{\varepsilon_2^{zz}}$ for both $NaBrF_4$ and $RbBrF_4$ compounds. The energy values corresponding to these prominent peaks are given in Table III.9, which these energies originate from the optical transition between the highest occupied valence band and the lowest unoccupied conduction band.

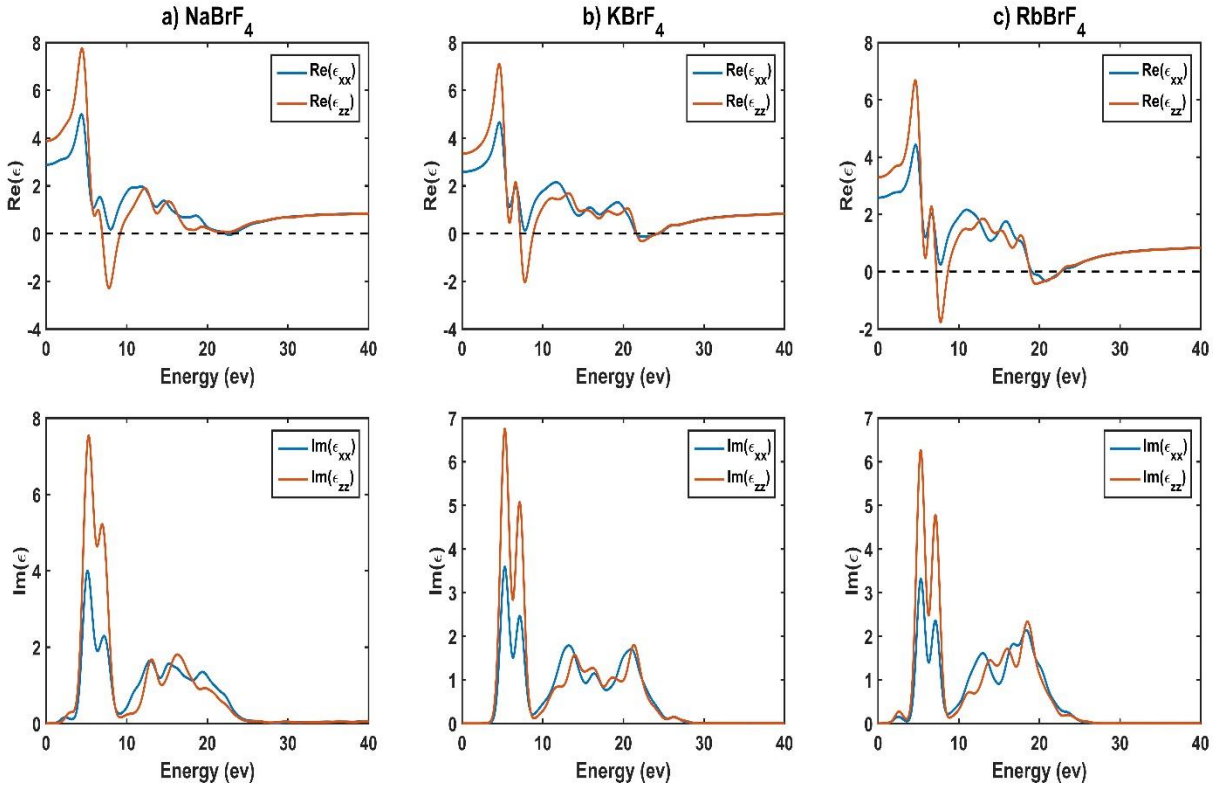

Figure III.9 The spectra of the real and the imaginary parts of dielectric function for $ABrF_4$ (A = Na, K and Rb) ternary compounds.

Regarding the absorption spectra displayed in Figure III.10, where represent the maximum absorbance in the ultraviolet (UV) optical range, which the first main peaks situated around 5.6 eV, proposes that these ternary compounds can be used for the production of the specified UV optoelectronic devices. Furthermore, the absorption thresholds start at about 2.98 eV for $NaBrF_4$, 3.17 eV for $KBrF_4$ and 3.23 eV for $RbBrF_4$, which is closely enough to the calculated band gap. Moreover, the absorption curves show a fast decrease in the higher most energy region, which is the typical feature of semiconductor compounds.

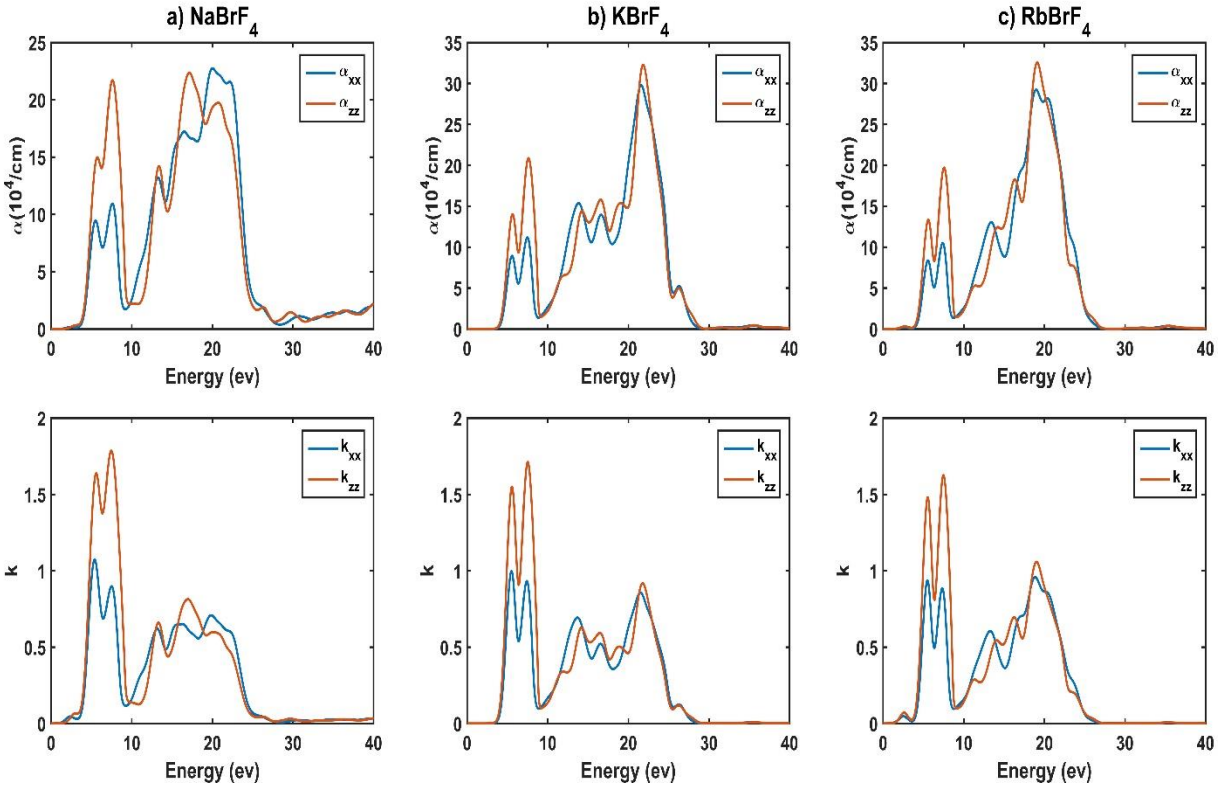

Figure III.10 The spectra of the absorption coefficient $\boldsymbol{\alpha}$ and the extinction coefficient $\boldsymbol{k}$ for $ABrF_4$ (A = Na, K and Rb) ternary compounds.

The real part of the dielectric function $\boldsymbol{\varepsilon_1}$ (called also the dispersive part), has prominent peaks situated around 4.45 eV, 4.60 eV and 4.62 eV for $NaBrF_4$, $KBrF_4$ and $RbBrF_4$, respectively. The most important point in the spectrum of the real part, is the zero-frequency limit $\boldsymbol{\varepsilon_1(0)}$ i.e., when the curves of $\boldsymbol{\varepsilon_1(\omega)}$ cross zero frequency, which represents the dielectric response of the material to a static electric field according to the Drude behavior. The calculated values $\boldsymbol{\varepsilon_1^{xx}(0)}$ and $\boldsymbol{\varepsilon_1^{zz}(0)}$, for $ABrF_4$ (A=Na, K and Rb) ternary compounds are mentioned in Table III.9. It is clear that the value of $\boldsymbol{\varepsilon_1(0)}$ decreases when moving from Na to Rb, whereas the value of the band gaps as we find out in the electronic properties increase in the same direction, which indicates an inversely proportional relationship between the energy gap $\boldsymbol{E_g}$ and the zero-frequency limit of dielectric function $\boldsymbol{\varepsilon(0)}$ according to Penn model [54]:

$$\boldsymbol{\varepsilon(0) = 1 + \left(\frac{\hbar\omega_p}{E_g}\right)^2} \qquad \textbf{(III.40)}$$

Where $\boldsymbol{\omega_p}$ is the plasma frequency and $\hbar$ is the reduced Planck constant.

Figure III.10, displays also the spectra of the extinction coefficient $\boldsymbol{k(\omega)}$. The maximum peak of $\boldsymbol{k(\omega)}$ corresponding to the energies 7.46 eV, 7.51 eV and 7.45 eV, for $NaBrF_4$, $KBrF_4$ and $RbBrF_4$, respectively. Where this energies value corresponds to the zero of the real part of the dielectric function $\boldsymbol{\varepsilon_1(\omega)}$. In the fact, the value of $\boldsymbol{\varepsilon_1(\omega)}$ equals to zero means the non-existence of the dispersion on the material, and consequently due to the greater value of the extinction coefficient $\boldsymbol{k(\omega)}$ than the reflectivity $\boldsymbol{R(\omega)}$ as shown in Figure III.11. Furthermore, the zero-frequency of reflectivity $\boldsymbol{R(0)}$ for herein studied compounds is mentioned in Table III.9.

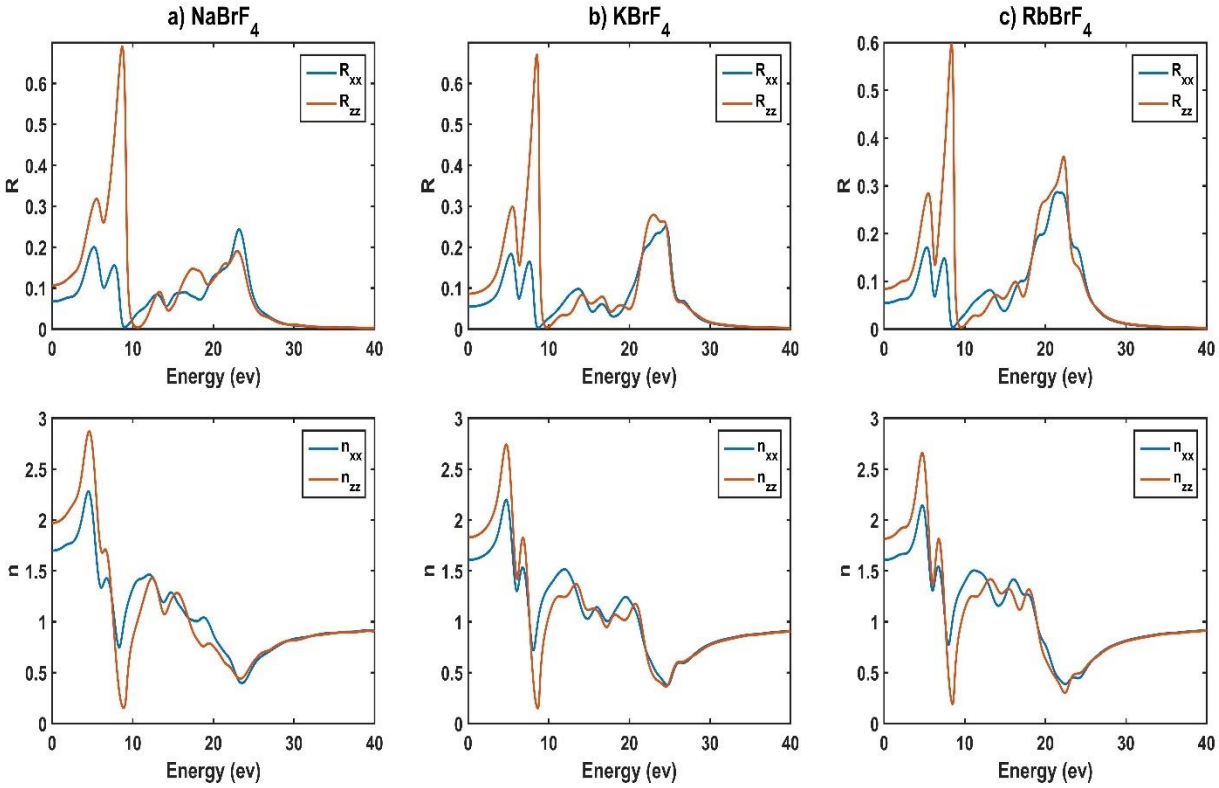

Figure III.11 The spectra of the optical reflectivity $\boldsymbol{R}$ and the refractive index $\boldsymbol{n}$ for $ABrF_4$ (A = Na, K and Rb) ternary compounds.

The variation of the refractive index $\boldsymbol{n}$ as a function of the angular frequency $\boldsymbol{\omega}$ showed the phenomenon of dispersion, as displayed in Figure III.11, where $\boldsymbol{n(\omega)}$ profile closely follows the shape of the dispersive part $\boldsymbol{\varepsilon_1(\omega)}$ spectrum. The prominent peak value of the refractive index found at about 4.59 eV, 4.72 eV and 4.73 eV for $NaBrF_4$, $KBrF_4$ and $RbBrF_4$, respectively. As we previously demonstrated, the dispersion phenomenon does not exist when the $\boldsymbol{\varepsilon_1(\omega)}$ equals to zero. For this reason, we find the value of the refractive index is approximately equal to one. Whereas the value of the refractive index **(**strictly equals one**)**, is corresponding to the absolute vacuum when the phenomena of refraction or dispersion of light are absolutely absent. It is important to note that in this energy region (from 7.4 to 7.6 eV) and in the higher energy region (higher than 25 eV) the two components of the refractive index are collinear, while outside these energy intervals, the materials show the optical property of birefringence. Furthermore, the obtained results of the static refractive index $\boldsymbol{n(0)}$ are mentioned in Table III.9, which confirms the values calculated by the semi-empirical relation $\boldsymbol{n(0) = \sqrt{\varepsilon_1(0)}}$, and indicating the reliability of our results.

Table III.9 Calculated the maximum peak values of $\boldsymbol{\varepsilon_2^{xx}(\omega)}$ and $\boldsymbol{\varepsilon_2^{zz}(\omega)}$, the static dielectric constant $\boldsymbol{\varepsilon_1^{xx}(0)}$ and $\boldsymbol{\varepsilon_1^{zz}(0)}$, the zero-frequency limit of the reflectivity $\boldsymbol{R^{xx}(0)}$ and $\boldsymbol{R^{zz}(0)}$ and the static refractive index $\boldsymbol{n^{xx}(0)}$ and $\boldsymbol{n^{zz}(0)}$ for $ABrF_4$ (A=Na, K and Rb) ternary compounds.

Compounds	**$NaBrF_4$**	**$KBrF_4$**	**$RbBrF_4$**
$\boldsymbol{\varepsilon_2^{xx}(\omega)}$	**5.13**	**5.31**	**5.31**
$\boldsymbol{\varepsilon_2^{zz}(\omega)}$	**5.27**	**5.31**	**5.28**
$\boldsymbol{\varepsilon_1^{xx}(0)}$	**2.88**	**2.58**	**2.57**
$\boldsymbol{\varepsilon_1^{zz}(0)}$	**3.88**	**3.34**	**3.30**
$\boldsymbol{R^{xx}(0)}$	**0.07**	**0.06**	**0.05**
$\boldsymbol{R^{zz}(0)}$	**0.11**	**0.09**	**0.08**
$\boldsymbol{n^{xx}(0)}$	**1.697**	**1.607**	**1.606**
$\boldsymbol{n^{zz}(0)}$	**1.969**	**1.828**	**1.815**

The increase in the number of free transporters created when photons are absorbed results an increase in electrical conductivity, hence the photoconductivity effect has been established, as shown in Figure III.12, the shape of the photoconductivity shares similar characteristics with the absorptive part $\boldsymbol{\varepsilon_2(\omega)}$ spectrum. Moreover, the photoconductivity does not appear when the photon energy is below the gap energy corresponding to the herein studied compounds, i.e., the photons do not have energy sufficient enough to overcome the band gap in these semiconductor compounds [55].

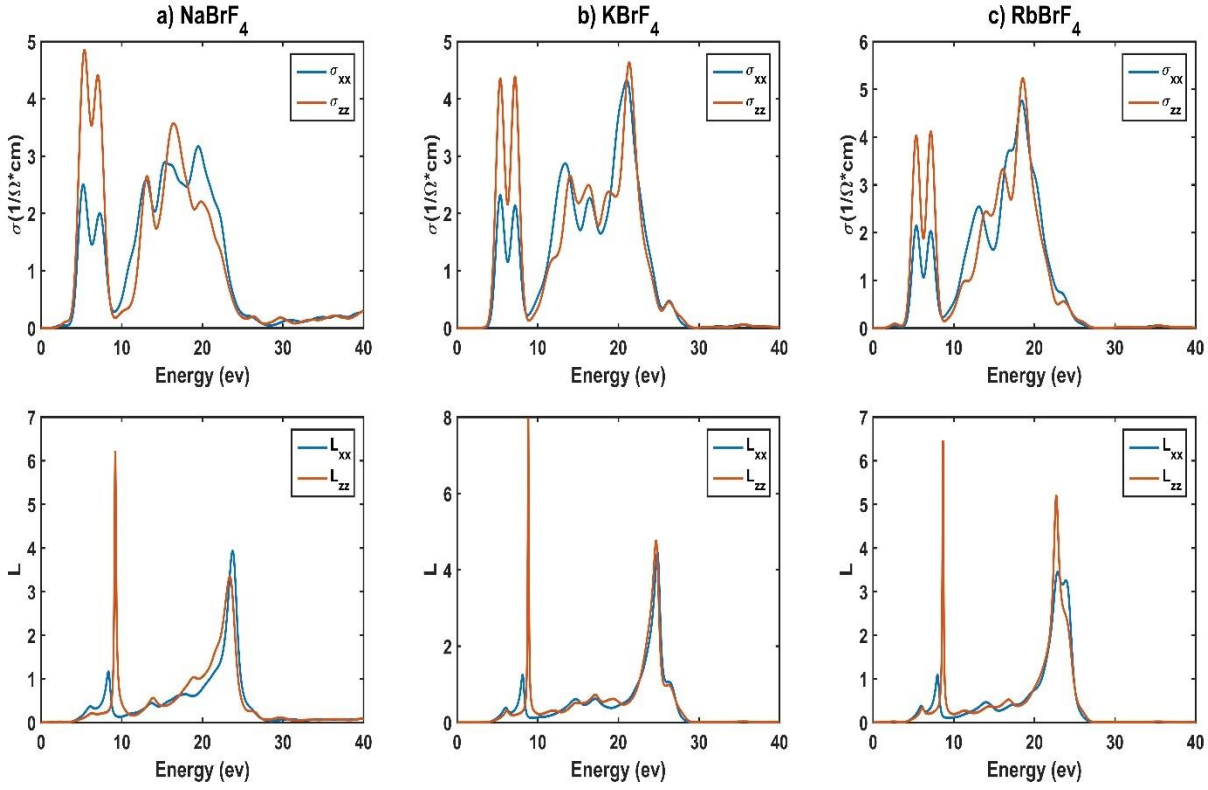

Figure III.12 The spectra of the photoconductivity $\boldsymbol{\sigma}$ and the energy loss function $\boldsymbol{L}$ for $ABrF_4$ (A = Na, K and Rb) ternary compounds.

The fast-moving electron in the material is losing energy and it depends on the photon energy [56]. In order to understand more of this phenomenon, we plotted the energy loss function $\boldsymbol{L(\omega)}$ in Figure III.12. The photon energy values corresponding to the prominent peaks of the energy loss function are 9.18 eV, 8.83 eV and 8.66 eV for $NaBrF_4$, $KBrF_4$ and $RbBrF_4$, respectively. We can notice that the highest value of loss energy depends on plasma energy $\hbar\boldsymbol{\omega_p}$ which the plasma resonance occurs when the absorptive part $\boldsymbol{\varepsilon_2(\omega)}$ takes a smallest value and the dispersive part $\boldsymbol{\varepsilon_1(\omega)}$ reaches zero again.

This study demonstrates the first investigation of the optical properties for $NaBrF_4$, $KBrF_4$ and $RbBrF_4$ compounds. For that, we hope our calculation can help to offer theoretical grounds for future experimental applications on these compounds.

References

[1] O. Materials, Bulk Crystal Growth of Electronic , Optical & Wiley Series in Materials for Electronic and Optoelectronic, 2005. https://books.google.dz/books

[2] R. Burkhalter, I. Dohnke, J. Hulliger, Growing of bulk crystals and structuring waveguides of fluoride materials for laser applications, 2001. https://doi.org/10.1016/S0960-8974(01)00002-X.

[3] S. Siegel, The crystal structure of KBrF 4 , Acta Crystallogr. 9 (1956) 493–495. https://doi.org/10.1107/s0365110x56001340.

[4] W.G. Sly, R.E. Marsh, A note on the structure of KBrF 4, Acta Crystallogr. 10 (1957) 378–379. https://doi.org/10.1107/s0365110x57001139.

[5] A.J. Edwards, G.R. Jones, Fluoride crystal structures. Part VIII. Neutron diffraction studies of potassium tetrafluorobromate(III) and potassium tetrafluoroaurate(III), J. Chem. Soc. A Inorganic, Phys. Theor. Chem. (1969) 1936–1938. https://doi.org/10.1039/J19690001936.

[6] A.I. Popov, Y.M. Kiselev, V.F. Sukhoverkhov, N.A. Chumaevskij, O.A. Krasnyanskaya, A.T. Sadikova, Investigation of thermal stability of alkali metal tetrafluorobromates (3), Zh. Neorg. Khim.; 32:5 (1987).

[7] A.R. Mahjoub, A. Hoser, J. Fuchs, K. Seppelt, Die Struktur von $BrF_6^{\ominus}$ und verwandten Verbindungen, Angew. Chemie. 101 (1989) 1528–1529. https://doi.org/10.1002/ange.19891011108.

[8] S.I. Ivlev, R. V. Ostvald, F. Kraus, A new look at NaBrF4: the most BrF3-rich tetrafluoridobromate(III) by mass, Monatshefte Fur Chemie. 147 (2016) 1661–1668. https://doi.org/10.1007/s00706-016-1799-2.

[9] S.I. Ivlev, F. Kraus, Redetermination of the crystal structure of K[BrF 4] from single-crystal X-ray diffraction data , IUCrData. 3 (2018). https://doi.org/10.1107/s2414314618006466.

[10] S.I. Ivlev, A.J. Karttunen, R. Ostvald, F. Kraus, RbBrF4 Revisited, Zeitschrift Fur Anorg. Und Allg. Chemie. 641 (2015) 2593–2598. https://doi.org/10.1002/zaac.201500647.

[11] A. V. Malin, S.I. Ivlev, R. V. Ostvald, F. Kraus, Rubidium tetrafluoridobromate(III): redetermination of the crystal structure from single-crystal X-ray diffraction data, IUCrData. 4 (2019). https://doi.org/10.1107/s2414314619015955.

[12] S. Ivlev, P. Woidy, V. Sobolev, I. Gerin, R. Ostvald, F. Kraus, On tetrafluorobromates (III): Crystal structures of the dibromate CsBr 2F7 and the monobromate CsBrF4, Zeitschrift Fur Anorg. Und Allg. Chemie. 639 (2013) 2846–2850. https://doi.org/10.1002/zaac.201300290.

[13] A. V. Malin, S.I. Ivlev, R. V. Ostvald, F. Kraus, Redetermination of the crystal structure of caesium tetrafluoridobromate (III) from single-crystal X-ray diffraction data, IUCrData. 5 (2020) 3–8. https://doi.org/10.1107/s2414314620001145.

[14] V.N. Mitkin, A.A. Galitsky, T.M. Korda, Application of fluoroxidants for the decomposition and analysis of platinum metals and gold in black shale ores, Fresenius. J. Anal. Chem. 365 (1999) 374–376. https://doi.org/10.1007/s002160051504.

[15] V.N. Mitkin, Physical-chemical basis for application of fluoroxidants in noble metal analytical chemistry, Spectrochim. Acta - Part B At. Spectrosc. 56 (2001) 135–175. https://doi.org/10.1016/S0584-8547(00)00303-7.

[16] V.N. Mitkin, S.B. Zayakina, G.N. Anoshin, New technique for the determination of trace noble metal content in geological and process materials, Spectrochim. Acta - Part B At. Spectrosc. 58 (2003) 311–328. https://doi.org/10.1016/S0584-8547(02)00154-4.

[17] V.N. Mitkin, S.B. Zayakina, V.G. Tsimbalist, A.A. Galizky, Application of potassium tetrafluorobromate to the rapid decomposition and determination of noble metals in chromites and related materials, Spectrochim. Acta - Part B At. Spect. 58 (2003) 297–310. https://doi.org/10.1016/S0584-8547(02)00155-6.

[18] S. Ivlev, P. Woidy, F. Kraus, I. Gerin, R. Ostvald, Tetrafluorobromates for urban mining of noble metals: A case study on iridium metal, Eur. J. Inorg. Chem. (2013) 4984–4987. https://doi.org/10.1002/ejic.201300618.

[19] T. Shishimi, S. Hara, BrF3-KHF2: An air-stable fluorinating reagent, J. Fluor. Chem. 168 (2014) 55–60. https://doi.org/10.1016/j.jfluchem.2014.08.019.

[20] S.J. Clark, M.D. Segall, C.J. Pickard, P.J. Hasnip, M.I.J. Probert, K. Refson, M.C. Payne, First principles methods using CASTEP, Zeitschrift Fur Krist. 220 (2005) 567–570. https://doi.org/10.1524/zkri.220.5.567.65075.

[21] J.P. Perdew, A. Ruzsinszky, G.I. Csonka, O.A. Vydrov, G.E. Scuseria, L.A. Constantin, X. Zhou, K. Burke, Restoring the density-gradient expansion for exchange in solids and surfaces, Phys. Rev. Lett. 100 (2008) 1–4. https://doi.org/10.1103/PhysRevLett.100.136406.

[22] Hendrik J Monkhorst, J.D. Pack, Special points for Brillouin-zone integration Monkhorst and Pack, Phys. Rev. B. 13 (1976) 5188–5192. http://prb.aps.org/pdf/PRB/v13/i12/p5188_1.

[23] F. Birch, Finite elastic strain of cubic crystals, Phys. Rev. 71 (1947) 809–824. https://doi.org/10.1103/PhysRev.71.809.

[24] R. Belghit, H. Belkhir, D. Heciri, M. Bououdina, M.T. Kadri, R. Ahuja, First principles study of structural, mechanical and electronic properties of the ternary alkali metal oxides KNaO and RbNaO, Chem. Phys. Lett. 706 (2018) 684–693. https://doi.org/10.1016/j.cplett.2018.07.013.

[25] S. Chandrasekar, S. Santhanam, A calculation of the bulk modulus of polycrystalline materials, J. Mater. Sci. 24 (1989) 4265–4267. https://doi.org/10.1007/BF00544497.

[26] F. Mouhat, F.X. Coudert, Necessary and sufficient elastic stability conditions in various crystal systems, Phys. Rev. B - Condens. Matter Mater. Phys. 90 (2014) 0–3. https://doi.org/10.1103/PhysRevB.90.224104.

[27] W. Voigt, Lehrbuch der Kristallphysik, 1966. https://doi.org/10.1007/978-3-663-15884-4.

[28] A. Reuss, Berechnung der Fließgrenze von Mischkristallen auf Grund der Plastizitätsbedingung für Einkristalle ., ZAMM - J. Appl. Math. Mech. / Zeitschrift Für Angew. Math. Und Mech. 9 (1929) 49–58. https://doi.org/10.1002/zamm.19290090104.

[29] S.P. Sun, X.P. Li, H.J. Wang, Y. Jiang, D.Q. Yi, Prediction on anisotropic elasticity, sound velocity, and thermodynamic properties of MoSi2 under pressure, J. Alloys Compd. 652 (2015) 106–115. https://doi.org/10.1016/j.jallcom.2015.08.207.

[30] R. Hill, The elastic behaviour of a crystalline aggregate, Proc. Phys. Soc. Sect. A. 65 (1952) 349–354. https://doi.org/10.1088/0370-1298/65/5/307.

[31] M.L. Cohen, Calculation of bulk moduli of diamond and zinc-blende solids, Phys. Rev. B. 32 (1985) 7988–7991. https://doi.org/10.1103/PhysRevB.32.7988.

[32] S.F. Pugh, XCII. Relations between the elastic moduli and the plastic properties of polycrystalline pure metals, London, Edinburgh, Dublin Philos. Mag. J. Sci. 45 (1954) 823–843. https://doi.org/10.1080/14786440808520496.

[33] FRANTSEVICH, I. N., Elastic constants and elastic moduli of metals and insulators, Ref. B. (1982). https://ci.nii.ac.jp/naid/10004038718.

[34] D.H. Wu, H.C. Wang, L.T. Wei, R.K. Pan, B.Y. Tang, First-principles study of structural stability and elastic properties of MgPd3 and its hydride, J. Magnes. Alloy. 2 (2014) 165–174. https://doi.org/10.1016/j.jma.2014.06.001.

[35] J. Haines, J.M. Léger, G. Bocquillon, Synthesis and design of superhard materials, Annu. Rev. Mater. Sci. 31 (2001) 1–23. https://doi.org/10.1146/annurev.matsci.31.1.1.

[36] O.L. Anderson, H.H. Demarest, Elastic constants of the central force model for cubic structures: Polycrystalline aggregates and instabilities, J. Geophys. Res. 76 (1971) 1349–1369. https://doi.org/10.1029/jb076i005p01349.

[37] M.A. Rahman, M.K. Ahmed, Physical Properties of BaNiSn 3-type Compounds LaTGe 3 (T= Rh, Ir, Pd): An ab-initio Investigation, n.d. https://www.researchgate.net/publication/339383954.

[38] T. Sugimoto, Development of an automatic vickers hardness testing system using image processing technolog takao sugimoto and tadao kawaguchi, IEEE Trans. Ind. Electron. 44 (1997) 696–702. https://doi.org/10.1109/41.633474.

[39] X.-Q. Chen, H. Niu, D. Li, Y. Li, Intrinsic Correlation between Hardness and Elasticity in Polycrystalline Materials and Bulk Metallic Glasses, 2 (2011). https://doi.org/10.1016/j.intermet.2011.03.026.

[40] H. Zhai, X. Li, J. Du, First-principles calculations on elasticity and anisotropy of tetragonal tungsten dinitride under pressure, Mater. Trans. 53 (2012) 1247–1251. https://doi.org/10.2320/matertrans.M2011373.

[41] S.I. Ranganathan, M. Ostoja-Starzewski, Universal elastic anisotropy index, Phys. Rev. Lett. 101 (2008) 3–6 https://doi.org/10.1103/PhysRevLett.101.055504

[42] K. Lau, A. McCurdy, Elastic anisotropy factors for orthorhombic, tetragonal, and hexagonal crystals, Phys. Rev. B - Condens. Matter Mater. Phys. 58 (1998) 8980–8984. https://doi.org/10.1103/PhysRevB.58.8980

[43] H. Siethoff, K. Ahlborn, Debye-temperature-elastic-constants relationship for materials with hexagonal and tetragonal symmetry, J. Appl. Phys. 79 (1996) 2968–2974. https://doi.org/10.1063/1.361293.

[44] O.L. Anderson, A simplified method for calculating the debye temperature from elastic constants, J. Phys. Chem. Solids. 24 (1963) 909–917. https://doi.org/10.1016/0022-3697(63)90067-2

[45] J. Feng, B. Xiao, R. Zhou, W. Pan, D.R. Clarke, Anisotropic elastic and thermal properties of the double perovskite slab-rock salt layer Ln 2SrAl 2O 7 (Ln = La, Nd, Sm, Eu, Gd or Dy) natural superlattice structure, Acta Mater. 60 (2012) 3380–3392. https://doi.org/10.1016/j.actamat.2012.03.004.

[46] W. Setyawan, S. Curtarolo, High-throughput electronic band structure calculations: Challenges and tools, Comput. Mater. Sci. 49 (2010) 299–312. https://doi.org/10.1016/j.commatsci.2010.05.010.

[47] S.Z. Karazhanov, P. Ravindran, A. Kjekshus, H. Fjellvåg, B.G. Svensson, Electronic structure and optical properties of ZnX (X=O, S, Se, Te): A density functional study, Phys. Rev. B - Condens. Matter Mater. Phys. 75 (2007) 1–14. https://doi.org/10.1103/PhysRevB.75.155104.

[48] Z.M. Gibbs, F. Ricci, G. Li, H. Zhu, K. Persson, G. Ceder, G. Hautier, A. Jain, G.J. Snyder, Effective mass and Fermi surface complexity factor from ab initio band structure calculations, Npj Comput. Mater. 3 (2017) 1–6. https://doi.org/10.1038/s41524-017-0013-3.

[49] O. Rubel, F. Tran, X. Rocquefelte, P. Blaha, Perturbation approach to ab initio effective mass calculations, Comput. Phys. Commun. 261 (2021) 107648. https://doi.org/10.1016/j.cpc.2020.107648.

[50] W. Khan, A.H. Reshak, Optoelectronic and thermoelectric properties of KAuX5 (X = S, Se): A first principles study, J. Mater. Sci. 49 (2014) 1179–1192. https://doi.org/10.1007/s10853-013-7798-3.

[51] M. Faizan, H. Ullah, S.H. Khan, S.M. Ramay, S.A.S. Qaid, A. Mahmood, M. Ali, Carrier effective masses and thermoelectric properties of novel Ag3AuSe2 and Ag3AuTe2 compounds, Int. J. Mod. Phys. B. 31 (2017) 1–8. https://doi.org/10.1142/S0217979217502538.

[52] R. de L. Kronig, On the Theory of Dispersion of X-Rays, JOSA, Vol. 12, Issue 6, Pp. 547-557. 12 (1926) 547–557. https://doi.org/10.1364/JOSA.12.000547.

[53] T. Ghellab, H. Baaziz, Z. Charifi, K. Bouferrache, M.A. Saeed, A. Telfah, Ab initio full-potential study of the fundamental properties of chalcopyrite semiconductors XPN 2 (X = H, Cu), Mater. Res. Express. 6 (2019). https://doi.org/10.1088/2053-1591/ab1325.

[54] D.R. Penn, Wave-number-dependent dielectric function of semiconductors, Phys. Rev. 128 (1962) 2093–2097. https://doi.org/10.1103/PhysRev.128.2093.

[55] J. Sun, X.F. Zhou, Y.X. Fan, J. Chen, H.T. Wang, X. Guo, J. He, Y. Tian, First-principles study of electronic structure and optical properties of heterodiamond BC2 N, Phys. Rev. B - Condens. Matter Mater. Phys. 73 (2006) 1–10. https://doi.org/10.1103/PhysRevB.73.045108.

[56] R. Belghit, H. Belkhir, M.T. Kadri, D. Heciri, M. Bououdina, R. Ahuja, Structural, elastic, electronic and optical properties of novel antiferroelectric KNaX (X = S, Se, and Te) compounds: First principles study, Phys. B Condens. Matter. 545 (2018) 18–29. https://doi.org/10.1016/j.physb.2018.05.025.

Conclusion

Conclusion

In this work, we carried out an ab-initio study on the structural, mechanical, electronic, and optical properties of ternary compounds of the form $ABrF_4$ where (A = Na, K and Rb), which crystallize in the tetragonal structure and belong to the space group I4/mcm (No. 140), based on the Density Functional Theory (DFT) and the Plane Wave Pseudopotential approach (PP-PW) as implemented in the CASTEP code. The various properties studied were calculated using the generalized gradient approximation of Perdew-Burke-Ernzerhof for solids (GGA PBE-sol) to deal with the exchange and correlation energy.

First of all, a precise geometrical optimization was performed on the crystal structure, then the structural, mechanical, electronic, and optical properties of the three materials $NaBrF_4$, $KBrF_4$, and $RbBrF_4$ were calculated in detail. The results of our study can be summarized as follows:

- The results of structural properties, such as the ground states parameters are in good agreement with the earlier experimental values.
- Based on the results of elastic constants and polycrystalline moduli, it can be concluded that these ternary compounds have ductile behavior, and among them, the $NaBrF_4$ compound exhibits the largest thermal conductivity and presents the hardest and stiffest material.
- The outcome of our investigation in electronic properties indicates that $NaBrF_4$ is a semiconductor material with a direct band gap, whereas, $KBrF_4$ and $RbBrF_4$ are semiconductors materials with indirect band gap.
- Both elastic and electronic properties including the Poisson's ratio, the band structure form, and the maps of the valance charge densities manifest obvious the ionic nature of the herein studied compounds.
- From the results of the optical properties, we conclude that these semiconductor materials could be useful for specific implementations in ultra-violet optoelectronic devices due to the vast absorption in the UV region.

Finally, these results can be used to aid, accelerate, and guide future experimental works.

Physica B 624 (2022) 413450

Contents lists available at ScienceDirect

Physica B: Physics of Condensed Matter

journal homepage: www.elsevier.com/locate/physb

The first foreseen of structural, mechanical, electronic and optical properties of novel alkali metal tetrafluoridobromate $ABrF_4$ (A=Na, K and Rb)

Ishak Mebarkia [a,*], Aïssa Manallah [a], Rafik Belghit [b]

[a] Applied Optics Laboratory, Institute of Optics and Precision Mechanics, University of Setif 1, 19000, Setif, Algeria
[b] Laboratory Studies of Surface and Interfaces of Solid Materials (LESIMS), Department of Physics, Faculty of Sciences, University Badji Mokhtar, 23000, Annaba, Algeria

ARTICLE INFO

Keywords:
Ab-initio
$ABrF_4$
Optoelectronic properties
Mechanical properties
Semiconductors

ABSTRACT

This study deals with the first theoretical investigation of structural, mechanical, electronic, and optical properties of $ABrF_4$ (A = Na, K, and Rb) ternary compounds using ab-initio calculations within the framework of the density functional theory (DFT) using the pseudo-potential plane-wave method. The structural parameters are in agreement with the experimental values stated in the literature. The elastic constants indicate that these compounds are ductile. For a better and in-depth confirming the anisotropic character of the mechanical properties, several indexes such as the universal anisotropic, and the percentage elastic anisotropy for compression and shear have been investigated. The electronic properties indicate that these compounds are wide-band gap semiconductor materials. The optical properties including the dielectric function, the absorption and extinction coefficients, the optical reflectivity and conductivity, the refractive index, and the energy loss function have been studied in detail. The wide optical absorption range in the ultraviolet (UV) region suggests that these materials could be useful for specific implementations in UV optoelectronic devices; therefore, this theoretical investigation is probable to motivate future experimental works.

1. Introduction

For several years great effort has been devoted to discovering new efficient optical materials that are required for Ultraviolet (UV) region applications in the fields of medical treatment, optical communications, semiconductor processing, electrical and electronics industries … etc. The alkali metal complex fluorides single crystals, that have a large UV optical absorption range, wide-band gaps, and lower refractive indices compared to those of oxides, are promising UV optical materials to fulfill this objective [1,2].

One of the motivating categories belonging to the alkali metal complex fluorides family is known as the alkali metal tetrafluoridobromates, which are inherently centrosymmetric and favorable for optoelectronic technologies, viz., for manufacturing UV optical components for the generation of long-wavelength radiation, optical amplifiers, and diode-pumped lasers … etc [3,4]. The ternary compound of alkali metal tetrafluoridobromate with the general formula $ABrF_4$ consists of sharing one of the alkali elements (A = Na, K, Rb, and Cs) as a cation with BrF_4 anion. Since the 1950s, several attempts have been carried out to determine the crystal structure of $ABrF_4$ (A = Na, K, Rb, and Cs) ternary compounds. During the past century, all syntheses on these crystals executed using powder X-ray diffraction data and powder neutron diffraction data [5–9], have been agreeing that $NaBrF_4$, $KBrF_4$, $RbBrF_4$, and $CsBrF_4$ crystallize in tetragonal space group type I4/mcm (No. 140). While the fractional coordinates of the atoms, the anisotropic displacement parameters, and the standard uncertainties are still vague.

In the recent few years, various experimental methods supported by theoretical calculations have been performed to investigate the synthesis and characterization with higher precision. Ivlev et al. (2016) [10] done the first refinement of the crystal structure of $NaBrF_4$ using single-crystal X-ray diffraction data and indicate that Na, Br, and F atoms are located in the Wyckoff sites 4a (0, 0, 1/4), 4d (1/2, 0, 0) and 16l (0.33524, 0.16476, 0.13080), respectively. They reinforced also this study using of powder X-ray diffraction data, Raman and Infrared spectroscopy, and theoretical studies using first-principles calculations based on the density functional theory (DFT) within the generalized gradient

* Corresponding author. P.O. Box 19000, Setif, Algeria.
E-mail address: ishak.mebarkia@univ-setif.dz (I. Mebarkia).

https://doi.org/10.1016/j.physb.2021.413450
Received 26 December 2020; Received in revised form 6 September 2021; Accepted 27 September 2021
Available online 30 September 2021

approximation (GGA) and local density approximation (LDA). Subsequently, Ivlev and Kraus (2018) [11] redetermined the crystal structure of $KBrF_4$ from single-crystal X-ray diffraction data, where suggest that K, Br, and F atoms occupy the Wyckoff sites 4a (1/2, 1/2, 1/4), 4d (1/2,0, 1/2) and 16l (0.65508, 0.15508, 0.37889), respectively. The same principle was carried out on the $RbBrF_4$ compound in two successive publications, where Ivlev et al. (2015) [12] revisited this compound by powder X-ray diffraction data, also using of Infrared and Raman spectroscopy, as well as theoretical calculations based on hybrid density functional method. Whereas Malin et al. (2019) [13], performed the first determination of the crystal structure of $RbBrF_4$ based on single-crystal X-ray diffraction data, which the authors confirmed that the Wyckoff positions regarding Rb, Br, and F atoms, respectively are 4a (1/2, 1/2, 3/4), 4d (1/2, 0,1/2) and 16l (0.6501, 0.1501, 0.61660).

Recently, research has demonstrated that $CsBrF_4$ crystallizes in orthorhombic structure space group type Immm (No. 71), rather than the tetragonal structure, where Ivlev et al. (2013) [14] executed the synthesis of $CsBrF_4$ crystal using powder X-ray diffraction data process, whereas Malin et al. (2020) [15] has been done the redetermination of this crystal structure using single-crystal X-ray diffraction data to improve the results of the fractional coordinates of the atoms and the anisotropic displacement parameters with high precision.

Due to the high content of bromine trifluoride BrF_3 in these crystals and their chemical characteristics, which makes them useful fluorinating oxidizers in different fields of chemical technologies [16–21]. It is significant to emphasize that until now, neither the experimental studies nor the theoretical calculations were published regarding the fundamental physical properties of these compounds, such as mechanical, electronic, and optical properties, which motivates us to investigate these properties and remove the theoretical lacking of the alkali metal tetrafluoridobromates that crystallize in tetragonal structure ($NaBrF_4$, $KBrF_4$, and $RbBrF_4$).

In the present work, we focus for the first time on the investigation of the structural, mechanical, electronic, and optical properties of $ABrF_4$ (A = Na, K, and Rb) ternary compounds using ab-initio calculations within the framework of density functional theory (DFT). The remainder of the paper is organized as follows, section 2 briefly describes the used computational details, section 3 presents and discusses our obtained results of total energy first-principles calculations. Finally, Section 4 summarizes the results of this work and draws conclusions.

2. Theoretical calculation methods

All first-principle calculations were performed within the framework of the density functional theory (DFT) using the Cambridge Serial Total Energy Package (CASTEP) code based on the plane-wave pseudo-potential (PP-PW) method [22]. The electronic exchange potential was described using the generalized gradient approximation (GGA) with the Perdew-Burke-Ernzerhof (PBE-sol) exchange-correlation function developed especially for solids [23]. The interaction between the valence electrons with ion, nuclei, and the core electrons for the herein treated atoms were described by norm-conserving pseudo-potentials. The pseudo-atomic calculations were performed as the valence electron structures 5s1 for Rb, 4s1 for K, 3s1 for Na, 4s2 4p5 for Br and 2s2 2p5 for F.

The plane-wave basis set cut-off energy was 60 Ry and the Brillouin zone (BZ) sampling with 4 × 4 × 2 mesh of Monkhorst-Pack special k-points [24], which corresponds to 3 irreducible points in the first BZ. The structural parameters were optimized using Broyden-Fletcher-Goldfarb-Shanno (BFGS) minimization [25,26]. The self-consistent convergence of the total energy change 2×10^{-5} eV/atom, the maximum force is 0.05 eV/Å, the maximum stress within 0.1 GPa, and the maximum atom displacement within 0.002 Å.

Table 1
The experimental values of the atom positions in Wyckoff sites of $ABrF_4$ (A = Na, K and Rb) ternary compounds.

	$NaBrF_4$	$KBrF_4$	$RbBrF_4$
Alkali atom	4a (0, 0, 1/4)[a,b]	4c (0, 0, 0)[c] 4a (0, 0, 1/4)[d,e] 4a (1/2, 1/2, 1/4)[f]	4c (0, 0, 0)[g] 4a (0, 0, 1/4)[h] 4a (1/2, 1/2, 3/4)[i]
Br	4d (1/2, 0, 0)[a,b]	4b (0, 1/2, 1/4)[c] 4d (0, 1/2, 0)[d,e] 4d (1/2, 0, 1/2)[f]	4d (0, 1/2, 0)[g,h] 4d (1/2, 0, 1/2)[i]
F	16l (0.6633, −0.1633, 0.1299)[a] 16l (0.33524, 0.16476, 0.13080)[b]	16l (0.161, 0.661, 0.147)[c] 16l (0.152, 0.652, 0.880)[d] 16l (0.152, 0.652, 0.121)[e] 16l (0.65508, 0.15508, 0.37889)[f]	16l (0.1490, −0.3510, 0.1162)[g] 16l (0.151, −0.349, 0.1193)[h] 16l (0.6501, 0.1501, 0.61660)[i]

Note: The experimental values means by.
- Powder X-ray diffraction data: [a]Ref.10, [c]Ref.5, [d]Ref.6, [g]Ref.9, [h]Ref.12.
- Powder neutron diffraction data: [e]Ref.7.
- Single crystal X-ray diffraction data: [b]Ref.10, [f]Ref.11, [i]Ref.13.

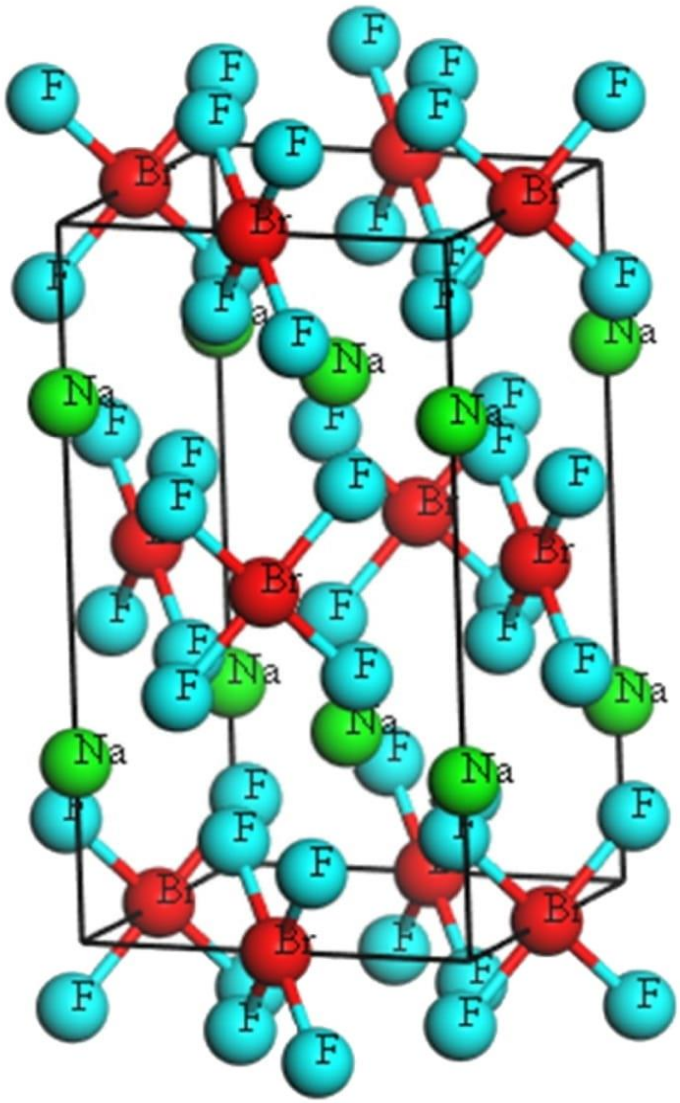

Fig. 1. (Color online) the conventional cell of $NaBrF_4$ compound. (For interpretation of the references to colour in this figure legend, the reader is referred to the Web version of this article.)

Table 2
Lattice constants a and c (in Å), c/a ratio, the internal coordinates of Fluorine atom x_F,y_F and z_F, the bond lengths Br–F and A–F (in Å), the angles F–Br–F# (in °), the Bulk modulus B_0 and its pressure derivative B_0' of $ABrF_4$ (A = Na, K and Rb) ternary compounds.

Compounds	Parameters	Present work	Other calculations	Experimental works
$NaBrF_4$	a	5.7814	5.546[d], 5.788[e]	5.762[a], 5.7848[b], 5.7239[c]
	c	10.4294	10.09[d], 10.44[e]	10.327[a], 10.400[b], 10.331[c]
	c/a	1.8039	1.8193[d], 1.8037[e]	1.7922[a], 1.7978[b], 1.8048[c]
	x_F	0.33452	/	0.6633[b], 0.33524[c]
	y_F	0.16548	/	−0.1633[b], 0.16476[c]
	z_F	0.13140	/	0.1299[b], 0.13080[c]
	Br–F	1.926	1.909[d], 1.933[e]	1.90[b], 1.899[c]
	Na–F	2.4871	2.362[d], 2.487[e]	2.499[b], 2.4674[c]
	F–Br–F#1	89.265	88.6[d], 89.2[e]	89.4[b], 89.25[c]
	F–Br–F#2	90.735	91.4[d], 90.8[e]	90.6[b], 90.75[c]
	B_0	28.09621	/	/
	B′	6.89523	/	/
$KBrF_4$	a	6.1769	/	6.192[a], 6.162[f], 6.174[g], 6.17[h], 6.0999[i]
	c	11.1626	/	11.108[a],11.081[f], 11.103[g], 11.1[h], 11.0509[i]
	c/a	1.8071	/	1.7939[a],1.7982[f], 1.7983[g], 1.7990[h], 1.8116[i]
	x_F	0.65585	/	0.161[f], 0.152[g], 0.152[h], 0.65508[i]
	y_F	0.15585	/	0.661[f], 0.652[g], 0.652[h], 0.15508[i]
	z_F	0.37835	/	0.147[f], 0.880[g], 0.121[h], 0.37889[i]
	Br–F	1.9229	/	1.81[f], 1.88[g], 1.89[h], 1.8924[i]
	K–F	2.7384	/	2.84[f], 2.75[g], 2.77[h], 2.7112[i]
	F–Br–F#1	90.15	/	89.1[h], 89.98[i]
	F–Br–F#2	89.85	/	90.9[h], 90.02[i]
	B_0	20.42155	/	/
	B′	6.42551	/	/
$RbBrF_4$	a	6.3895	6.20[m], 6.94[n]	6.401[a], 6.351[j], 6.37181[k], 6.2991[l]
	c	11.5819	11.74[m], 8.93[n]	11.1538[a], 11.489[j], 11.4934[k], 11.4659[l]
	c/a	1.8126	1.8935[m], 1.2867[n]	1.7425[a], 1.8090[j], 1.8037[k], 1.8202[l]
	x_F	0.6508	0.154[m], 0.1458[n]	0.1490[j], 0.151[k], 0.6501[l]
	y_F	0.1508	−0.346[m], −0.3542[n]	−0.3510[j], −0.349[k], 0.1501[l]
	z_F	0.6171	0.1145[m], 0.1411[n]	0.1162[j], 0.1193[k], 0.61660[l]
	Br–F	1.9225	1.91[m], 1.91[n]	1.8903[j], 1.932[k], 1.8905[l]
	Rb–F	2.8769	2.84[m], 2.94[n]	2.7653[j], 2.851[k], 2.8447[l]
	F–Br–F#1	90.28	89.7[m], 82.7[n]	89.861[j], 90.4[k], 90.01[l]
	F–Br–F#2	89.72	90.3[m], 97.3[n]	90.139[j], 89.6[k], 89.99[l]
	B_0	18.27326	/	/
	B′	6.75771	/	/

Note: [a]Ref.8, [b, c, d, e]Ref.10, [f]Ref.5, [g]Ref.6, [h]Ref.7, [i]Ref.11, [j]Ref.9, [k, m, n]Ref.12, [l]Ref.13.

3. Results and discussion

3.1. Structural properties

$NaBrF_4$, $KBrF_4$, and $RbBrF_4$ compounds crystallize at ambient conditions in the tetragonal structure with the space group I4/mcm (No. 140), where the conventional cell contains four formula units (Z = 4) in which F, Br, and the alkali atoms are predicted experimentally to positioned at the Wyckoff sites given in Table 1.

To determine the equilibrium structural parameters including the lattice parameters (a and c), the internal coordinates of Fluorine atom (x_F, y_F, and z_F), and the inter-atomic distances, we have used the latest experimental parameters obtained by single-crystal X-ray diffraction data to build the initial crystal structure, then both c/a ratio and the internal coordinates x_F, y_F and z_F are relaxed for each volume. The conventional cell of $NaBrF_4$ is illustrated in Fig. 1 as a prototype for the herein studied compounds, where the $[BrF_4]^-$ anion shows the square-planar structure and the coordination of the cation element by F atoms is a square anti-prismatic polyhedron. Table 2 mentions the calculated results for the ground states parameters such as the lattice constants a and c, the tetragonal ratio c/a, the internal coordinates x_F, y_F, and z_F, the bond lengths that connect the Fluorine atom to other elements, the values of minimum and maximum angle F–Br–F, the Bulk modulus B_0 and the Bulk modulus pressure derivative B' for the studied ternary compounds using GGA PBE-sol approximation along with the experimental data, as well as the other theoretical calculations for comparison.

The Bulk modulus B_0 and its pressure derivative B_0' obtained from fitting of the variation total energies (E) versus the associated cell volumes (V) to the following Birch-Murnaghan isothermal equation of states (EOS) [27]:

$$E(V) = E_0 + \frac{9V_0B_0}{16}\left\{\left[\left(\frac{V_0}{V}\right)^{\frac{2}{3}} - 1\right]^3 B_0' + \left[\left(\frac{V_0}{V}\right)^{\frac{2}{3}} - 1\right]^2\left[6 - 4\left(\frac{V_0}{V}\right)^{\frac{2}{3}}\right]\right\} \quad (1)$$

where E_0 and V_0 are the energy and volume at zero pressure, respectively. We can notice that there is an excellent agreement between our calculated results of the optimized structural parameters and the earlier experimental ones for all studied compounds, whereas the results obtained in this study are in good agreement with the available theoretical values expect for the $NaBrF_4$ compound, which the authors took their experimental values obtained from single-crystal X-ray diffraction data, then optimized the structures by LDA PW92 and GGA PBE-sol approximations, contrary to $RbBrF_4$ when the theoretical calculations based on the experimental values obtained by powder X-ray diffraction data and treated by PBE0 hybrid density functional method. We note also the nonexistence of theoretical investigation for the $KBrF_4$ compound.

For $NaBrF_4$, $KBrF_4$ and $RbBrF_4$ compounds, the calculated lattice constants a and c as well as c/a ratio deviate from the measured ones by only (1.0046%, 0.9525%, 0.0499%), (1.2623%, 1.0108%, 0.2484%) and (1.4351%, 1.0117%, 0.4175%), respectively. These insignificant deviations confirm the validity of our performed calculations. Moreover, the lattice constants a and c and the bond lengths that connect the Fluorine atom F to the Alkali elements A increase when the A atom is replaced in the sequence Na→K→Rb in the $ABrF_4$ series. This trend can be justified by the increase of the atomic radii in the same sequence, when ($r^{Na} = 1.90$) < ($r^{K} = 2.43$) < ($r^{Rb} = 2.65$).

The F–Br–F# angles are defined as differing only slightly from 90° and their sum equal 180°, where our calculations have achieved with good coincidence to the experimental and theoretical studies. Furthermore, the bulk modulus calculated in this sub-section will be used later to confirm the reliability of our calculations by comparing it with the corresponding one in the next sub-section.

3.2. Mechanical properties

The examination of the elastic constants and the polycrystalline moduli of crystals have proved their eligibility to realize many mechanical properties such as stability, strength, stiffness, hardness, and brittleness or ductility behavior of materials and some other physical properties, such as inter-atomic potentials, phonon spectra and equation

Table 3
The calculated values of the elastic stiffness constants C_{ij} (in GPa), the ratios C_{33}/C_{11} and C_{66}/C_{44}, the Cauchy pressures $[C_{12}–C_{66}]$ and $[C_{13}–C_{44}]$, and the elastic compliance constants S_{ij} (in 1/GPa) for $ABrF_4$ (A = Na, K and Rb) ternary compounds.

Compounds	$NaBrF_4$	$KBrF_4$	$RbBrF_4$
C_{11}	37.95067	25.94675	21.71127
C_{12}	26.55510	15.94402	12.68495
C_{13}	18.15587	13.96060	15.50370
C_{33}	57.82495	34.06575	33.23418
C_{44}	17.60895	10.26875	9.15633
C_{66}	22.36172	13.00377	9.80792
C_{33}/C_{11}	1.52	1.31	1.53
C_{66}/C_{44}	1.27	1.27	1.07
$C_{12}–C_{66}$	4.19	2.94	2.88
$C_{13}–C_{44}$	0.55	3.69	6.35
S_{11}	0.0532921	0.0664076	0.0804797
S_{12}	−0.0344613	−0.0335651	−0.0303074
S_{13}	−0.0059125	−0.0134593	−0.0234053
S_{33}	0.0210064	0.0403866	0.0519266
S_{44}	0.0567893	0.0973828	0.1092140
S_{66}	0.0447193	0.0769008	0.1019585

of state [28]. Usually, the elastic constants of polycrystalline materials depend on the elastic constants of the component single crystals, and to calculate the elastic constants of polycrystals, numerical simulations of the aggregate mass have been used, or have used some well-known approximations such as those of Voigt, Reuss, and Hill [29].

Since the herein studied compounds crystallize within a tetragonal structure at ambient conditions, six elastic stiffness constants are considered (C_{11}, C_{12}, C_{13}, C_{33}, C_{44}, and C_{66}). The calculated elastic stiffness and compliance constants (C_{ij} and S_{ij}) for $ABrF_4$ (A = Na, K and Rb) ternary compounds, are listed in Table 3. These values can be considered as a reference for future research works because we note the absence of any previous data on the elastic constants in the literature for these studied materials.

According to the following four necessary and sufficient conditions for elastic stability in the tetragonal structures [30]: $C_{11} > |C_{12}|$; $(C_{11}+C_{12})\,C_{33} > 2(C_{13})^2$; $C_{44} > 0$; $C_{66} > 0$, the elastic Stiffness constants C_{ij} of the herein studied compounds as shown in Table 3 confirm the previous mechanical stability conditions showing that $NaBrF_4$, $KBrF_4$, and $RbBrF_4$ compounds are mechanically stable. Moreover, this study has shown that all studied compounds have $C_{33} > C_{11}$ where $C_{33}/C_{11} > 1$ as indicate in Table 3, which specifies that the bonding strength along [001] direction is stronger than the bonding strength along [100] and [010] directions. While $C_{66} > C_{44}$ or $C_{66}/C_{44} > 1$, which indicates that along [100] direction, the shear deformation in the plan (001) is more difficult than the corresponding one in the plan (010).

The polycrystalline moduli of studied compounds in this paper have been calculated by using the Voigt [31] and Reuss [32] approximations. The bulk modulus (B) and shear modulus (G) can be evaluated by the obtained elastic Stiffness constants C_{ij} as follows [33]:

$$B_V = \frac{2(C_{11}+C_{12})+C_{33}+4C_{13}}{9} \tag{2}$$

$$B_R = \frac{(C_{11}+C_{12})C_{33}-2C_{13}^2}{C_{11}+C_{12}+2C_{33}-4C_{13}} \tag{3}$$

$$G_V = \frac{2C_{11}-C_{12}-2C_{13}+C_{33}+6C_{44}+3C_{66}}{15} \tag{4}$$

$$G_R = \frac{15}{\frac{18B_V}{(C_{11}+C_{12})C_{33}-2C_{13}^2}+\frac{6}{(C_{11}-C_{12})}+\frac{6}{C_{44}}+\frac{3}{C_{66}}} \tag{5}$$

In the above equations, the subscripts (V and R) of bulk modulus and shear modulus indicate the Voigt approximation and Reuss approximation, respectively. According to the Hill approximation [34], the polycrystalline moduli (Bulk modulus B, shear modulus G, Young's modulus E, Poisson's ratio ν, and Lamé's coefficients μ and λ) can be estimated by the following equations:

Table 4
The calculated values of Bulk modulus B (in GPa), shear modulus G (in GPa), Young modulus E (in GPa), Poisson ratio ν, Lamé's coefficients μ and λ, Pugh's ratio B/G and Vickers hardness H_V for $ABrF_4$ (A = Na, K and Rb) ternary compounds.

Compounds	$NaBrF_4$	$KBrF_4$	$RbBrF_4$
B_V	28.82888	19.29885	18.22682
B_R	28.55676	19.14445	17.05031
G_V	16.23989	9.51452	7.82174
G_R	12.81612	8.57269	7.07155
B	28.69282	19.22165	17.63857
G	14.52800	9.04361	7.44664
E	37.29029	23.45273	19.58395
ν	0.28339	0.29665	0.31495
μ	14.52804	9.04358	7.44665
λ	19.00749	13.19258	12.67414
B/G	1.9750	2.1254	2.3687
H_V	2.1937	1.3656	1.1244

$$B = \frac{B_V + B_R}{2} \tag{6}$$

$$G = \frac{G_V + G_R}{2} \tag{7}$$

$$E = \frac{9BG}{3B+G} \tag{8}$$

$$\nu = \frac{3B-2G}{6B+2G} \tag{9}$$

$$\mu = \frac{E}{2(1+\nu)} \tag{10}$$

$$\lambda = \frac{\nu E}{(1+\nu)(1-2\nu)} \tag{11}$$

The results of the mechanical properties of our studied compounds are listed in Table 4. We can note the excellent agreement between the values of the bulk modulus calculated from the elastic Stiffness constants C_{ij} as shown in Table 4, and the corresponding ones fitted to the Birch–Murnaghan EOS in the previous sub-section for all studied compounds. This consequence is good proof of the reliability of our calculation. On the other hand, the Bulk modulus value decreases when the alkali atom A is replaced in the following sequence Na→K→Rb in the $ABrF_4$ compounds, suggesting the increase in volume V of the considering compounds, which is in agreement with the Cohen's approximation $B \sim V^{-1}$ [35].

The shear modulus G and the Young modulus E are usually used to predict the rigidity of solids. Our obtained results indicate that G and E moduli decrease when moving from $NaBrF_4$ to $KBrF_4$ to $RbBrF_4$ which fundamentally originates from decrease C_{44} and indicating the diminution in the stiffness of these compounds in the same direction.

Several methods were developed to predict the mechanical nature of the material and classify it as brittle (fragile) or ductile (malleable). In this study, we have used the three most common methods to prove the reliability of our calculation. Pugh [36] has suggested an empirical relationship linking the bulk modulus B to the shear modulus G, when the material is ductile the B/G ratio is greater than 1.75; otherwise, the material is brittle. As shown in Table 4, the values of B/G are larger than 1.75 for all herein studied compounds, which indicate their ductile nature. However, Frantsevich [37] proposed a rule regarding the value of Poisson's ratio ν. If $\nu > 0.26$, the compound is classifying as malleable, while if $\nu < 0.26$, the compound is considered fragile. Our calculated values of Poisson's ratio for $NaBrF_4$, $KBrF_4$, and $RbBrF_4$ compounds are larger than 0.26, signalizing once more the ductile behavior of these

compounds, which is good agreement with Pugh evaluation. Moreover, the criteria of the Cauchy [38] pressures (C_{12}–C_{66}) and (C_{13}–C_{44}) indicating the ductile particularity of the material when the two Cauchy pressures have positive values. As shown in Table 3 the calculated elastic stiffness constants lead to positive values of Cauchy pressures for all studied compounds, which confirm once again that these compounds are mechanically ductile.

One of the usefulness of Poisson's ratio is to inform about the character of the chemical bonding. Regarding the covalent materials, the value of Poisson's ratio is small ($\nu = 0.1$), while for ionic materials it takes higher value ($\nu = 0.25$) [39]. As shown in Table 4, the values of Poisson's ratio for all studied compounds are Close to 0.25, suggesting the ionic character is present in their chemical bonding. Furthermore, the ionic crystals can be classified into two groups via the value of Poisson's ratio: central force crystals and non-central force crystals [40]. For central force crystals, the Poisson's ratio takes a value greater than 0.25 and less than 0.5, whereas for non-central force crystals it equals 0.25 or 0.5 [41]. Since the calculated value of Poisson's ratio for $NaBrF_4$, $KBrF_4$ and $RbBrF_4$ are lying between the range of 0.25–0.50, these compounds present central force.

The hardness of materials is a very important mechanical property in industrial applications, such as used to estimate the corrosion and strength in the machine parts manufacturing industries [42]. Numerous semi-empirical models have been established to calculate the hardness of materials. In this study, we have calculated the Vickers hardness H_V affirmed by Chen, which is linearly correlating with the shear modulus G [43] such as $H_V = 0.151G$. The calculated values of Vickers hardness are listed in Table 4. Which indicates that $NaBrF_4$ is the hardest material between the herein studied compounds.

The micro-cracks existing in the crystals are usually due to elastic anisotropy. Therefore it is significant to estimate the elastic anisotropy in materials with a view to ameliorate their strength and perfect their structure to some extent [44]. In practical terms, every elastic single crystal is anisotropic [45]. In this case, it is worthy to predict theoretically the elastic anisotropy by using some anisotropy indexes, such as:

- The universal anisotropic A^U which is valid to all types of elastic single crystals, as introduced and established by Shivakumar's work [45], based on bulk and shear moduli:

$$A^U = 5\frac{G_V}{G_R} + \frac{B_V}{B_R} - 6 \geq 0 \tag{12}$$

- the percentage elastic anisotropy for compression A_B and shear A_G, as given [44]:

$$A_B = \frac{B_V - B_R}{B_V + B_R} \tag{13}$$

$$A_G = \frac{G_V - G_R}{G_V + G_R} \tag{14}$$

In the relations mentioned above of A^U, A_B, and A_G, the subscripts V and R refer to the Voigt and Reuss estimates, respectively. For an isotropic system, these elastic anisotropy indexes (A^U, A_B, and A_G) take a value of zero, i.e. The magnitude of the deviation of these elastic anisotropy indexes from zero measures the degree of elastic anisotropy possessed by a crystal.

The shear anisotropic factors A_1, A_2, and A_3 are based on the elastic stiffness constants C_{ij}, which give an estimation of the degree of anisotropy in bonding between atoms in different crystallographic planes. Regarding the tetragonal structure, only the shear anisotropic factors along the shear planes (100) and (001) are sufficient and can be written as following [46]:

$$A_1 = A_{(100)} = \frac{4C_{44}}{C_{11} + C_{33} - C_{13}} \tag{15}$$

Table 5
Universal anisotropic index A^U, bulk (compression) and shear anisotropic A_B and A_G, shear anisotropic factors A_1 and A_2 for $ABrF_4$ (A = Na, K and Rb) ternary compounds.

Compounds	A^U	A_B	A_G	A_1	A_2
$NaBrF_4$	1.34526	0.00474	0.11783	1.18451	3.92463
$KBrF_4$	0.55738	0.00402	0.05207	1.27994	2.60004
$RbBrF_4$	0.59943	0.03335	0.05037	1.53000	2.17318

$$A_2 = A_{(001)} = \frac{2C_{66}}{C_{11} - C_{12}} \tag{16}$$

In the situation of an isotropic crystal, the shear anisotropic factors A_1, A_2 must be equal to one, where each value greater or lesser than the unity is a measurement of the level of the mechanical anisotropy in the matter. In this work, these anisotropic indexes have been calculated and listed in Table 5, which suggests that the elastic properties of the herein studied compounds are anisotropic. Moreover, from these calculated values, $NaBrF_4$ exhibits the highest universal anisotropic than the other studied compounds, and we can notice that the percentage elastic anisotropy for shear modulus A_G is larger than the percentage elastic anisotropy for Bulk modulus A_B for all studied compounds, which indicates that the shear modulus appears more grounded directional reliance than the bulk modulus. On the other hand, the shear anisotropic factor A_2 along the shear plane (001) is greater than the shear anisotropic factor A_1 along the shear plane (100), which principally result from the obtained stiffness elastic constants, where $C_{66} > C_{44}$, show the atomic bondings in the crystallographic plane (001) is more anisotropic than the corresponding ones lying on the crystallographic plane (100).

A precious design to check the anisotropy of mechanical properties is plotting the polycrystalline moduli in three-dimensional (3D) space based on the following mechanical moduli (Bulk modulus B, Young's modulus E, shear modulus G and Poisson's ratio ν) with directional dependence for a tetragonal structure:

$$B = \frac{1}{S} \tag{17}$$

$$E = \frac{1}{S'} \tag{18}$$

$$G = \frac{3}{9S' - S} \tag{19}$$

$$\nu = \frac{1}{2}\left(1 - \frac{S}{3S'}\right) \tag{20}$$

where:

$$S = (S_{11} + S_{12} + S_{13})\left(l_1^2 + l_2^2\right) + (2S_{13} + S_{33})l_3^2 \tag{21}$$

$$S' = S_{11}\left(l_1^4 + l_2^4\right) + (2S_{13} + S_{44})\left(l_1^2 l_3^2 + l_2^2 l_3^2\right) + S_{33}l_3^4 + (2S_{12} + S_{66})l_1^2 l_2^2 \tag{22}$$

In the above relations, S_{ij} is the elastic compliance constants; l_1, l_2, and l_3 refer the directional cosines to the x, y, and z axes within spherical coordinates, respectively. For the entire isotropy of any polycrystalline modulus previously mentioned, it takes a sphere form in the 3D space, whereas the curvature from the appearance of the sphere detects the rate of anisotropy. As shown in Fig. 2, for all studied compounds, both young's and shear moduli present a stronger anisotropic degree than that illustrated in bulk modulus and Poisson's ratio. Furthermore, the highest degree of anisotropy for Bulk modulus and the lowest one for shear modulus is showing in the $RbBrF_4$ compound, which affirms the results given in Table 5. In addition to that, for more distinguished the anisotropy of polycrystalline moduli in their crystallographic planes (100), (010), and (001). The projection of the shape of these moduli has been plotted into these planes and showed in Fig. 3. As shown in Fig. 3,

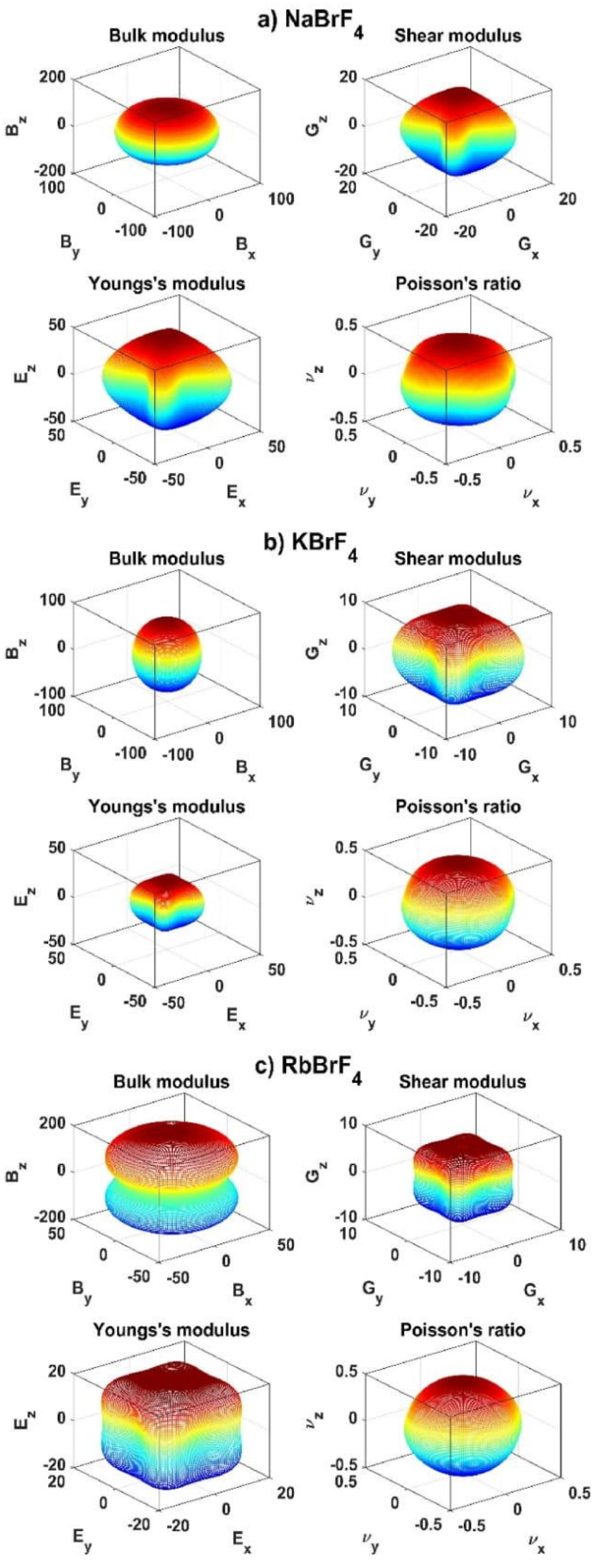

Fig. 2. 3D representation of Bulk modulus "B", shear modulus "G", Young's modulus "E" and Poisson's ratio "ν" for $ABrF_4$ (A = Na, K and Rb) ternary compounds.

the projections on (010) and (100) planes are identical, which is a consequence of the tetragonal structure of the herein studied compounds. We can confirm for all studied compounds that bulk modulus and Poisson's ratio show weaker anisotropic magnitude compared to that of young's and shear moduli, especially in the plane (001) where the bulk modulus appears the shape of the perfect circle. Regarding the shear modulus, it is clear that it showed more anisotropy in the plane (001) than in the (100) plane, which is reliable to the estimation found in Table 5, where $A_{(001)} > A_{(100)}$ for all studied compounds.

The Debye temperature is a significant parameter of a solid, Due to its direct correlation to the thermal conductivity, melting temperature, elastic constants, and polycrystalline moduli [47,48]. Several empirical methods have been developed to calculate Debye temperature θ_D, where, the most common one is proportional to the averaged sound velocity ν_m, by the following equation [48]:

$$\theta_D = \frac{h}{k_B}\left[\frac{3q}{4\pi}\left(\frac{N_A\rho}{M}\right)\right]^{\frac{1}{3}}\nu_m \tag{23}$$

where h and k_B signify Plank's and Boltzmann's constants, respectively; q is the number of atoms in the unit cell, N_A is Avogadro's number, ρ is the density, M is the molecular weight of the solid, and ν_m is the average sound velocity which given by:

$$\nu_m = \left[\frac{1}{3}\left(\frac{2}{\nu_t^3}+\frac{1}{\nu_l^3}\right)\right]^{-\frac{1}{3}} \tag{24}$$

Here, ν_l and ν_t are respectively the longitudinal and transverse sound velocity calculated from shear modulus G, Bulk modulus B, and the density ρ under Navier's relations:

$$\nu_l = \left(\frac{B+\frac{4G}{3}}{\rho}\right)^{\frac{1}{2}} \tag{25}$$

$$\nu_t = \left(\frac{G}{\rho}\right)^{\frac{1}{2}} \tag{26}$$

The calculated parameters, such as Debye temperature θ_D, the density ρ, as well as the average, longitudinal and transverse sound velocity ν_m, ν_l and ν_t, respectively are mentioned in Table 6. Through the results obtained in Table 6, among the herein studied compounds $NaBrF_4$ exhibits the highest Debye Temperature, which implies the largest thermal conductivity and melting temperature, as well as the chemical bonding powerful in the crystal structure and higher hardness, which that in good agreement with our results obtained by calculating the Vickers hardness H_V. Furthermore, we can be noted that the longitudinal sound velocities of all studied compounds are much faster than transverse sound velocities. In this reason and for deeper study of this phenomenon, the longitudinal and transverse sound velocities (ν_l and ν_t, respectively) in the principal directions are calculated and listed in Table 7 using Christoffel's equation [49] based on the elastic stiffness constants C_{ij} and the density ρ as follows:

For [100]:

$$\begin{cases} [100]\nu_l = \sqrt{\dfrac{C_{11}}{\rho}} \\ [001]\nu_{t1} = \sqrt{\dfrac{C_{44}}{\rho}} \\ [010]\nu_{t2} = \sqrt{\dfrac{C_{66}}{\rho}} \end{cases} \tag{27}$$

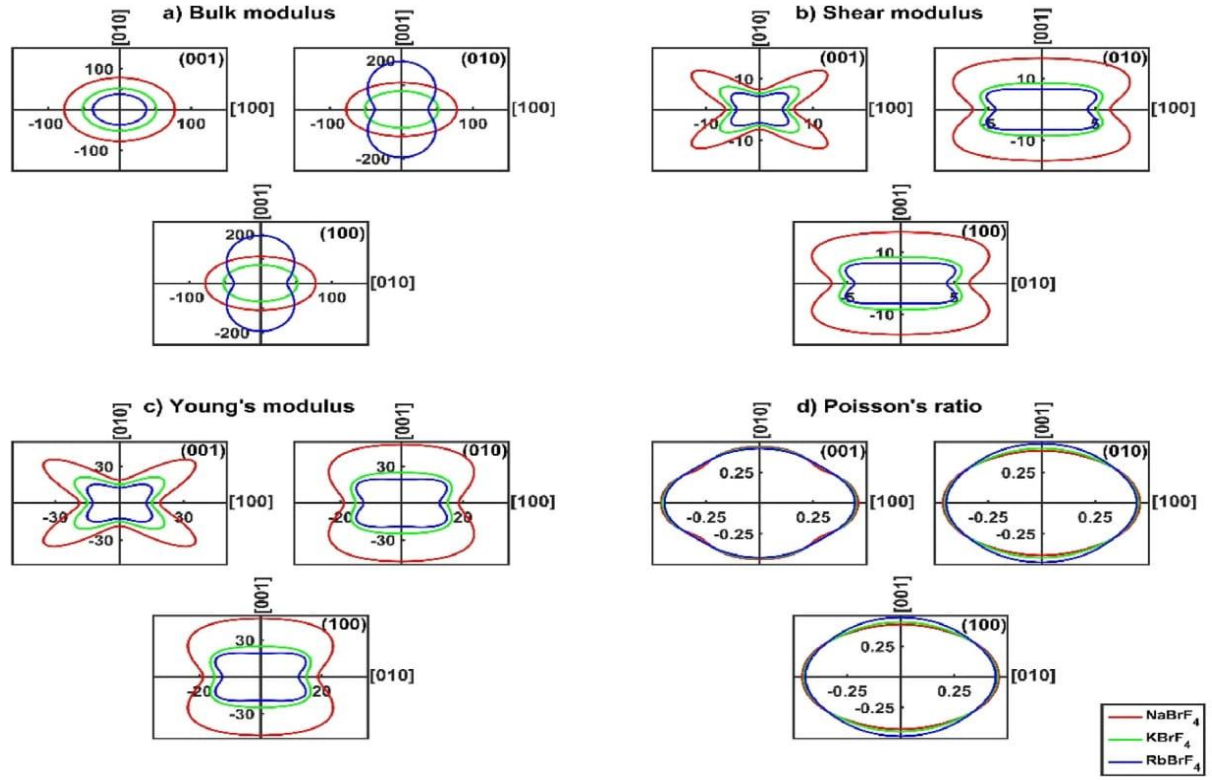

Fig. 3. The planar contours of Bulk modulus "B", shear modulus "G", Young's modulus "E" and Poisson's ratio "ν" for $ABrF_4$ (A = Na, K and Rb) ternary compounds are shown for (001), (010) and (100) crystallographic planes.

Table 6
The elastic Debye temperature θ_D (in K), the density ρ, the average, longitudinal and transverse sound velocity ν_m, ν_l and ν_t (in m/s) for $ABrF_4$ (A = Na, K and Rb) ternary compounds.

Compounds	θ_D	ρ	v_m	v_l	v_t
$NaBrF_4$	278.13220	3.45366	2286.15330	3730.50832	2050.98882
$KBrF_4$	218.54463	3.05692	1920.39024	3198.82194	1720.00226
$RbBrF_4$	181.48469	3.42031	1651.29016	2839.0001	1475.52815

Table 7
The longitudinal and transverse sound velocities in the principal directions (in km/s) for $ABrF_4$ (A = Na, K and Rb) ternary compounds.

Compounds	[100]			[001]			[110]		
	$[100]v_l$	$[001]v_{t1}$	$[010]v_{t2}$	$[001]v_l$	$[100]v_{t1}$	$[010]v_{t2}$	$[110]v_l$	$[100]v_{t1}$	$[1\bar{1}0]v_{t2}$
$NaBrF_4$	3.3149	2.2580	2.5446	4.0918	2.5446	2.5446	3.9766	2.2580	1.2844
$KBrF_4$	2.9134	1.8328	2.0625	3.3382	2.0625	2.0625	3.3325	1.8328	1.2791
$RbBrF_4$	2.5195	1.6362	1.6934	3.1172	1.6934	1.6934	2.8099	1.6362	1.1487

For [001]:

$$\begin{cases} [001]\nu_l = \sqrt{\dfrac{C_{33}}{\rho}} \\ [100]\nu_{t1} = [010]\nu_{t2} = \sqrt{\dfrac{C_{66}}{\rho}} \end{cases} \quad (28)$$

For [110]:

$$\begin{cases} [110]\nu_l = \sqrt{\dfrac{(C_{11}+C_{12}+2C_{66})}{2\rho}} \\ [001]\nu_{t1} = \sqrt{\dfrac{C_{44}}{\rho}} \\ \left[1\bar{1}0\right]\nu_{t2} = \sqrt{\dfrac{(C_{11}-C_{12})}{2\rho}} \end{cases} \quad (29)$$

It is evident that the $NaBrF_4$ compound with large elastic stiffness constants has the fastest sound velocities than the two other compounds. Furthermore, the longitudinal sound velocities of all studied compounds are the fastest along [001] principal direction. The anisotropic shown in sound velocities indicates one more elastic anisotropy for these

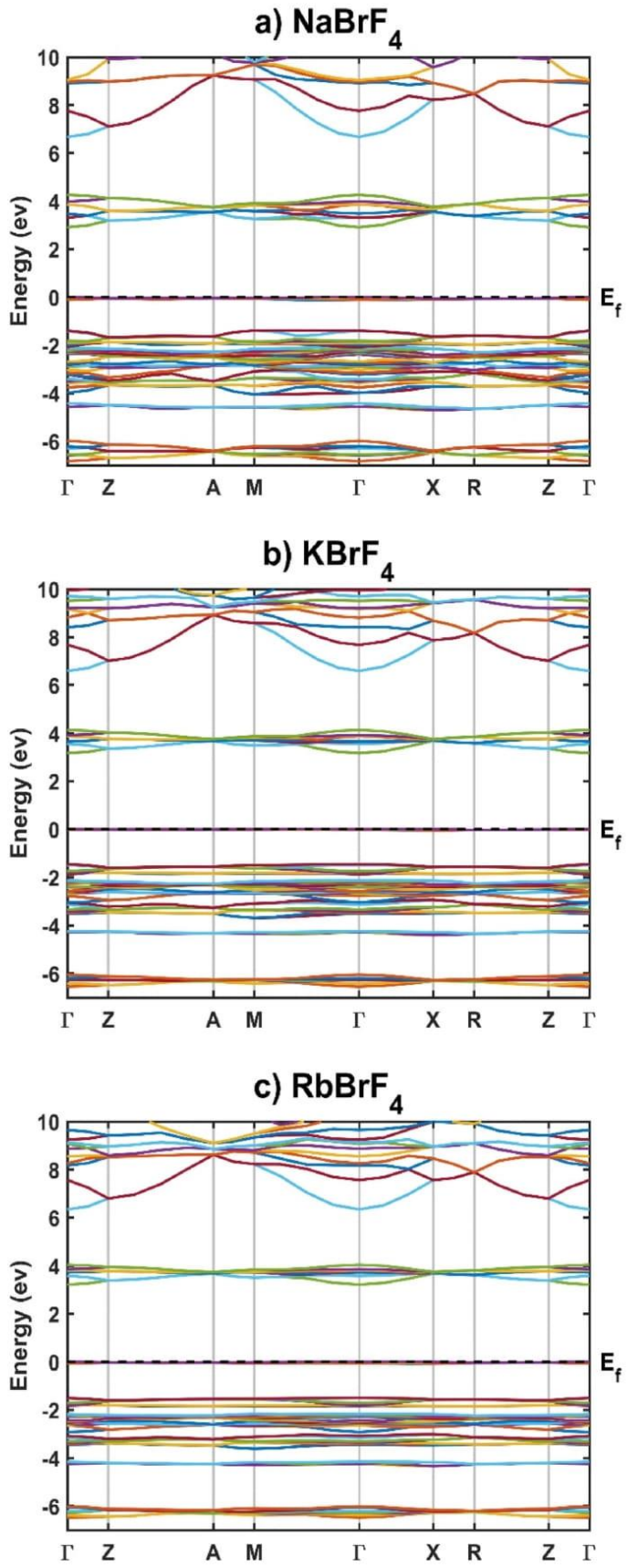

Fig. 4. The band structure of $ABrF_4$ (A = Na, K and Rb) ternary compounds.

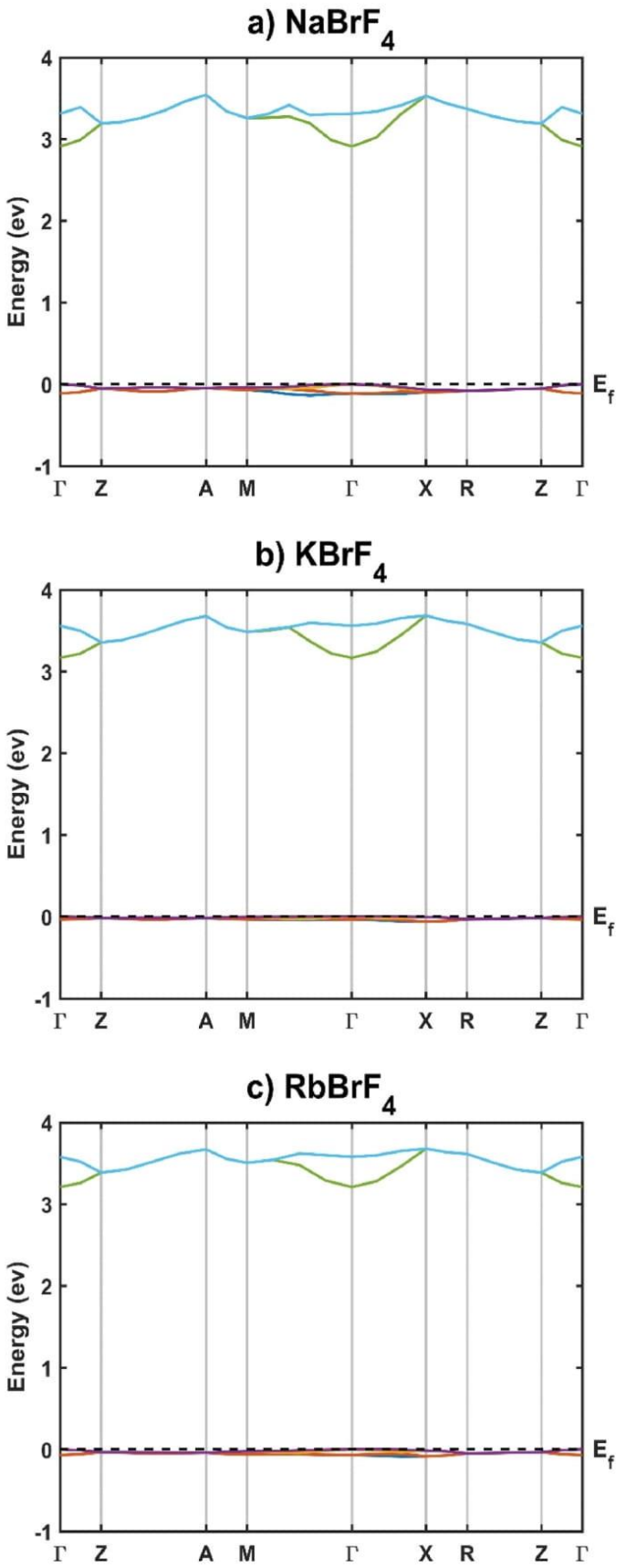

Fig. 5. The enlarged view of the band structure around both maximum valence band and minimum conduction band of $ABrF_4$ (A = Na, K and Rb) ternary compounds.

Table 8
The calculated effective masses (in units of the rest free electron mass m_e) for $ABrF_4$ (A = Na, K and Rb) ternary compounds. m_e^*, m_{hh}^*, and m_{lh}^* stand for, respectively, electron, heavy hole, and light hole.

Compounds	m_e^*	m_{hh}^*	m_{lh}^*
$NaBrF_4$	0,00287	0,02654	0,01165
$KBrF_4$	0,00307	0,22,927	0,01875
$RbBrF_4$	0,00272	0,06963	0,01705

compounds.

Since there are no previous experimental and theoretical data reported in the literature for $NaBrF_4$, $KBrF_4$, and $RbBrF_4$ ternary compounds, we can consider our results as the first prediction of their mechanical properties.

3.3. Electronic properties

In this sub-section, the electronic band structure along the Brillouin zone (BZ) high symmetry lines for $ABrF_4$ (A = Na, K and Rb) ternary compounds are depicted in Fig. 4. The horizontal dashed line positioned at 0 eV clarifies the Fermi level E_F, where the highest energy of the valence band has been selected. The Enlarged view of the band structure around both the maximum of the valence band (VBM) and the minimum of the conduction band (CBM) have been plotted in Fig. 5.

The gap between the conduction and valence bands calculated in this study is 2.909 eV, 3.166 eV, and 3.210 eV for $NaBrF_4$, $KBrF_4$, and $RbBrF_4$, respectively, which gives these compounds the property to become wide-band gap semiconductor materials. As shown in Fig. 5. $NaBrF_4$ is a semiconductor compound with a direct band gap, owing to its VBM and its CBM are sited at Γ point, whereas, $KBrF_4$ and $RbBrF_4$ are semiconductors compounds together with an indirect band gap, which their VBM are located near the point Γ in the Γ-X direction, while their CBM situated at the Γ point. We can note also that the highest electronegativity value of Na atom (χ^{Na}) makes the band gap of $NaBrF_4$ the smallest among the other compounds, where according to Pauling scale we find: ($\chi^{Na} = 0.93$) > ($\chi^{K} = \chi^{Rb} = 0.82$). These results can be considered as a source for future research work since there are no experimental or theoretical band gap values for all studied compounds.

It is clear in Fig. 5, that the topmost part of the valence band (VB) is quasi flat and less dispersive than the lower part of the conduction band (CB), which indicates that the VB holes are heavier than the CB electrons, hence, the VB holes are less mobile than the CB electrons and consequently, the electrons are localized [50]. Furthermore, the contribution of the electrons to the conductivity is predicted to be higher than that of the holes. Thereby, the predominant ionic nature of the chemical bonding is predicted in $ABrF_4$ (A = Na, K and Rb) ternary compounds. We can note also that the VBM appears less dispersive in both $KBrF_4$ and $RbBrF_4$ compounds than that of $NaBrF_4$.

For semiconductors, the effective mass of the charge carriers is an appropriate descriptor of the electronic band structure, which is used to identify the effective density of states and carrier concentrations [51, 52]. The parabolic effective mass approach is one of the best methods applied to calculate the effective mass (m^*) by the parabolic fitting of the E(k) diagram (the energy E versus the wave vector k) around the CBM or the VBM, in agreement with the following relation [53,54]:

$$\frac{1}{m^*} = \frac{1}{\hbar^2}\frac{\partial^2 E(k)}{\partial k^2} \tag{30}$$

where $\hbar$ is the reduced Planck constant. The calculated values of the effective mass for electrons m_e^*, heavy holes m_{hh}^* and light holes m_{lh}^* are

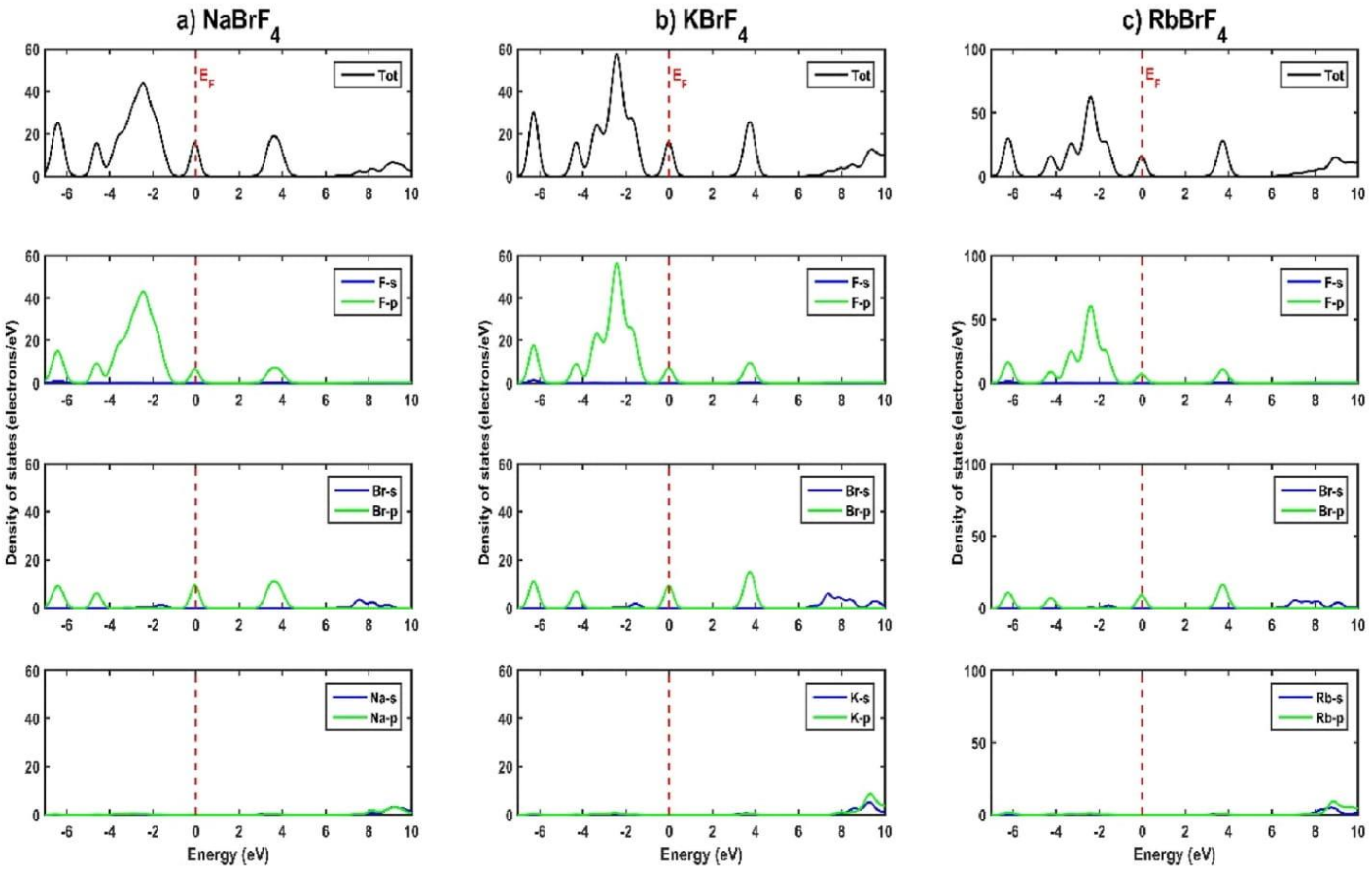

Fig. 6. The calculated total and partial densities of states for $ABrF_4$ (A = Na, K and Rb) ternary compounds.

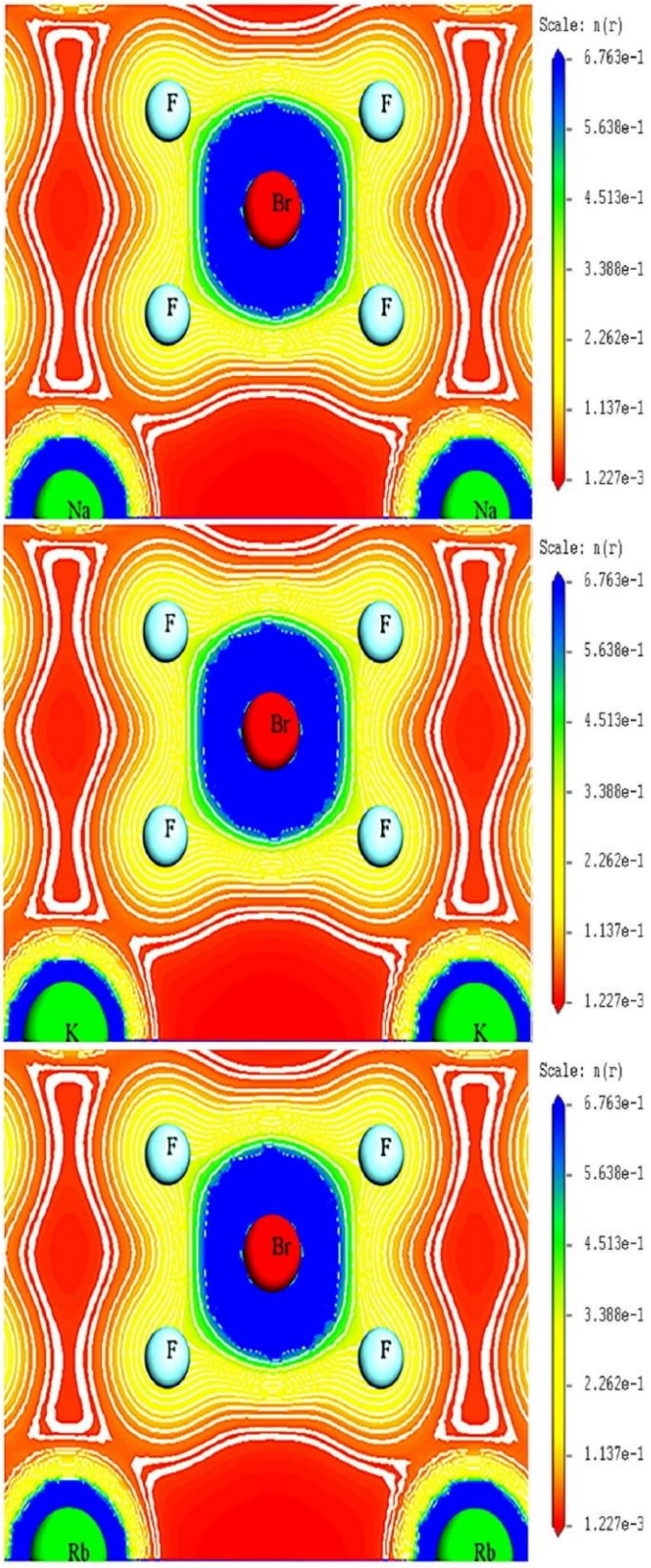

Fig. 7. 2D representation of the calculated valence charge densities in the (010) crystallographic plane for $ABrF_4$ (A = Na, K and Rb) ternary compounds.

mentioned in Table 8 for the herein studied compounds. The obtained data show that the value of the effective hole mass is greater than the value of the effective electron mass for all herein studied compounds, which confirm that the VB holes are heavier than the CB electrons, and suggesting that $ABrF_4$ (A = Na, K and Rb) materials are p-type semiconductors. On the other hand, the calculated electron effective mass is smaller in $RbBrF_4$ than that of $NaBrF_4$ and is much smaller than that of $KBrF_4$. Thus our computations predict higher mobility of electrons in $RbBrF_4$ relative to both $NaBrF_4$ and $KBrF_4$.

For understanding the electronic nature better and deeper, the total density of states (TDOS) and partial density of states (PDOS) of all studied compounds are plotted in Fig. 6, where the Fermi level E_F is considered as the origin of energies. As shown in Fig. 6, the profile of the density of states of the semiconductors compounds with indirect band gap (IBS) such as $KBrF_4$ and $RbBrF_4$, is almost similar with slight differences can be noted, while the $NaBrF_4$ semiconductor compound with direct band gap (DBS) has a different profile of the density of states. We can note that for all studied compounds, the valence band is dominated by F "p" states with a small contribution of Br "p" states. Whereas, the conduction bands are primarily Br, F, and the alkali element "p" like states with a little participation of Br and the alkali atom "s" states.

Furthermore, to understanding the nature of chemical bonding between the different atoms, the maps of the valence charge densities in the (010) plane for $ABrF_4$ (A = Na, K and Rb) ternary compounds are plotted in Fig. 7. It is clear that the ionic character appears in the region between A^+ cations and $(BrF_4)^-$ anions, where demonstrates the reliability of our previously obtained results of Poisson's ratio value and band structure form.

3.4. Optical properties

When the materials interact with an external electromagnetic field such as light, the response of the matter generally depends on the frequency of this field. During this interaction (light-matter), the optical properties of the material appear. The main optical parameters of the material such as absorption coefficient$\alpha(\omega)$, extinction coefficient $k(\omega)$, optical reflectivity $R(\omega)$, refractive index $n(\omega)$, optical conductivity $\sigma(\omega)$, and energy loss function $L(\omega)$ can be calculated from its dielectric permittivity ε, where it is often treated as a complex function of the angular frequency ω of the applied field:

$$\varepsilon(\omega) = \varepsilon_1(\omega) + i\varepsilon_2(\omega) \tag{31}$$

where $\varepsilon_1(\omega)$is the real part of the dielectric function which can be estimated from the imaginary part $\varepsilon_2(\omega)$ using the normalized Kramers-Kronig relation based on the principal value of the Cauchy integral "P" as follows [55]:

$$\varepsilon_1(\omega) = 1 + \frac{2}{\pi} P \int_0^{+\infty} \frac{\omega' \varepsilon_2(\omega')}{\omega' 2 - \omega^2} d\omega' \tag{32}$$

As $ABrF_4$ (X = Na, K and Rb) ternary compounds are crystallized in tetragonal structure, the dielectric functions include only two components ε^{xx} and ε^{zz}, where ε^{xx} concerning the polarization of the applied electric field E along the x and y directions (i.e. $E \perp$ c-axis), while ε^{zz} is related to the polarization of E along z direction (i.e. $E \parallel$ c-axis) [56].

In this study, optical spectra of both perpendicular and parallel to the electric field are plotted versus photon energy in the range of (0–40 eV) for the herein studied compounds.

Fig. 8 displays the real and the imaginary parts of the dielectric function for $ABrF_4$ (A = Na, K, Rb), where we can notice that the peaks are move and shift towards the lowermost energy region by replacing the alkali atoms from Na to K to Rb, which this behavior is shown previously in the calculations of the band structure and the density of states. Furthermore, it is clear that the anisotropy between the components of the dielectric function at the energy region less than 25 eV, makes ε^{zz} the

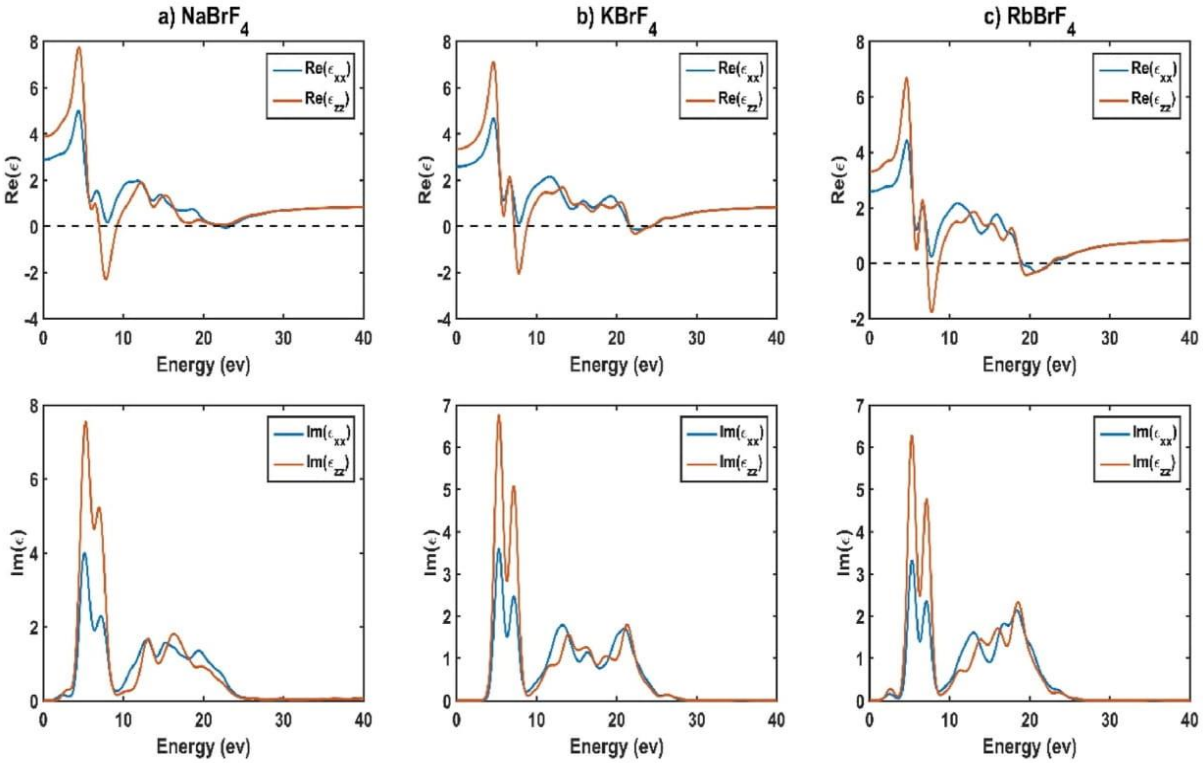

Fig. 8. The spectra of the real and the imaginary parts of dielectric function for $ABrF_4$ (A = Na, K and Rb) ternary compounds.

Table 9
Calculated the maximum peak values of $\varepsilon_2^{xx}(\omega)$ and $\varepsilon_2^{zz}(\omega)$, the static dielectric constant $\varepsilon_1^{xx}(0)$ and $\varepsilon_1^{zz}(0)$, the zero frequency limit of the reflectivity $R^{xx}(0)$ and $R^{zz}(0)$ and the static refractive index $n^{xx}(0)$ and $n^{zz}(0)$ for $ABrF_4$ (A = Na, K and Rb) ternary compounds.

Compounds	$NaBrF_4$	$KBrF_4$	$RbBrF_4$
$\varepsilon_2^{xx}(\omega)$	5.13	5.31	5.31
$\varepsilon_2^{zz}(\omega)$	5.27	5.31	5.28
$\varepsilon_1^{xx}(0)$	2.88	2.58	2.57
$\varepsilon_1^{zz}(0)$	3.88	3.34	3.30
$R^{xx}(0)$	0.07	0.06	0.05
$R^{zz}(0)$	0.11	0.09	0.08
$n^{xx}(0)$	1.697	1.607	1.606
$n^{zz}(0)$	1.969	1.828	1.815

dominant component for these compounds.

The imaginary part of the dielectric constant ε_2 (called also the absorptive part) has a significant peak located at the lower energy region with a small shift between the two components ε_2^{xx} and ε_2^{zz} for both $NaBrF_4$ and $RbBrF_4$ compounds. The energy values corresponding to these prominent peaks are given in Table 9, which these energies originate from the optical transition between the highest occupied valence band and the lowest unoccupied conduction band.

Regarding the absorption spectra displayed in Fig. 9, where represent the maximum absorbance in the ultraviolet (UV) optical range, which the first main peaks situated around 5.6 eV, proposes that these ternary compounds can be used for the production of the specified UV optoelectronic devices. Furthermore, the absorption thresholds start at about 2.98 eV for $NaBrF_4$, 3.17 eV for $KBrF_4$, and 3.23 eV for $RbBrF_4$, which is closely enough to the calculated band gap. Moreover, the absorption curves show a fast decrease in the higher most energy region, which is the typical feature of semiconductor compounds.

The real part of the dielectric function ε_1 (called also the dispersive part), has prominent peaks situated around 4.45 eV, 4.60 eV, and 4.62 eV for $NaBrF_4$, $KBrF_4$, and $RbBrF_4$, respectively. The most important point in the spectrum of the real part, is the zero frequency limit $\varepsilon_1(0)$ i.e when the curves of $\varepsilon_1(\omega)$ cross zero frequency, which represents the dielectric response of the material to a static electric field according to the Drude behavior. The calculated values $\varepsilon_1^{xx}(0)$ and $\varepsilon_1^{zz}(0)$ for $ABrF_4$ (A = Na, K and Rb) ternary compounds are mentioned in Table 9. It is clear that the value of $\varepsilon_1(0)$ decreases when moving from Na to Rb, whereas the value of the band gaps as we find out in the electronic properties increase in the same direction, which indicates an inversely proportional relationship between the energy gap Eg and the zero-frequency limit of dielectric function $\varepsilon(0)$ according to Penn model [57]:

$$\varepsilon(0) = 1 + \left(\frac{\hbar\omega_p}{E_g}\right)^2 \tag{33}$$

where ω_p is the plasma frequency and $\hbar$ is the reduced Planck constant. Fig. 9, displays also the spectra of the extinction coefficient $k(\omega)$. The maximum peak of $k(\omega)$ corresponding to the energies 7.46 eV, 7.51 eV and 7.45 eV, for $NaBrF_4$, $KBrF_4$ and $RbBrF_4$, respectively. Where this energies value corresponds to the zero of the real part of the dielectric function $\varepsilon_1(\omega)$. In the fact, the value of $\varepsilon_1(\omega)$ equals to zero means the non-existence of the dispersion on the material, and consequently due to the greater value of the extinction coefficient $k(\omega)$ than the reflectivity $R(\omega)$ as shown in Fig. 10. Furthermore, the zero-frequency of reflectivity $R(0)$ for herein studied compounds is mentioned in Table 9.

The variation of the refractive index n as a function of the angular frequency ω showed the phenomenon of dispersion, as displayed in Fig. 10, where $n(\omega)$ profile closely follows the shape of the dispersive part $\varepsilon_1(\omega)$ spectrum. The prominent peak value of the refractive index found at about 4.59 eV, 4.72 eV, and 4.73 eV for $NaBrF_4$, $KBrF_4$ and $RbBrF_4$, respectively. As we previously demonstrated, the dispersion phenomenon does not exist when the $\varepsilon_1(\omega)$ equals to zero. For this reason, we find the value of the refractive index is approximately equal to one. Whereas the value of the refractive index (strictly equals one), is corresponding to the absolute vacuum when the phenomena of

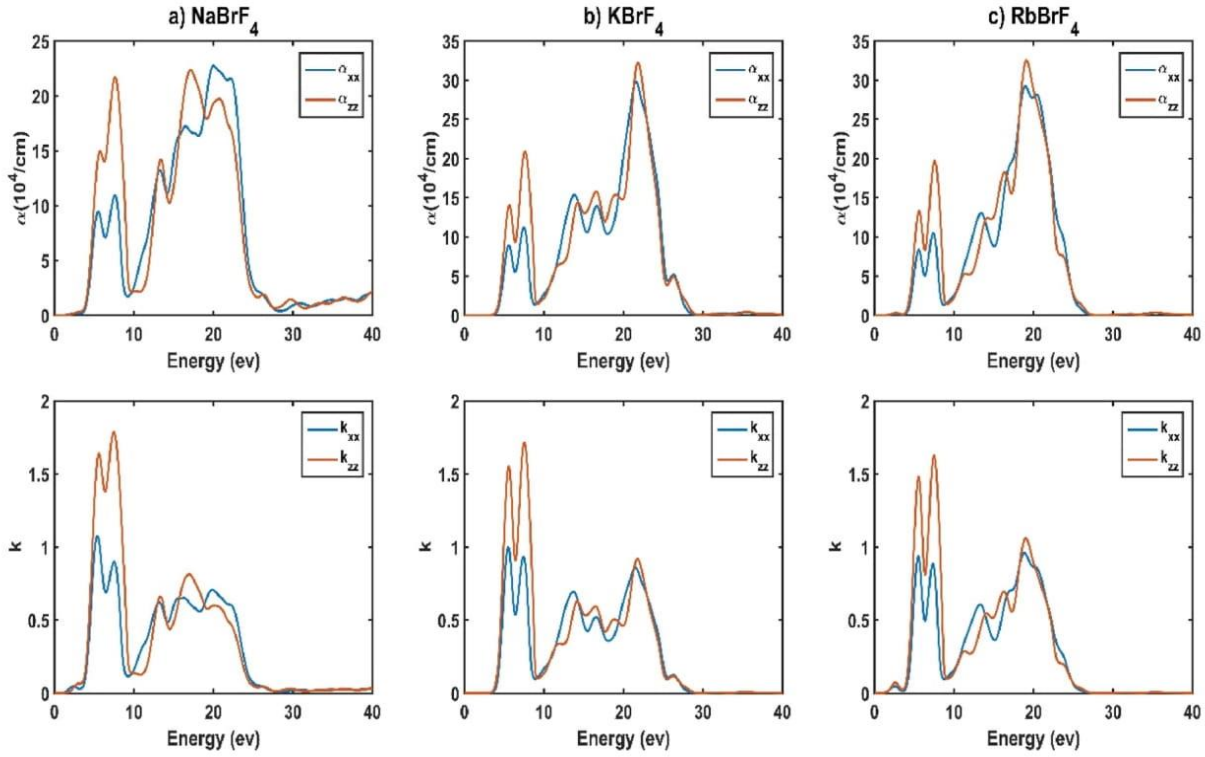

Fig. 9. The spectra of the absorption coefficient "α" and the extinction coefficient "k" for $ABrF_4$ (A = Na, K and Rb) ternary compounds.

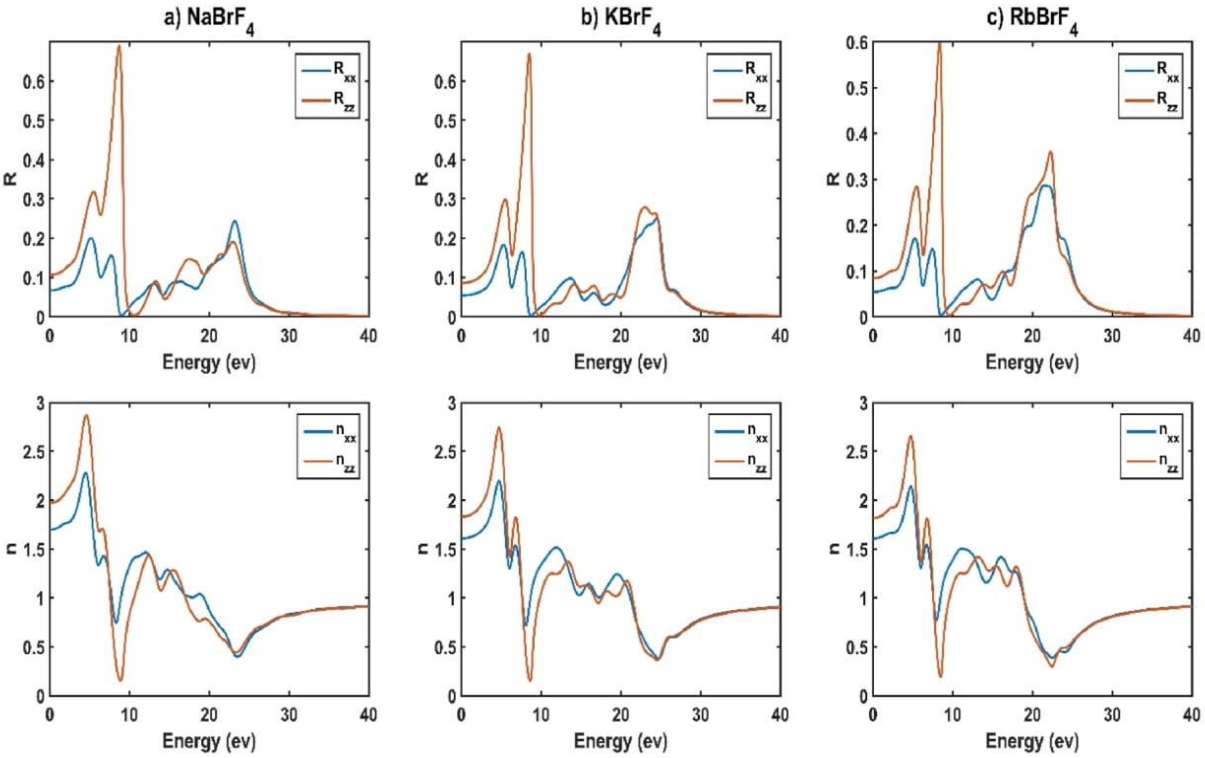

Fig. 10. The spectra of the optical reflectivity "R" and the refractive index "n" for $ABrF_4$ (A = Na, K and Rb) ternary compounds.

refraction or dispersion of light are absolutely absent. It is important to note that in this energy region (from 7.4 to 7.6 eV) and in the higher energy region (higher than 25 eV) the two components of the refractive index are collinear, while outside these energy intervals, the materials show the optical property of birefringence. Furthermore, The obtained results of the static refractive index n (0) are mentioned in Table 9, which confirms the values calculated by the semi-empirical relation $n(0) = \sqrt{\varepsilon_1(0)}$, and indicating the reliability of our results.

The increase in the number of free transporters created when photons are absorbed results an increase in electrical conductivity, hence

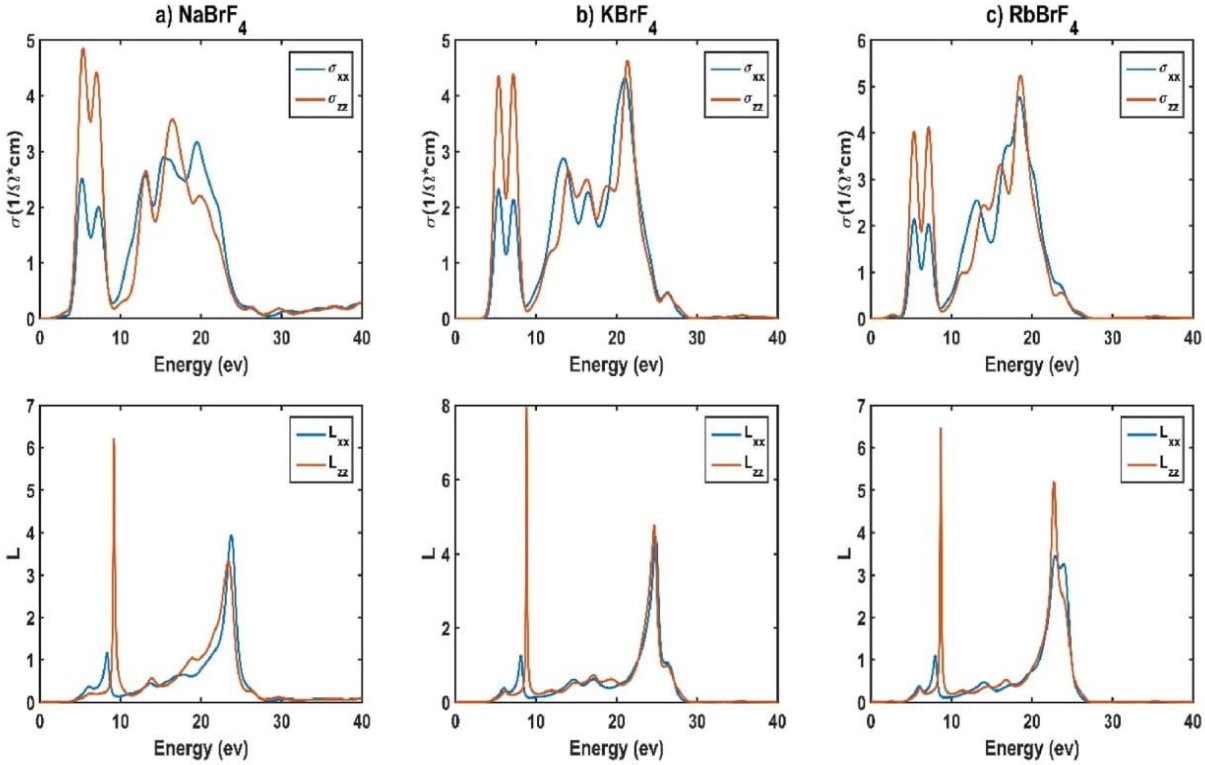

Fig. 11. The spectra of the optical conductivity "σ" and the energy loss function "L" for $ABrF_4$ (A = Na, K and Rb) ternary compounds.

the photoconductivity effect has been established, as shown in Fig. 11, the shape of the optical conductivity shares similar characteristics with the absorptive part $\varepsilon_2(\omega)$ spectrum. Moreover, the photoconductivity does not appear when the photon energy is below the gap energy corresponding to the herein studied compounds, i.e. the photons do not have energy sufficient enough to overcome the band gap in these semiconductors compounds [58].

The fast-moving electron in the material is losing energy and it depends on the photon energy [59]. In order to understand more of this phenomenon, we plotted the energy loss function $L(\omega)$ in Fig. 11. The photon energy values corresponding to the prominent peaks of the energy loss function are 9.18 eV, 8.83 eV, and 8.66 eV for $NaBrF_4$, $KBrF_4$, and $RbBrF_4$, respectively. We can notice that the highest value of loss energy depends on plasma energy $\hbar\omega_p$ which the plasma resonance occurs when the absorptive part $\varepsilon_2(\omega)$ takes a smallest value and the dispersive part $\varepsilon_1(\omega)$ reaches zero again.

This study demonstrates the first investigation of the optical properties for $NaBrF_4$, $KBrF_4$, and $RbBrF_4$ compounds. For that, we hope our calculation can help to offer theoretical grounds for future experimental applications on these compounds.

4. Conclusion

In this paper, we have studied the structural, mechanical, electronic and optical properties of alkali metal tetrafluoridobromate $NaBrF_4$, $KBrF_4$, and $RbBrF_4$ using the pseudo-potential plane-wave method within the generalized gradient approximation. The obtained results can be summarized as follow:

- The results of structural properties, such as the ground states parameters are in good agreement with the earlier experimental values.
- Based on the results of elastic constants and polycrystalline moduli, it can be concluded that these ternary compounds have ductile behavior, and among them, the $NaBrF_4$ compound exhibits the largest thermal conductivity and presents the hardest and stiffest material.
- The outcome of our investigation in electronic properties indicates that $NaBrF_4$ is a semiconductor material with a direct band gap, whereas, $KBrF_4$ and $RbBrF_4$ are semiconductors materials with indirect band gap.
- Both elastic and electronic properties including the Poisson's ratio, the band structure form, and the maps of the valance charge densities manifest obvious the ionic nature of the herein studied compounds.

Furthermore, the optical properties such as the real and the imaginary parts of the dielectric function, the absorption and the extinction coefficients, the optical reflectivity, the refractive index, the photoconductivity, and the energy loss function have been studied in details. The vast absorption in the UV region suggests that these materials could be useful for specific implementations in UV optoelectronic devices.

Author contribution statements

Ishak Mebarkia: Software, Investigation, Writing – original draft, and Visualization. **Aïssa Manallah:** Supervision. **Rafik Belghit:** Conceptualization, Methodology, and Validation.

Declaration of competing interest

The authors declare that they have no known competing financial interests or personal relationships that could have appeared to influence the work reported in this paper.

References

[1] S. Stepleton, Synthesis of Complex Fluorides for Optical Applications, All Diss, 2009. https://tigerprints.clemson.edu/all_dissertations/418. (Accessed 7 July 2021).
[2] A. Stevenson, H. Serier-Brault, … P.G.-J. of F., undefined 2011, Fluoride materials for optical applications: Single crystals, ceramics, glasses, and glass–ceramics,

Elsevier. (n.d.). https://www.sciencedirect.com/science/article/pii/S002211391100282X (accessed July 7, 2021).
[3] O. Materials, Bulk Crystal Growth of Electronic, Optical & Wiley Series in Materials for Electronic and Optoelectronic, 2005.
[4] R. Burkhalter, I. Dohnke, J. Hulliger, Growing of Bulk Crystals and Structuring Waveguides of Fluoride Materials for Laser Applications, 2001, https://doi.org/10.1016/S0960-8974(01)00002-X.
[5] S. Siegel, The crystal structure of KBrF 4, Acta Crystallogr. 9 (1956) 493–495, https://doi.org/10.1107/s0365110x56001340.
[6] W.G. Sly, R.E. Marsh, A note on the structure of $KBrF_4$, Acta Crystallogr. 10 (1957) 378–379, https://doi.org/10.1107/S0365110X57001139.
[7] A.J. Edwards, G.R. Jones, Fluoride crystal structures. Part VIII. Neutron diffraction studies of potassium tetrafluorobromate(III) and potassium tetrafluoroaurate(III), J. Chem. Soc. A Inorganic, Phys. Theor. Chem. (1969) 1936–1938, https://doi.org/10.1039/J19690001936.
[8] A.I. Popov, Y.M. Kiselev, V.F. Sukhoverkhov, N.A. Chumaevskij, O. A. Krasnyanskaya, A.T. Sadikova, Investigation of thermal stability of alkali metal tetrafluorobromates (3), Zh. Neorg. Khim. 32 (1987) 5.
[9] A.R. Mahjoub, A. Hoser, J. Fuchs, K. Seppelt, Die Struktur von BrF6⊖ und verwandten Verbindungen, Angew. Chem. 101 (1989) 1528–1529, https://doi.org/10.1002/ange.19891011108.
[10] S.I. Ivlev, R.V. Ostvald, F. Kraus, A new look at NaBrF4: the most BrF3-rich tetrafluoridobromate(III) by mass, Monatshefte Fur Chemie 147 (2016) 1661–1668, https://doi.org/10.1007/s00706-016-1799-2.
[11] S.I. Ivlev, F. Kraus, Redetermination of the crystal structure of K[BrF 4] from single-crystal X-ray diffraction data, IUCrData 3 (2018), https://doi.org/10.1107/s2414314618006466.
[12] S.I. Ivlev, A.J. Karttunen, R. Ostvald, F. Kraus, RbBrF4 revisited, Zeitschrift Fur Anorg. Und Allg. Chemie. 641 (2015) 2593–2598, https://doi.org/10.1002/zaac.201500647.
[13] A.V. Malin, S.I. Ivlev, R.V. Ostvald, F. Kraus, Rubidium tetrafluoridobromate(III): redetermination of the crystal structure from single-crystal X-ray diffraction data, IUCrData 4 (2019), https://doi.org/10.1107/s2414314619015955.
[14] S. Ivlev, P. Woidy, V. Sobolev, I. Gerin, R. Ostvald, F. Kraus, On tetrafluorobromates(III): crystal structures of the dibromate CsBr 2F7 and the monobromate CsBrF4, Zeitschrift Fur Anorg. Und Allg. Chemie. 639 (2013) 2846–2850, https://doi.org/10.1002/zaac.201300290.
[15] A.V. Malin, S.I. Ivlev, R.V. Ostvald, F. Kraus, Redetermination of the crystal structure of caesium tetrafluoridobromate(III) from single-crystal X-ray diffraction data, IUCrData 5 (2020) 3–8, https://doi.org/10.1107/s2414314620001145.
[16] V.N. Mitkin, A.A. Galitsky, T.M. Korda, Application of fluoroxidants for the decomposition and analysis of platinum metals and gold in black shale ores, Fresenius' J. Anal. Chem. 365 (1999) 374–376, https://doi.org/10.1007/s002160051504.
[17] V.N. Mitkin, Physical-chemical basis for application of fluoroxidants in noble metal analytical chemistry, Spectrochim. Acta Part B At. Spectrosc. 56 (2001) 135–175, https://doi.org/10.1016/S0584-8547(00)00303-7.
[18] V.N. Mitkin, S.B. Zayakina, G.N. Anoshin, New technique for the determination of trace noble metal content in geological and process materials, Spectrochim. Acta Part B At. Spectrosc. 58 (2003) 311–328, https://doi.org/10.1016/S0584-8547(02)00154-4.
[19] V.N. Mitkin, S.B. Zayakina, V.G. Tsimbalist, A.A. Galizky, Application of potassium tetrafluorobromate to the rapid decomposition and determination of noble metals in chromites and related materials, Spectrochim. Acta Part B At. Spectrosc. 58 (2003) 297–310, https://doi.org/10.1016/S0584-8547(02)00155-6.
[20] S. Ivlev, P. Woidy, F. Kraus, I. Gerin, R. Ostvald, Tetrafluorobromates for urban mining of noble metals: a case study on iridium metal, Eur. J. Inorg. Chem. (2013) 4984–4987, https://doi.org/10.1002/ejic.201300618.
[21] T. Shishimi, S. Hara, BrF3-KHF2: an air-stable fluorinating reagent, J. Fluor. Chem. 168 (2014) 55–60, https://doi.org/10.1016/j.jfluchem.2014.08.019.
[22] S.J. Clark, M.D. Segall, C.J. Pickard, P.J. Hasnip, M.I.J. Probert, K. Refson, M. C. Payne, First principles methods using CASTEP, Zeitschrift Fur Krist 220 (2005) 567–570, https://doi.org/10.1524/zkri.220.5.567.65075.
[23] J.P. Perdew, A. Ruzsinszky, G.I. Csonka, O.A. Vydrov, G.E. Scuseria, L. A. Constantin, X. Zhou, K. Burke, Restoring the density-gradient expansion for exchange in solids and surfaces, Phys. Rev. Lett. 100 (2008) 1–4, https://doi.org/10.1103/PhysRevLett.100.136406.
[24] Hendrik J Monkhorst, J.D. Pack, Special points for brillouin-zone integration Monkhorst and pack, Phys. Rev. B 13 (1976) 5188–5192. http://prb.aps.org/pdf/PRB/v13/i12/p5188_1.
[25] T.H. Fischer, J. Almlöf, General methods for geometry and wave function optimization, J. Phys. Chem. 96 (1992) 9768–9774, https://doi.org/10.1021/j100203a036.
[26] B.G. Pfrommer, M. Côté, S.G. Louie, M.L. Cohen, Relaxation of crystals with the quasi-Newton method, J. Comput. Phys. 131 (1997) 233–240, https://doi.org/10.1006/jcph.1996.5612.
[27] F. Birch, Finite elastic strain of cubic crystals, Phys. Rev. 71 (1947) 809–824, https://doi.org/10.1103/PhysRev.71.809.
[28] R. Belghit, H. Belkhir, D. Heciri, M. Bououdina, M.T. Kadri, R. Ahuja, First principles study of structural, mechanical and electronic properties of the ternary alkali metal oxides KNaO and RbNaO, Chem. Phys. Lett. 706 (2018) 684–693, https://doi.org/10.1016/j.cplett.2018.07.013.
[29] S. Chandrasekar, S. Santhanam, A calculation of the bulk modulus of polycrystalline materials, J. Mater. Sci. 24 (1989) 4265–4267, https://doi.org/10.1007/BF00544497.
[30] F. Mouhat, F.X. Coudert, Necessary and sufficient elastic stability conditions in various crystal systems, Phys. Rev. B Condens. Matter 90 (2014), https://doi.org/10.1103/PhysRevB.90.224104, 0–3.
[31] W. Voigt, Lehrbuch der Kristallphysik, 1966, https://doi.org/10.1007/978-3-663-15884-4.
[32] A. Reuss, Berechnung der Fließgrenze von Mischkristallen auf Grund der Plastizitätsbedingung für Einkristalle, ZAMM - J. Appl. Math. Mech./Z. Angew. Math. Mech. 9 (1929) 49–58, https://doi.org/10.1002/zamm.19290090104.
[33] S.P. Sun, X.P. Li, H.J. Wang, Y. Jiang, D.Q. Yi, Prediction on anisotropic elasticity, sound velocity, and thermodynamic properties of MoSi2 under pressure, J. Alloys Compd. 652 (2015) 106–115, https://doi.org/10.1016/j.jallcom.2015.08.207.
[34] R. Hill, The elastic behaviour of a crystalline aggregate, Proc. Phys. Soc. 65 (1952) 349–354, https://doi.org/10.1088/0370-1298/65/5/307.
[35] M.L. Cohen, Calculation of bulk moduli of diamond and zinc-blende solids, Phys. Rev. B 32 (1985) 7988–7991, https://doi.org/10.1103/PhysRevB.32.7988.
[36] S.F. Pugh, XCII. Relations between the elastic moduli and the plastic properties of polycrystalline pure metals, London, Edinburgh, Dublin Philos. Mag. J. Sci. 45 (1954) 823–843, https://doi.org/10.1080/14786440808520496.
[37] I.N. Frantsevich, Elastic Constants and Elastic Moduli of Metals and Insulators, Ref. B, 1982. https://ci.nii.ac.jp/naid/10004038718. (Accessed 22 December 2020). accessed.
[38] D.H. Wu, H.C. Wang, L.T. Wei, R.K. Pan, B.Y. Tang, First-principles study of structural stability and elastic properties of MgPd3 and its hydride, J. Magnes. Alloy. 2 (2014) 165–174, https://doi.org/10.1016/j.jma.2014.06.001.
[39] J. Haines, J. Léger, G. Bocquillon, Synthesis and design of superhard materials, Annu. Rev. Mater. Res. 31 (2001) 1–23, https://doi.org/10.1146/annurev.matsci.31.1.1.
[40] O.L. Anderson, H.H. Demarest, Elastic constants of the central force model for cubic structures: polycrystalline aggregates and instabilities, J. Geophys. Res. 76 (1971) 1349–1369, https://doi.org/10.1029/jb076i005p01349.
[41] M.A. Rahman, M.K. Ahmed, Physical Properties of BaNiSn 3-type Compounds LaTGe 3 (T= Rh, Ir, Pd): An ab-initio Investigation, n.d. https://www.researchgate.net/publication/339383954 (accessed December 22, 2020).
[42] T. Sugimoto, Development of an automatic vickers hardness testing system using image processing technolog takao sugimoto and tadao kawaguchi, IEEE Trans. Ind. Electron. 44 (1997) 696–702, https://doi.org/10.1109/41.633474.
[43] X.-Q. Chen, H. Niu, D. Li, Y. Li, Intrinsic Correlation between Hardness and Elasticity in Polycrystalline Materials and Bulk Metallic Glasses, vol. 2, 2011, https://doi.org/10.1016/j.intermet.2011.03.026.
[44] H. Zhai, X. Li, J. Du, First-principles calculations on elasticity and anisotropy of tetragonal tungsten dinitride under pressure, Mater. Trans. 53 (2012) 1247–1251, https://doi.org/10.2320/matertrans.M2011373.
[45] S.I. Ranganathan, M. Ostoja-Starzewski, Universal elastic anisotropy index, Phys. Rev. Lett. 101 (2008) 3–6, https://doi.org/10.1103/PhysRevLett.101.055504.
[46] K. Lau, A. McCurdy, Elastic anisotropy factors for orthorhombic, tetragonal, and hexagonal crystals, Phys. Rev. B Condens. Matter 58 (1998) 8980–8984, https://doi.org/10.1103/PhysRevB.58.8980.
[47] H. Siethoff, K. Ahlborn, Debye-temperature-elastic-constants relationship for materials with hexagonal and tetragonal symmetry, J. Appl. Phys. 79 (1996) 2968–2974, https://doi.org/10.1063/1.361293.
[48] O.L. Anderson, A simplified method for calculating the debye temperature from elastic constants, J. Phys. Chem. Solid. 24 (1963) 909–917, https://doi.org/10.1016/0022-3697(63)90067-2.
[49] J. Feng, B. Xiao, R. Zhou, W. Pan, D.R. Clarke, Anisotropic elastic and thermal properties of the double perovskite slab-rock salt layer Ln 2SrAl 2O 7 (Ln = La, Nd, Sm, Eu, Gd or Dy) natural superlattice structure, Acta Mater. 60 (2012) 3380–3392, https://doi.org/10.1016/j.actamat.2012.03.004.
[50] S.Z. Karazhanov, P. Ravindran, A. Kjekshus, H. Fjellvåg, B.G. Svensson, Electronic structure and optical properties of ZnX (X=O, S, Se, Te): a density functional study, Phys. Rev. B Condens. Matter 75 (2007) 1–14, https://doi.org/10.1103/PhysRevB.75.155104.
[51] Z.M. Gibbs, F. Ricci, G. Li, H. Zhu, K. Persson, G. Ceder, G. Hautier, A. Jain, G. J. Snyder, Effective mass and Fermi surface complexity factor from ab initio band structure calculations, Npj Comput. Mater. 3 (2017) 1–6, https://doi.org/10.1038/s41524-017-0013-3.
[52] O. Rubel, F. Tran, X. Rocquefelte, P. Blaha, Perturbation approach to ab initio effective mass calculations, Comput. Phys. Commun. 261 (2021) 107648, https://doi.org/10.1016/j.cpc.2020.107648.
[53] W. Khan, A.H. Reshak, Optoelectronic and thermoelectric properties of KAuX5 (X = S, Se): a first principles study, J. Mater. Sci. 49 (2014) 1179–1192, https://doi.org/10.1007/s10853-013-7798-3.
[54] M. Faizan, H. Ullah, S.H. Khan, S.M. Ramay, S.A.S. Qaid, A. Mahmood, M. Ali, Carrier effective masses and thermoelectric properties of novel Ag3AuSe2 and Ag3AuTe2 compounds, Int. J. Mod. Phys. B 31 (2017) 1–8, https://doi.org/10.1142/S0217979217502538.
[55] C. Ambrosch-Draxl, J.O. Sofo, Linear optical properties of solids within the full-potential linearized augmented planewave method, Comput. Phys. Commun. 175 (2006) 1–14, https://doi.org/10.1016/j.cpc.2006.03.005.
[56] T. Ghellab, H. Baaziz, Z. Charifi, K. Bouferrache, M.A. Saeed, A. Telfah, Ab initio full-potential study of the fundamental properties of chalcopyrite semiconductors XPN 2 (X = H, Cu), Mater. Res. Express 6 (2019), https://doi.org/10.1088/2053-1591/ab1325.

[57] D.R. Penn, Wave-number-dependent dielectric function of semiconductors, Phys. Rev. 128 (1962) 2093–2097, https://doi.org/10.1103/PhysRev.128.2093.
[58] J. Sun, X.F. Zhou, Y.X. Fan, J. Chen, H.T. Wang, X. Guo, J. He, Y. Tian, First-principles study of electronic structure and optical properties of heterodiamond BC2 N, Phys. Rev. B Condens. Matter 73 (2006) 1–10, https://doi.org/10.1103/PhysRevB.73.045108.
[59] R. Belghit, H. Belkhir, M.T. Kadri, D. Heciri, M. Bououdina, R. Ahuja, Structural, elastic, electronic and optical properties of novel antiferroelectric KNaX (X = S, Se, and Te) compounds: first principles study, Phys. B Condens. Matter 545 (2018) 18–29, https://doi.org/10.1016/j.physb.2018.05.025.

Abstract

This study deals with the first theoretical investigation of structural, mechanical, electronic, and optical properties of $ABrF_4$ (A = Na, K, and Rb) ternary compounds using ab-initio calculations within the framework of the density functional theory (DFT) using the pseudo-potential plane-wave method. The structural parameters are in agreement with the experimental values stated in the literature. The elastic constants indicate that these compounds are ductile. For confirming the anisotropic of the mechanical properties, several indexes such as the universal anisotropic, and the percentage elastic anisotropy for compression and shear have been investigated. The electronic properties indicate that these compounds are wide-band gap semiconductor materials. The optical properties including the dielectric function, the absorption and extinction coefficients, the optical reflectivity and photoconductivity, the refractive index, and the energy loss function have been studied in detail. The wide optical absorption range in the ultraviolet (UV) region suggests that these materials could be useful for specific implementations in UV optoelectronic devices; therefore, this theoretical investigation is probable to motivate future experimental works.

Keywords: *First-principles calculations; density functional theory; $ABrF_4$; elastic and Optoelectronic properties.*

Résumé

Cette étude traite la première investigation théorique des propriétés structurelles, mécaniques, électroniques et optiques des composés ternaires $ABrF_4$ (A = Na, K et Rb) en utilisant des calculs ab-initio dans le cadre de la théorie de la fonctionnelle de la densité (DFT) par la méthode des ondes planes pseudo-potentielles. Les paramètres structuraux sont en accord avec les valeurs expérimentales indiquées dans la littérature. Les constantes élastiques indiquent que ces composés sont ductiles. Pour confirmer l'anisotropie des propriétés mécaniques, plusieurs indices tels que l'anisotropie universelle et le pourcentage d'anisotropie élastique pour la compression et le cisaillement ont été étudiés. Les propriétés électroniques indiquent que ces composés sont des matériaux semi-conducteurs à large bande interdite. Les propriétés optiques telles que la fonction diélectrique, les coefficients d'absorption et d'extinction, la réflectivité et la photoconductivité, l'indice de réfraction et la fonction de perte d'énergie ont été étudiées en détail. La large plage d'absorption optique dans la région ultraviolette (UV) suggère que ces matériaux pourraient être utiles pour des mises en œuvre spécifiques dans des dispositifs optoélectroniques UV ; par conséquent, cette investigation théorique est susceptible de motiver de futurs travaux expérimentaux.

Mots clés : *Calculs des premiers principes; la théorie fonctionnelle de la densité; $ABrF_4$; propriétés élastiques et optoélectroniques.*

ملخص

تتناول هذه الدراسة أول تحقيق نظري للخصائص التركيبية والميكانيكية والإلكترونية والبصرية للمركبات الثلاثية $ABrF_4$ (A=Na وK وRb) باستخدام حسابات المبادئ الأولى في إطار نظرية الكثافة الوظيفية باستخدام طريقة الموجة المستوية الكمونات الزائفة. تتوافق الثوابت الهيكلية مع القيم التجريبية الواردة في المراجع. الثوابت الميكانيكية تشير إلى أن هذه المركبات مرنة. لتأكيد الطابع المتباين للخواص الميكانيكية، تم فحص العديد من المؤشرات مثل المتباين الشامل، وتباين المرونة المئوية للضغط والقص. تشير الخصائص الإلكترونية إلى أن هذه المركبات عبارة عن مواد أشباه موصلات ذات فجوة نطاق واسعة. تمت دراسة الخصائص البصرية بما في ذلك دالة العزل الكهربائي ومعاملات الامتصاص والاخماد والانعكاس البصري والتوصيل الفتوني ومعامل الانكسار ودالة فقدان الطاقة بالتفصيل. يشير نطاق الامتصاص البصري الواسع في منطقة الأشعة فوق البنفسجية (UV) إلى أن هذه المواد يمكن أن تكون مفيدة لتطبيقات محددة في الأجهزة الإلكترونية الضوئية للأشعة فوق البنفسجية؛ لذلك، من المحتمل أن يكون هذا البحث النظري لتحفيز الأعمال التجريبية المستقبلية.

الكلمات المفتاحية: *حسابات المبادئ الأولى. نظرية الكثافة الوظيفية؛ $ABrF_4$ ؛ الخصائص المرنة والإلكترونية الضوئية.*